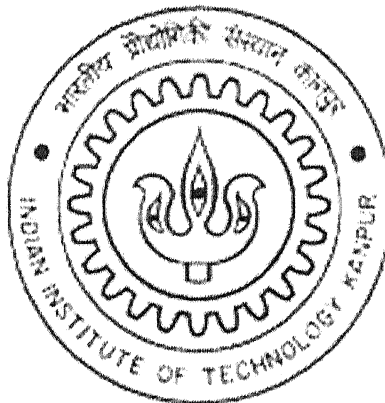# A UTILITY FRIENDLY THREE-LEVEL HIGH PERFORMANCE INDUCTION MOTOR DRIVE SYSTEM

A thesis submitted
in partial fulfillment of the requirements
For the degree of

MASTER OF TECHNOLOGY

by

G Kiran

to the

Department of Electrical Engineering
INDIAN INSTITUTE OF TECHNOLOGY, KANPUR
May 2005

TH
EE/2005/M
K63u

CERTIFICATE

This is to certify that the work contained in this thesis entitled "**A Utility Friendly Three-Level High Performance Induction Motor Drive System**", by **G. Kiran,** has been carried out under my supervision and that this work has not been submitted elsewhere for any degree.

Dr. Shyama. P. Das

Associate Professor

Department of Electrical Engineering

Indian Institute of Technology

Kanpur, India

Dedicated to my parents

ACKNOWLEDGMENTS

I sincerely thank my friends G. Srikanth, R. Pavan kumar sukla, E. Rammohan, Hema Rani, S. Srikanth, G. Radha Krishna, K. N. Srinivas, D. D. Praveen Kumar, Bhaumik Sherdiwala, Navin Mohan Naidu, K. Jayalakshmi, Ujjwala D, and many others who made my stay at IIT a memorable thing in my life. My stay at IITK will remain fresh and evergreen in my memory with the warmth and affection extended by my friends.

The thesis wouldn't have been completed without the active participation of our technical staff. I am very thankful to Mr. K E Hole of PCB Lab and Mr. Tiwari of electrical workshop.

Finally I would express my thanks to all those who have helped me directly or indirectly in the progress and completion of work.

Kiran Gajula

Abstract

In the present thesis, the torque and the flux of a three-level induction motor are directly and independently controlled by using "Direct Torque and Flux Control (DTFC)" method. A three-level Synchronous Link Converter (SLC) is used as the front-end converter for drawing unity power factor sinusoidal current from utility. Hence the drive is utility friendly and capable of four quadrant operation. High performance induction motor drives require accurate independent torque and flux control over a wide range of speed range. DTFC is less complex and gives better control characteristics. The main difference between DTFC and traditional AC drive method controls is that with DTFC there is no separate voltage and frequency-controlled PWM modulator.

The DTFC method gives attractive performance in terms of fast torque response, simple control scheme without coordinate transformation, and robustness against the motor parameter variation. It has been developed on the space vector approach, where the torque and flux of an induction motor can be controlled directly and independently. In the DTFC, the motor torque and flux are calculated from the primary variables and they are controlled directly and independently by selecting optimum inverter switch modes. The conventional DTFC suffers from flux demagnetization at low speed due to increased stator resistance drop. A modified control scheme has been developed in the present work to avoid this problem for better response at low speed condition. The real time algorithm of the drive system has been implemented with a PC, which uses PCL-208 data acquisition card for data transfer.

Keywords: *Direct Torque and Flux Control (DTFC), Synchronous Link Converter (SLC), Three-level inverter, Induction Motor, Look up table, Space vector modulation.*

Contents

List of Figures

List of Tables

List of Symbols

i_a, i_b, i_c — Source currents supplied to Synchronous Link Converter

ΔI — Hysteresis current band

v_{as}, v_{bs}, v_{cs} — Supply Voltages given to Synchronous Link Converter

V_{dc1}, V_{dc2}, V_{dc} — upper, lower and total DC link Voltage

$i_{qs}, i_{ds}, i_{qr}, i_{dr}$ — Stator and rotor q, d-axis currents

V_{ao}, V_{bo}, V_{co} — Voltage inputted by inverter

$f_{qs}, f_{ds}, f_{qr}, f_{dr}$ — Stator and rotor q, d-axis fluxes

ω_c, ω_r — Speed of arbitrary reference frame and rotor speed

f_s, f_{s_ref}, f_r — Stator, stator reference and rotor fluxes

θ_s — Stator flux angle

θ_n — Sector no. n

ct, cf — Status of Torque and Flux

γ — Slip angle or torque angle

T_e, T_{e_ref} — Electromagnet torque and reference torque

L_s, L_r, L_m — Stator, rotor and magnetizing inductances, per-phase

K_p, K_i — PI controller gains

R_s, R_r — Stator and rotor per phase resistances

Chapter 1

Introduction

1.1 Background

Motion control is required in large a number of industrial and domestic applications like transportation systems, rolling mills, paper machines, textile mills, machine tools, fans, pumps, robots, washing machines, etc. One major application of electric drives is in electric traction. Electric traction includes electric trains, electric buses, trams, battery driven and solar powered vehicles.

In the field of electric traction, the ac electrification at commercial frequency began during the year 1955. The overhead catenary supply was fed at 25.0 kV, 50 Hz, single phase supply. Such a system needed power conversion on the Locomotives / Motor coaches for feeding the dc traction motors. Initially power conversion was done by means of mercury arc rectifiers. The maintenance cost of mercury arc rectifier was very high. In order to overcome this drawback, semiconductor diode rectifier was used to feed the dc traction motors. Such system has drawbacks such as, regeneration was not possible resulting in wastage of considerable wastage of power in the dynamic braking resistors, reduced life and increased maintenance of braking equipment. The multi-stage phase controlled converters operating in sequence control and the pulse width modulated

converters were used for obtaining the continuous control of tractive force/speed. Although these schemes ensured the better utilization of adhesion, the system has drawbacks due to the use of dc traction motors such as: the increased maintenance due to presence of commutator and brush gears, comparatively lower torque to weight ratio, lower operating speeds, lower efficiency compared with the ac traction motors.

To overcome these drawbacks, the three phase ac motors have been employed. Such a drive has several important features like regenerative braking capability, very little maintenance, better utilization of available adhesion, higher average speed, higher torque-to-weight ratio, higher voltage and higher efficiency. Both synchronous and the asynchronous induction motors are used in the three phase ac motor traction drives.

For almost a century, induction machine (IM) has been the work-horse of industry due to its robustness, low cost, and less maintenance. Before power electronics was introduced, induction motors were mainly used for essentially constant speed applications because of the unavailability of the variable-frequency voltage or current supply. The advancement of power electronics has made it possible to vary the frequency of the voltage or current supplies relatively easily, thus has extended the used of induction motor in variable speed drive applications; but due to the inherent coupling of flux and torque components in IM, it could not provide the torque performance comparable to the DC machine.

The only effective way of producing a variable speed induction motor drive is to supply the induction motor with three phase voltages of variable frequency and variable amplitude. A variable frequency is required because the rotor speed depends on the speed of the rotating magnetic field provided by the stator. A variable voltage is required

because the motor impedance at low frequencies and consequently the current has to be limited by the means of reducing the supply voltage.

It is in this area considerable research effort has been devoted with the aim to find even simpler methods of speed control for induction machines. One method, which has gained popularity over the last decade, is Direct Torque and Flux Control.

Historically, several general controllers have been developed for induction motor control:

- Scalar controllers: Despite the fact that "Voltage-Frequency" (V/f) is the simplest controller, it is the most widespread, and is used in the majority of the industrial applications. It is known as scalar control [1] as it acts by imposing a constant relation between voltage and frequency without any phase angle control. The controller structure is very simple and it is normally used without speed feedback. In this control scheme, the performance of the machine improves in the steady state only, but the transient response is poor. However, this controller doesn't achieve a good accuracy in both speed and torque responses, mainly due to the fact that the stator flux and torque are not directly controlled.

- Vector controllers: In 1971, Blaschke [2] proposed a scheme, which aims as the control of an induction motor like a separately excited dc motor, called field orientation control, vector control, or transvector control [3]. The idea of vector controlled AC motor drives is based on the excellent control properties of DC motors, where torque and motor magnetic flux can be independently controlled. In this scheme, the induction motor is analysed from a synchronously rotating reference frame where all the fundamental ac variables appear to be dc ones. The torque and flux component of currents are identified and controlled independently to achieve a

good dynamic response. However, there is a necessity of transforming the variables in the synchronously rotating reference frame to the stator reference frame to effect the control of actual currents/voltages. This transformation contains transcendental functions like sine, cosine, and also introduces computational complexity into the system. Additionally, the transformation also needs the appropriate flux vector angle, which is either calculated by adding the calculated slip angle and measured rotor angle as in indirect vector control [4, 5] or by estimating the flux angle directly by employing a flux observer as in direct vector control. Thus the accuracy of the vector control is largely governed by the accuracy with which flux angle is calculated and rotating reference frame variables are transformed into the stator variables.

- Field Acceleration method: This method is based on maintaining the amplitude of magnetic field in the air gap as constant and there is an adjustment in the speed of rotation of the field to produce the desired value of the torque. This also means when the air gap flux is kept constant, all other variables like voltage, current and torque become functions of slip frequency and torque control is achieved by accelerating and decelerating the rotation of flux [6, 7].

- Direct Torque and Flux Control (DTFC) has emerged over the last decade to become one possible alternative to the well-known vector control of induction machines. Its main characteristic is the good performance, and it gives results as good as the classical vector control but with several advantages based on its simple structure and having four quadrant control capability. In DTFC [8-19] it is possible to control

directly the stator flux and the torque by selecting the appropriate inverter state. Thus the flux and torque are directly controlled by closed loop feedback as opposed to the vector control where the flux and torque are indirectly controlled by the direct and quadrature axis components of stator current vector. DTFC uses feedback control of torque and stator flux, which are computed with measured voltages and currents. The method uses stator reference frame model of the induction motor for its implementation, thereby avoiding trigonometric operations in the coordinate transformations of the synchronous reference frames [7]. The scheme uses stator flux linkages controls that enable the flux-weakening operation of the induction motor to be straight forward compared to rotor flux-weakening as the stator flux is directly proportional to the induced emf. This reduces the dependence of the scheme on many motor parameters, thus making it robust, especially in the flux-weakening region. Thus the scheme depends only on stator resistance of the motor [20]. For flux and torque control, this scheme requires the position of the flux phasor, which is difficult to obtain at low and zero speeds from measured voltages and currents. At such low speed, the stator induced emfs are very small, making scaling and accurate problematic; also the stator-resistance variations introduce significant error in the flux-phasor computation. Thus the low-speed operation suffers with this scheme without stator resistance compensation [10, 15, 18]. There is also a possible instability problem, due to parameter sensitivity. The drive system becomes unstable if the measured stator resistance in the controller is higher than the actual machine resistance [22]. Although majority of applications are in the medium power range, the DTFC algorithm is equally applicable for the high-power motor drives. Most of the

three-level inverters are generally used in driving the high power induction motors. In the high power three level inverter applications, the inverter switching frequency is limited below 1 kHz [21]. This limitation on the switching frequency results from a consideration that the higher the switching frequency, the heavier the cooling apparatus for the respective switching semiconductors. As a result, such a consideration on the low switching frequency of the inverter is taken into account design the DTFC algorithm suitable for three-level inverter-fed induction motors [23, 24, 25].

In the inverter-fed induction motor drives, a dc power source is required to feed the dc link. Traditionally, the power conversion from ac to dc was achieved by uncontrolled diode rectifiers or thyristorised controlled converters. Such converters have drawbacks such as harmonics in the input current, and output dc voltage, in addition to low input power factor for thyristors controlled converters particularly at low output voltages. Furthermore, four quadrant operation is not possible without employing a dual converter. Modern electric traction drives require the front-end ac to dc converter to have both rectifying and regenerating abilities. Dual converter used under such requirements has complexity in power and control circuits. The use of synchronous link three level converter (SLC) [26,27] as a front-end converter ensures near sinusoidal input current, reduced harmonic current injection into the utility and near unity power factor operation under forward and reverse power flow conditions.

1.2 Objectives of the Thesis

The objective of the present work is to realize a variable speed three-level inverter-fed induction motor drive where the torque and the flux of an induction motor is controlled directly and independently by using Direct Torque and Flux control method. At the same time, unity input power factor is maintained by using a three phase three level SLC as the front-end ac to dc converter. The dc link voltage is regulated by a closed loop feedback using a PI controller. Unity power factor at the utility interface is obtained by controlling the front-end converter switches in such a way that the source currents follow the reference currents which are in phase with the respective source voltages. Thus the present drive is utility friendly.

A PC is used to achieve the closed-loop operation. Thus, the present thesis deals with the design, simulation and PC-based implementation of a four quadrant direct torque and flux controlled induction motor drive system using three level inverter.

1.3 Summary of the chapters

The work presented in this thesis is organized in five chapters as given below:

Chapter 2 describes the basic operation of a three phase three level synchronous link converter. Modeling and simulation has been made with resistive load. Simulation results are presented at the end of the chapter.

Chapter 3 highlights the main feature of the proposed DTFC scheme along with description of its principle and basic concept of the torque and flux control. Mathematical modeling of induction motor and control algorithm of the proposed DTFC scheme using

three-level VSI is also presented in the chapter. Simulation has been made with the synchronous link converter used as the front-end converter. Typical simulation results are presented at the end of the chapter.

Chapter 4 describes the hardware fabrication and PC-based implementation of control scheme using a high performance data acquisition card. Brief discussions about the power circuit and the control circuit are given with requisite diagrams. Experimental results are presented at the end of the chapter.

Chapter 5 enumerates the main contributions of the present thesis and suggests the scope for the future work.

Chapter 2

Modeling and Simulation of Three Level Synchronous Link Converter

2.1 Introduction

The power conversion from *ac* to *dc* has been traditionally dominated by uncontrolled rectifiers or phase controlled converters. Such converters have the inherent drawbacks such as, harmonics in the input current and output voltages, in addition to low input power factor particularly at low output voltages. Variable speed drive applications require *ac* to *dc* converters to have both rectifying and regenerating abilities. Dual converters can be used under such requirements, but they have complex power and control circuits. The Synchronous Link Converter (SLC) can be used as the front-end converter where sinusoidal input current with four quadrant operation is required.

Synchronous Link Converter has several advantages such as sinusoidal input currents, unity power factor, inherent regenerative capability and these make SLC a plausible choice for *ac* to *dc* converter in a variable speed drive applications. In recent years, multilevel converters have become popular in medium and high power applications due to their ability to meet the increasing demand of power ratings. This chapter deals with the modeling and simulation of a three phase three-level Synchronous Link Converter, which can be used as a front-end converter for a variable speed drive system.

2.2 Principle of Three-phase Three-level Synchronous Link Converter

The power circuit configuration for the three-phase three-level is shown in Fig 2.1. It is operated in controlled current boost type converter mode. The source currents (i_a, i_b, i_c) are made to follow sinusoidal reference currents within a hysteresis band. The hysteresis band width determines the source current profile, its harmonic spectrum and the switching frequency of the devices. From Fig. 2.1, the source currents (i_a, i_b, i_c)can be increased by turning on the upper two switches (A1 & A2, B1 & B2, C1 &C2) and source currents can be decreased by turning on the lower two switches (A3 & A4, B3 & B4, C3 &C4). The dc link capacitor voltage is kept constant throughout the operation.
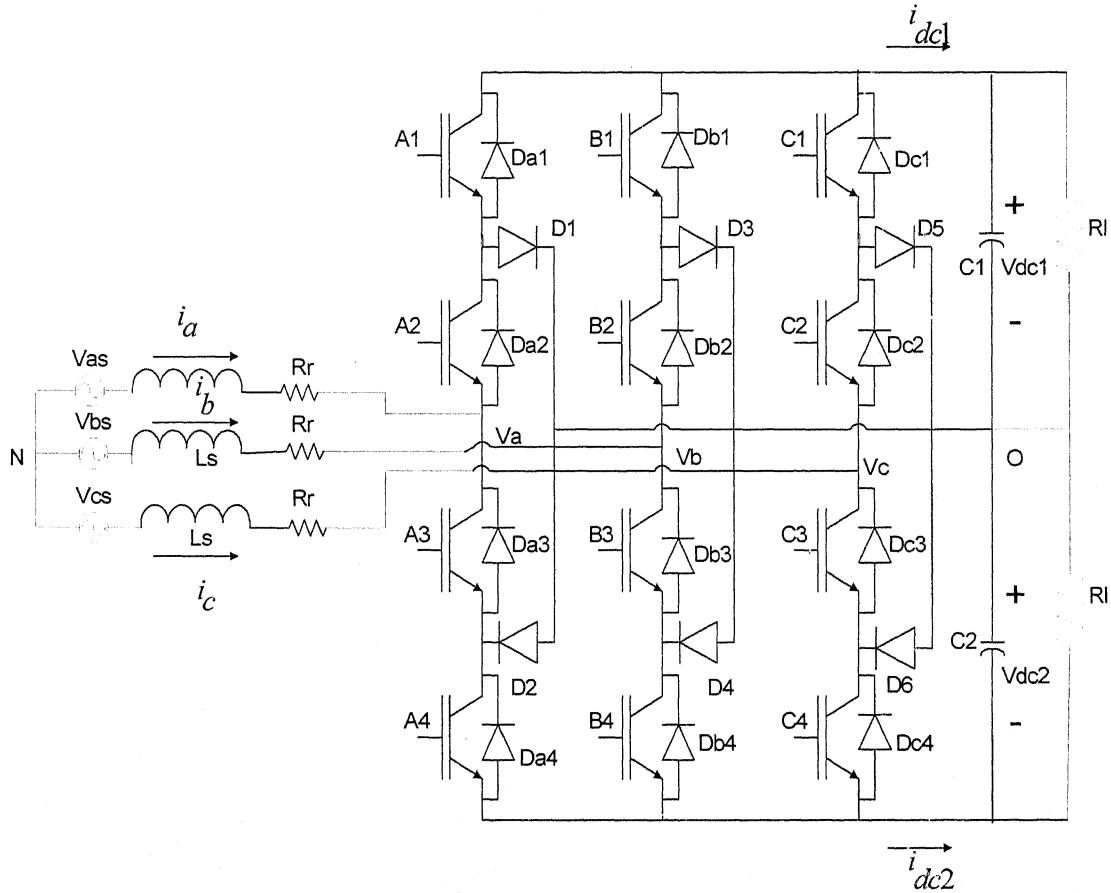
Fig. 2.1 Three-phase Three-level Synchronous Link Converter

The switching logic employing hysteresis current control can be written as follows.

If $i_a \geq i_{a\_ref} + \Delta I$ then switches A1 and A2, turn on.

If $i_a < i_{a\_ref} - \Delta I$ then switches A3 and A4, turn on.

Where ΔI is the hysteresis band on the reference current. Similarly, the same logic can be applied for other phase currents also.

2.3 Hysteresis Current Control Scheme
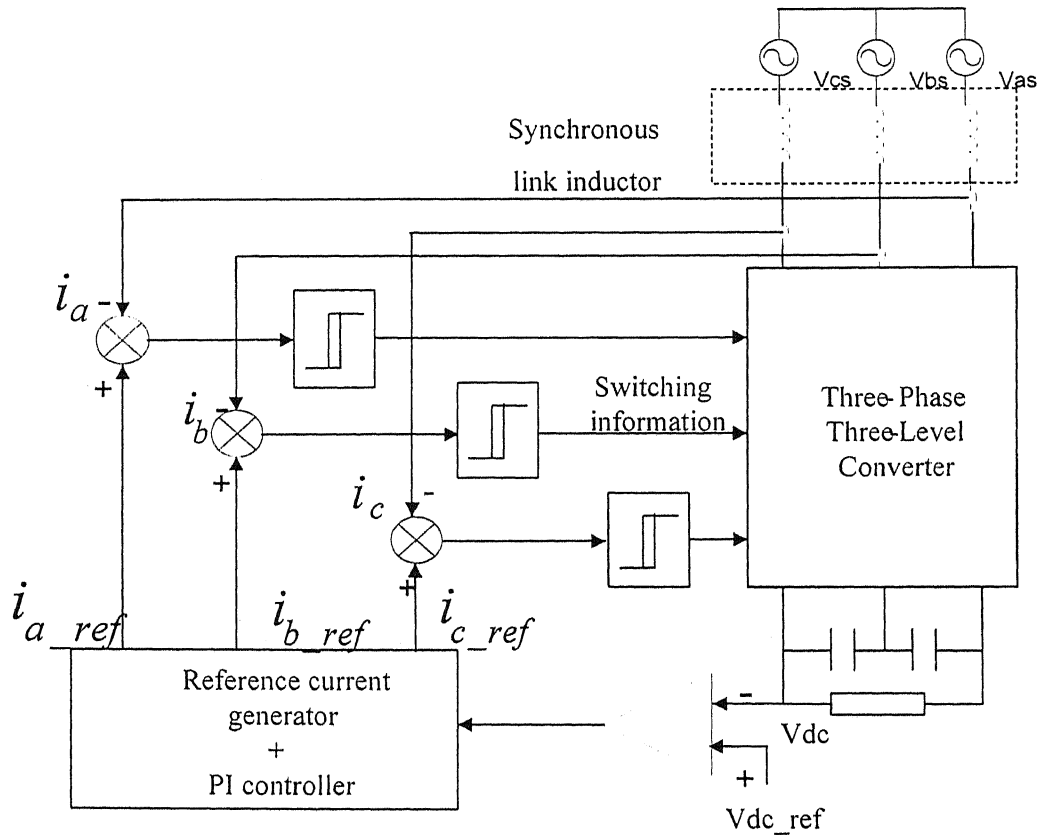
Fig 2.2 Hysteresis current control scheme for SLC

The hysteresis current control scheme block diagram is shown in Fig. 2.2. The dc link voltage is compared with the reference dc link voltage to control the amplitude of the reference currents. The error between the actual dc link voltage and reference dc link voltage is processed through a PI controller, which gives the amplitude of the reference

currents. The amplitude is multiplied by sin(wt), sin(wt-120), sin(wt-240) respectively, which are in phase with the respective phase voltages, to generate the reference source currents of the converter. The switches are controlled in such a way that the actual currents follow the reference currents with in the present hysteresis band.

2.4 Modeling of Three-phase Three-level SLC

The modeling of SLC is divided into two stages. In the first stage, we obtain the expressions for the current dynamics, and in the second, we obtain the expressions to describe the dynamics of the capacitor voltages.

A. The inductor current dynamics

Direct application of Kirchoff's voltage law (KVL) yields,

$$v_{as} = L_s \frac{di_a}{dt} + R_r i_a + v_{ao} + v_{on} \tag{2.1}$$

$$v_{bs} = L_s \frac{di_b}{dt} + R_r i_b + v_{bo} + v_{on} \tag{2.2}$$

$$v_{cs} = L_s \frac{di_c}{dt} + R_r i_c + v_{co} + v_{on} \tag{2.3}$$

Since source voltages are balanced and a three phase three wire system is considered, we can write the following equations

$$v_{as} + v_{bs} + v_{cs} = 0$$

$$i_a + i_b + i_c = 0$$

Adding all the three equations (2.1), (2.2) and (2.3), we get

$$v_{on} = -\frac{1}{3}(v_{ao} + v_{bo} + v_{co})$$

Eliminating v_{on} from (2.1), (2.2) and (2.3), we get

$$
\begin{bmatrix} v_{as} \\ v_{bs} \\ v_{cs} \end{bmatrix} = L_s \begin{bmatrix} \dfrac{di_a}{dt} \\ \dfrac{di_b}{dt} \\ \dfrac{di_c}{dt} \end{bmatrix} + R_r \begin{bmatrix} i_a \\ i_b \\ i_c \end{bmatrix} + \frac{1}{3} \begin{bmatrix} 2 & -1 & -1 \\ -1 & 2 & -1 \\ -1 & -1 & 2 \end{bmatrix} \begin{bmatrix} v_{ao} \\ v_{bo} \\ v_{co} \end{bmatrix} \tag{2.4}
$$

The pole voltages of the SLC v_{io} (where i = a, b, c) with respect to point O are

defined in terms of the switching variables S_{i1} and S_{i2} as follows:

$$
v_{io} = \left(S_{i1} v_{dc1} - S_{i2} v_{dc2} \right) \quad
\begin{cases}
S_{i1} = \begin{cases} 1 & \text{when switches } k_1 \text{ and } k_2 \text{ are on} \\ 0 & \text{else} \end{cases} \\[2mm]
S_{i2} = \begin{cases} 1 & \text{when switches } k_3 \text{ and } k_4 \text{ are on} \\ 0 & \text{else} \end{cases}
\end{cases} \tag{2.5}
$$

where $k = A,B,C$ and $i = a,b,c$

From equation (2.4) we can get,

$$
\begin{bmatrix} \dfrac{di_a}{dt} \\ \dfrac{di_b}{dt} \\ \dfrac{di_c}{dt} \end{bmatrix} = \frac{1}{L_s} \left[\begin{bmatrix} v_{as} \\ v_{bs} \\ v_{cs} \end{bmatrix} - R_r \begin{bmatrix} i_a \\ i_b \\ i_c \end{bmatrix} - \frac{1}{3} \begin{bmatrix} 2 & -1 & -1 \\ -1 & 2 & -1 \\ -1 & -1 & 2 \end{bmatrix} \begin{bmatrix} v_{a0} \\ v_{bo} \\ v_{co} \end{bmatrix} \right] \tag{2.6}
$$

Hence, the inductor current dynamics can be modeled as (2.6) where the SLC

pole voltages v_{ao}, v_{bo} and v_{co} are computed in (2.5).

B. *The capacitor voltage dynamics:*

The dc link currents i_{dc1} and i_{dc2} can be evaluated using Kirchoff's Current Law

(KCL) as follows,

$$i_{dc1} = \sum_{k=a}^{c} S_{k1} i_k \qquad S_{k1} = \begin{cases} 1 & \text{when switches } k_1 \text{ and } k_2 \text{ are on} \\ 0 & \text{else} \end{cases} \qquad (2.7)$$

$$i_{dc2} = \sum_{k=a}^{c} S_{k2} i_k \qquad S_{k2} = \begin{cases} 1 & \text{when switches } k_3 \text{ and } k_4 \text{ are on} \\ 0 & \text{else} \end{cases} \qquad (2.8)$$

$$C_1 \frac{dv_{dc1}}{dt} = i_{dc1} - \frac{v_{dc1}}{R_l} \quad \text{and} \quad C_2 \frac{dv_{dc2}}{dt} = -i_{dc2} - \frac{v_{dc2}}{R_l} \qquad (2.9)$$

$$C_1 = C_2 = C$$

We can simplify equation (2.9) as,

$$\begin{bmatrix} \dfrac{dv_{dc1}}{dt} \\ \dfrac{dv_{dc2}}{dt} \end{bmatrix} = \frac{1}{C} \begin{bmatrix} i_{dc1} - \dfrac{v_{dc1}}{R_l} \\ -i_{dc2} - \dfrac{v_{dc2}}{R_l} \end{bmatrix} \qquad (2.10)$$

Hence, the capacitor voltage dynamics can be modeled as (2.10) where the current i_{dc1} and i_{dc2} are given in equations (2.7) and (2.8) respectively.

The equations (2.6) and (2.10) can be solved by R-K fourth order method and the values of $V_{dc1}, V_{dc2}, i_a, i_b$ and i_c can be obtained. V_{dc} is the sum of V_{dc1} and V_{dc2}.

A computer program has been developed for resistive load. The data for simulation are given below.

1. Input supply voltage $v_{ph} = 230$ V (rms), 3Φ, 50 Hz.

2. Output dc voltage $V_{dc} = 350$ V.

3. Synchronous Link Inductor $L_r = 8 \, mH$.

4. DC link Capacitors $C_1 = C_2 = 1000 \mu F$.

5. Load resistance $R_l = 20 \, \Omega$.

In the simulation results, the input phase current waveforms, the source voltages, and the dc link voltages are shown in following figures. Fig. 2.3 shows that the dc link voltage is nearly constant during the operation. Fig 2.4 and 2.5 show that the sharing of voltage between capacitors is same. Figs. 2.6, 2.7 and 2.8 show that input phase currents are in phase with the respective voltages.

2.5 Conclusion

Due to advantages like reduced line current harmonics, unity power factor operation and bi-directional power flow capability, synchronous link converters are widely used as front-end converters in regenerative ac drives. Hysteresis current control scheme is used, and unity power factor operation is shown in simulation results. Usage of multilevel converter has increased the power rating and reduced the harmonic distortion. The use of multilevel converter in the front-end allows transformer less interface with high voltage utility for high power application.

2.6 Simulation results :
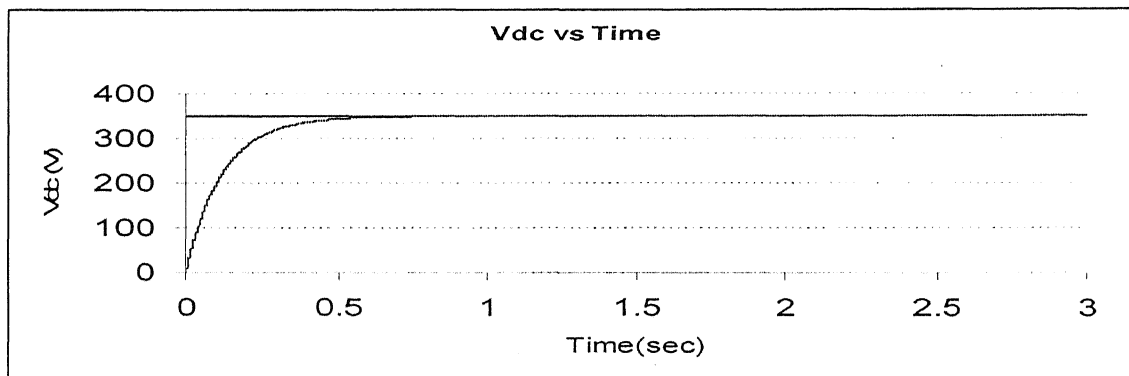
X-axis 1div = 0.5 sec (time)

Y-axis 1div = 100 V (DC voltage)

Fig. 2.3 Response of DC link voltage V_{dc}

Vdc1 vs Time
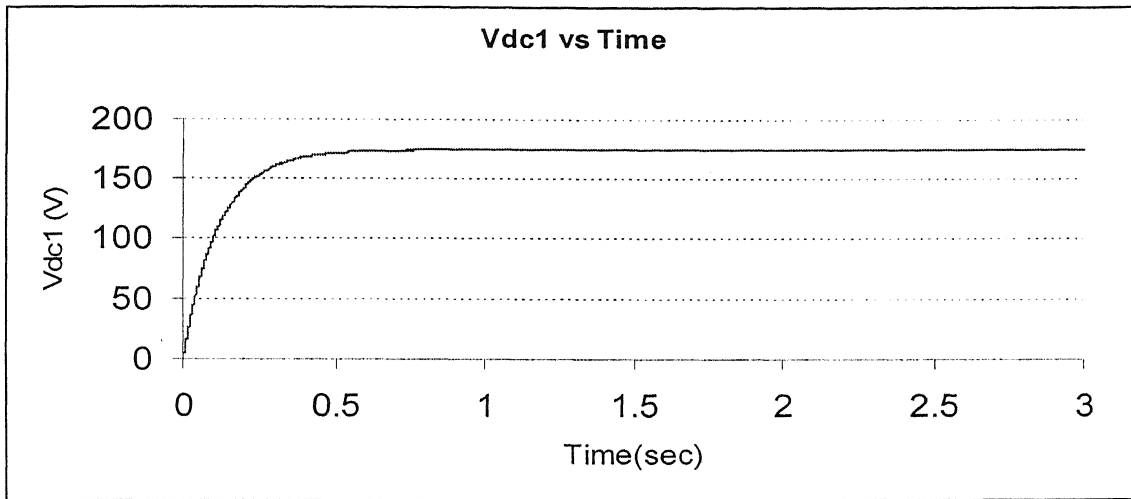
X-axis 1div = 0.5 sec (time)

Y-axis 1div = 100 V (DC voltage)

Fig. 2.4 Response of DC link voltage V_{dc1}

Vdc2 vs Time (sec)
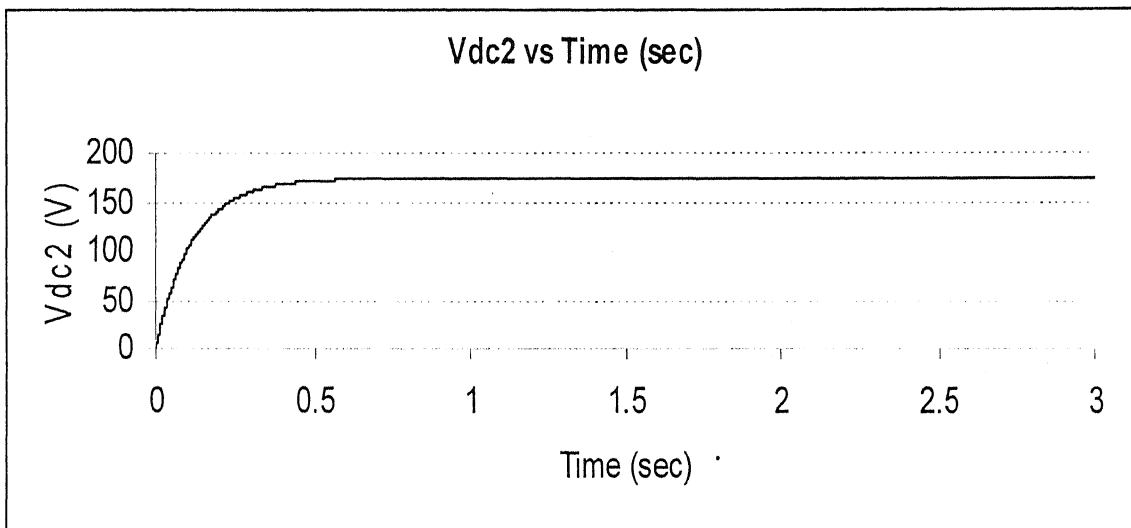
X-axis 1div = 0.5 sec (time)

Y-axis 1div = 100 V (DC voltage)

Fig. 2.5 Response of DC link voltage V_{dc2}

Vas,Ia vs Time
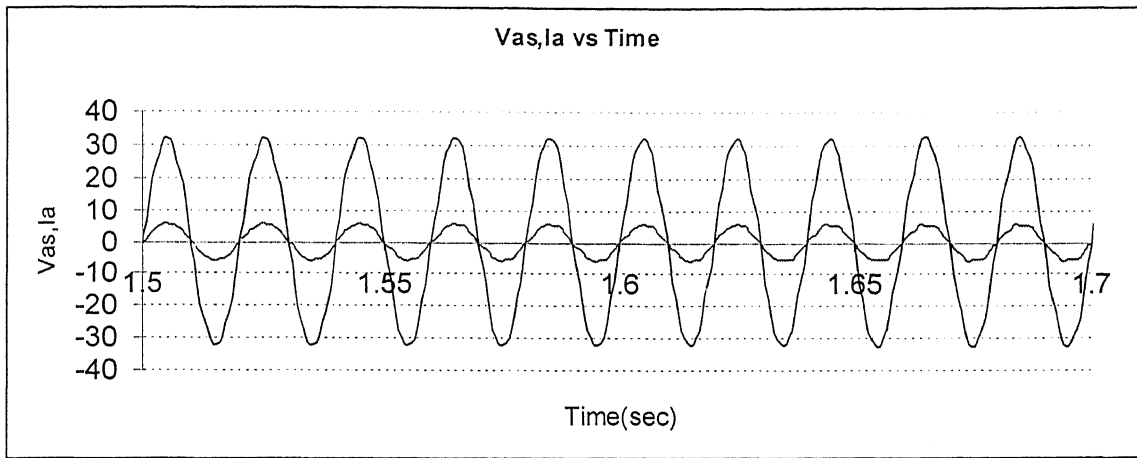
X-axis 1div = 0.05 sec (time)

Y-axis 1div = 100 V (source voltage, v_{as})

Y-axis 1div = 10 A (source current, i_a)

Fig. 2.6 Waveform of source voltage and source current for phase 'a'

Vbs,Ib vs Time
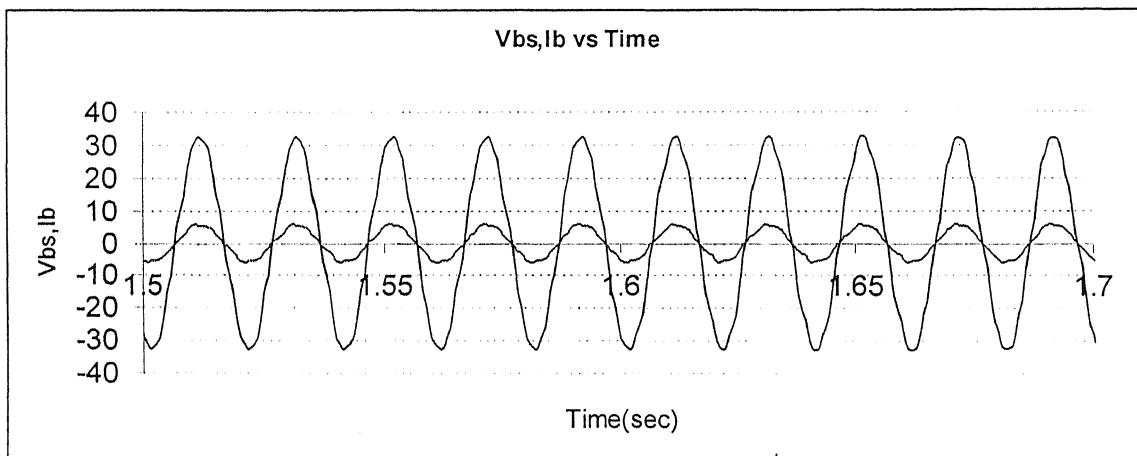
X-axis 1div = 0.05 sec (time)

y-axis 1div = 100 V (source voltage, v_{bs})

y-axis 1div = 10 A (source current, i_b)

Fig. 2.7 Waveform of source voltage and source current for phase 'b'

Vcs,Ic vs Time
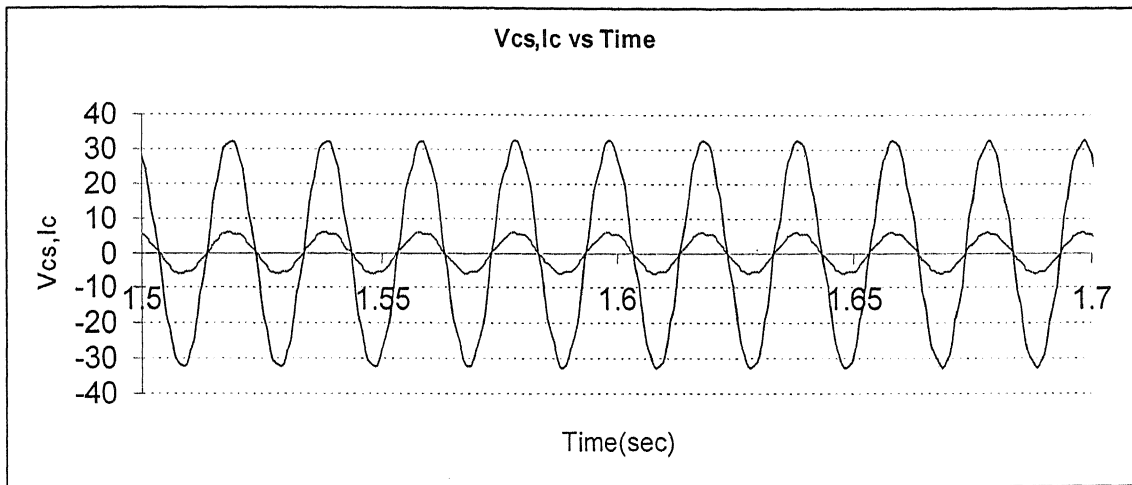
X-axis 1div = 0.05 sec (time)

Y-axis 1div = 100 V (source voltage, v_{cs})

Y-axis 1div = 10 A (source current, i_c)

Fig. 2.8 Waveform of source voltage and source current for phase 'c'

Source Currents vs Time
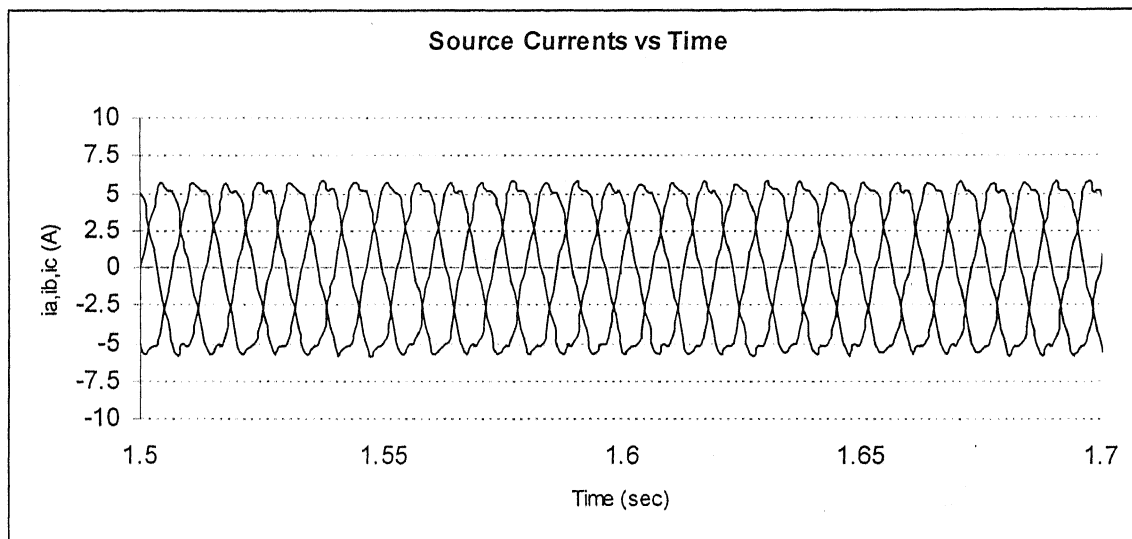
X-axis 1div = 0.05 sec (time)

Y-axis 1div = 10 A (source currents, i_a, i_b, i_c)

Fig. 2.9 Waveform of source currents

Chapter 3

Modeling and Simulation of Converter-Inverted fed Induction Motor Drive with Direct Torque and Flux Control

---

3.1 Introduction

The various control strategies for the control of the inverter-fed induction motor have resulted in good steady-state but poor dynamic response. From the plots of the dynamic responses, the cause of such poor dynamic response is found to be the deviation of the air gap flux linkages from their set values. The deviation is not only in magnitude but also in phase. The variations in the flux linkages have to be controlled by the magnitude and frequency of the stator and rotor phase currents and their instantaneous phases. Scalar control strategies have utilized the stator phase current magnitude and frequency and not their phases. This resulted in the deviation of the phase and magnitudes of the air gap flux linkages from their set values.

The oscillations in the air gap flux linkages results in oscillations in electromagnetic torque and, if left unchecked, result as speed oscillations. This is undesirable in many high-performance applications, such as in robotic actuators, centrifuges, servos, process drives, and rolling mills, where high precision, fast positioning, or speed control is required. Such requirement will not be met with the sluggishness of control due to the flux oscillations. Further, air gap flux variations

resulted in large excursions of stator currents, requiring large peak converter and inverter ratings to meet the dynamics. An enhancement of peak inverter rating increases cost and reduces the competitive edge of ac drives in marketplace, in spite of excellent advantages of the ac drives over dc drives.

Separately excited dc drives are simpler in control because they independently control flux, which, when maintained constant, contributes to an independent control of torque. This is made possible with separate control of field and armature current magnitudes, providing simplicity not possible with ac machine control. In contrast, ac induction motor drives require a coordinated control of stator current magnitudes, frequencies and their phases, making it a complex control. As with the dc drives, independent control of the flux and torque is possible in ac drives. The stator current phasor can be resolved, say, along the rotor flux linkages, and the component along the rotor flux linkages in the field-producing component, but this requires the position of the rotor flux linkages at every instant as it is dynamic unlike the dc machine. The requirement of phase, frequency, and magnitude control of the currents and hence of the flux phasor is made possible by inverter control.

Vector control made the ac drives equivalent to dc drives in the independent control of flux and torque and superior to them in their dynamic performance, because it relates to the phasor control of the rotor flux linkages. In vector control method, the machine control is achieved in a synchronously rotating reference frame in which the ac variables appear as dc quantities. The torque and flux components of stator current are identified and controlled independently to achieve good dynamic response. However in vector control there is a necessity of transforming the variables in synchronously rotating

reference frame to stator reference frame, to effect the control of actual motor current/voltages. This transformation requires trigonometric functions and so introduces computational complexity into the control system. Additionally, the transformation also needs the flux vector angle which is either calculated by adding the calculated slip angle and measured rotor angle as in the indirect control or by estimating the flux directed by employing a flux observer. Thus, the accuracy of vector control id largely governed by the accuracy with which the flux angle is calculated and rotating frame variables are transformed into the stator variables.

In recent years, the commercial applications of the field- oriented induction motor drives have greatly increased. DTFC strategy for ac motor control seems to be particularly useful for the adjustable speed drives, due to its robustness and functional simplicity. Despite its simplicity, DTFC is able to produce very fast torque and flux control and is robust with respect to motor parameters changes and to perturbations. Unlike the conventional vector control, DTFC requires no coordinate transformation of variables. Using the space-vector modulation (SVM) provides higher control resolution and helps improving the drive's behavior. The DTFC for ac drives is a strategy exclusively based on stator voltage control. The consecutive voltage vectors applied to the motor are directly selected on the basis of torque and flux errors. In this way, fast response and robust torque and flux control are obtained, without intermediate current control. The classic DTFC uses bang-bang torque and flux controllers, without decoupling. A simple switching logic (switching table) employs the output signals of these controllers to select the most appropriate voltage vector, i.e., the one which rapidly reduces the torque and flux errors.

High power induction motor drives using classical three-phase converters have the disadvantages of poor voltage and current qualities. To improve these values, the switching frequency has to be raised which causes additional switching losses. Another possibility is to put a motor input filter between the converter and motor, which causes additional weight. A further inconvenience is the limited voltage that can be applied to the induction motor determined by the blocking voltage of the semiconductor switches. For high power semiconductors, the switching frequency is limited by the maximal power loss. The aim of three-level converter is to generate motor currents of high quality by using more semi conducting devices. In particular, the converter is used for high-voltage motor drives. The series connection allows reaching much higher voltages than the blocking voltage of the semiconductors. The resulting switching frequency is a multiple of the switching frequency applied to the switches. Variable speed induction motors need regenerative braking capability. If diode or phase controlled rectifiers are used as a front end converter, regenerative braking is not possible. In addition, for these converters source current has harmonics, and the power factor is less then unity. The above problem can be solved by using the synchronous link three-level converter as the front-end converter.

The present chapter is devoted to the development of control scheme and digital simulation of direct torque and flux control of induction motor using three-level inverter with current control synchronous link converter as front-end converter. The induction motor is simulated in the stationary reference frame. Typical simulation results are given at the end of the chapter.

3.2 Converter – Inverter fed Induction Motor Drive

Fig. 3.1 shows the basic block diagram of three-level converter-inverter fed induction motor drive system. The drive system consists of two major parts: the driving part that contains the ac to dc three-level converter, three-level *dc* to *ac* inverter, and the induction motor, as well as the control part consists of the controller circuit and software. The three-level *ac* to *dc* converter is called synchronous link converter (SLC) to make the system utility friendly as discussed in chapter 2. Three-level inverter is used to control the induction motor. In the following sessions details of direct torque control of induction motor using three-level inverter will be given. Initially the dynamic modeling of induction motor has been done.
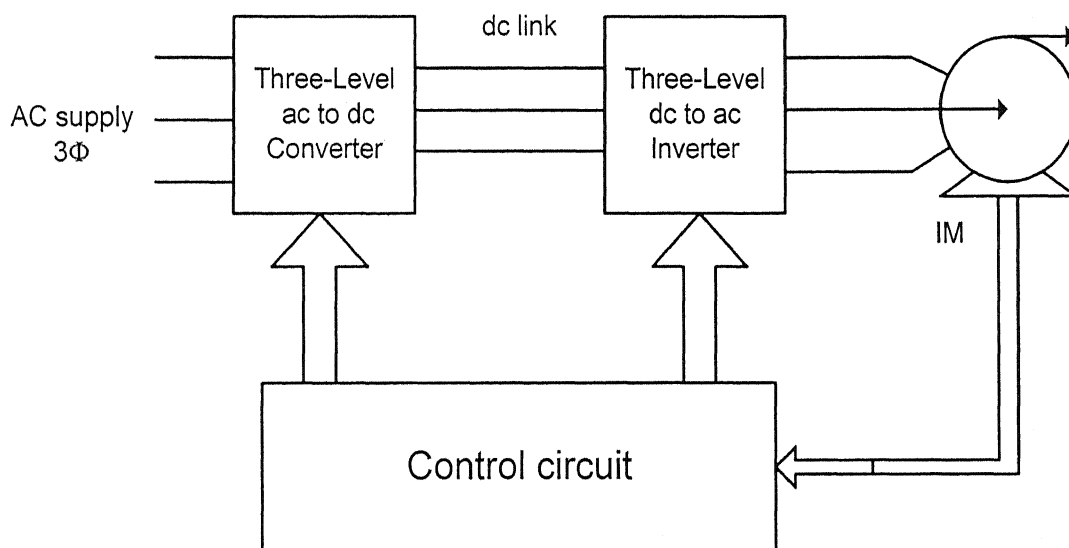
Fig 3.1 Block diagram of three-level converter-inverter fed induction motor drive

3.3 Dynamic Modeling of Induction Motor

A dynamic model of the machine subjected to control must be known in order to understand and design controlled drives. Due to the fact that every good control has to face any possible change of the plant, it could be said that the dynamic model of the machine could be just a good approximation of the real plant. Nevertheless, the model should incorporate all the important dynamic effects occurring during both steady-state and transient operations. Furthermore, it should be valid for any changes in the inverter's supply such as voltages or currents.

The dynamic model of the induction motor is derived by using a two-phase motor in direct and quadrature axes. The concept of power invariance is utilized in the modeling. According to the concept of power invariance, the power must be equal in the three-phase machine and its two-phase equivalent model.

The following assumptions are made to derive the dynamic model:

- Uniform air gap;

- Balanced rotor and stator windings with sinusoidally distributed mmf;

- Inductance vs. rotor position is sinusoidal; and

- Saturation and parameter changes are neglected.

3.3.1 Modeling of Induction Motor in Arbitrary Reference Frame

The dynamic equations of the induction motor in arbitrary reference frame can be represented by using flux linkages as variables. The stator and rotor flux linkages in arbitrary reference frame are defined by

$$f_{ds}^c = L_s \, i_{ds}^c + L_m \, i_{dr}^c \qquad (3.1)$$

$$f_{qs}^c = L_s \, i_{qs}^c + L_m \, i_{qr}^c \qquad (3.2)$$

$$f_{dr}^c = L_r \, i_{dr}^c + L_m \, i_{ds}^c \qquad (3.3)$$

$$f_{qr}^c = L_r \, i_{qr}^c + L_m \, i_{qs}^c \qquad (3.4)$$

The stator and rotor voltages can be written as

$$V_{ds}^c = i_{ds}^c \, R_s - \omega_c \, f_{qs}^c + p \, f_{ds}^c \qquad (3.5)$$

$$V_{qs}^c = i_{qs}^c \, R_s + \omega_c \, f_{ds}^c + p \, f_{qs}^c \qquad (3.6)$$

$$V_{dr}^c = i_{dr}^c \, R_r - \left(\omega_c - \omega_r\right) f_{qr}^c + p \, f_{dr}^c \qquad (3.7)$$

$$V_{qr}^c = i_{qr}^c \, R_r + \left(\omega_c - \omega_r\right) f_{dr}^c + p \, f_{qr}^c \qquad (3.8)$$

By substituting equations 3.1 - 3.4 into equations 3.5 - 3.8, the induction motor model in arbitrary reference frame is obtained. For simplicity superscript "c" is removed in the matrix.

$$\begin{bmatrix} V_{qs} \\ V_{ds} \\ 0 \\ 0 \end{bmatrix} = \begin{bmatrix} R_s + L_s p & \omega_c L_s & L_m p & \omega_c L_m \\ -\omega_c L_s & R_s + L_s p & -\omega_c L_m & L_m p \\ L_m p & \left(\omega_c - \omega_r\right)L_m & R_r + p L_r & \left(\omega_c - \omega_r\right)L_r \\ -\left(\omega_c - \omega_r\right)L_m & L_m p & -\left(\omega_c - \omega_r\right)L_r & R_r + p L_r \end{bmatrix} \begin{bmatrix} i_{qs} \\ i_{ds} \\ i_{qr} \\ i_{dr} \end{bmatrix} \qquad (3.9)$$

3.3.2 Modeling of Induction Motor in Stationary Reference Frame

The motor is fed from voltage source inverter as shown in fig. (3.2). For a given set of switching information, V_{ao}, V_{bo} and V_{co} have discrete instantaneous values.

Thus,

$$V_{an} = -\frac{1}{3}(2 * V_{ao} - V_{bo} - V_{co}) \tag{3.10}$$

$$V_{bn} = -\frac{1}{3}(2 * V_{bo} - V_{ao} - V_{co}) \tag{3.11}$$

$$V_{cn} = -\frac{1}{3}(2 * V_{co} - V_{bo} - V_{ao}) \tag{3.12}$$

Assuming that the direct phase winding axis (d-axis) of two-phase model is along the a-phase winding axis of the three-phase machine, transformation of ac voltage and current from a, b, c (3-phase) frame to d, q (2-phase) stationary reference frame gives

$$V_{ds} = \left(\frac{2}{3}\right)\left(V_{an} - 0.5\left(V_{bn} + V_{cn}\right)\right) \tag{3.13}$$

$$V_{qs} = \left(\frac{1}{\sqrt{3}}\right)\left(V_{bn} - V_{cn}\right) \tag{3.14}$$

$$i_{ds} = \left(\frac{2}{3}\right)\left(i_{an} - 0.5\left(i_{bn} + i_{cn}\right)\right) \tag{3.15}$$

$$i_{qs} = \left(\frac{1}{\sqrt{3}}\right)\left(i_{bn} - i_{cn}\right) \tag{3.16}$$

The DTFC scheme uses a stator reference frame model of the induction motor for its implementation. Therefore stator reference frame model is obtained by putting $\omega_c = 0$ in the arbitrary reference model of induction motor.

$$
\begin{bmatrix} V_{qs} \\ V_{ds} \\ 0 \\ 0 \end{bmatrix} = \begin{bmatrix} R_s + L_s p & 0 & L_m p & 0 \\ 0 & R_s + L_s p & 0 & L_m p \\ L_m p & -\omega_r L_m & R_r + pL_r & -\omega_r L_r \\ \omega_r L_m & L_m p & \omega_r L_r & R_r + pL_r \end{bmatrix} \begin{bmatrix} i_{qs} \\ i_{ds} \\ i_{qr} \\ i_{dr} \end{bmatrix}
\tag{3.17}
$$

The above set of differential equations can be solved by Runge-Kutta fourth order method and the values of i_{qs}, i_{ds}, i_{qr}, and i_{dr} can be obtained.

The d-axis and q-axis stator flux can be found from the equations (3.5) and (3.6) by putting $\omega_c = 0$ and removing the super script "c".

$$
V_{ds} = i_{ds} R_s + p f_{ds}
\tag{3.18}
$$

$$
V_{qs} = i_{qs} R_s + p f_{qs}
\tag{3.19}
$$

We can get
$$
f_{ds} = \int \left(V_{ds} - i_{ds} R_s \right) dt
\tag{3.20}
$$

$$
f_{qs} = \int \left(V_{qs} - i_{qs} R_s \right) dt
\tag{3.21}
$$

Therefore,

$$
f_s = \sqrt{f_{ds} * f_{ds} + f_{qs} * f_{qs}}
\tag{3.22}
$$

The position of stator flux and hence the sector can be obtained as

$$
\theta_s = \tan^{-1} \left(\frac{f_{qs}}{f_{ds}} \right)
\tag{3.23}
$$

The electromagnetic torque can be expressed as:

$$
T_e = (3/2)(P/2)\left(f_{ds} i_{qs} - f_{qs} i_{ds} \right)
\tag{3.24}
$$

The speed of the rotor in electrical rad/sec is

$$
\omega_r = (P/2)(1/J)\left(T_e - T_l - B(2/P)\omega_{ro} \right)
\tag{3.25}
$$

3.4 Direct Torque and Flux Control

DTFC main features are as follows:

- Direct control of flux and torque, which are computed from measured values of stator voltages and currents.

- Indirect control of stator currents and voltages.

- Approximately sinusoidal stator fluxes and stator currents.

- High dynamic performance.

The main advantages of DTFC are:

- Absence of coordinate transformation.

- Absences of voltage modulator block, as well as other controllers like PID for motor flux and torque.

- Minimal torque response time even better than vector controllers.

However, some disadvantages are also present such as:

- Possible problems during starting.

- Requirement of flux and torque estimators, implying the consequent parameters identification.

- Inherent torque and stator flux ripple.

3.4.1 Basic Concepts of DTFC

The torque expression given in Equation (3.24) can be expressed in the vector form as

$$\overline{T}_e = \frac{3}{2}\left(\frac{P}{2}\right)\overline{f}_s \times \overline{I}_s \tag{3.27}$$

where $\overline{f}_s = f_{qs} - j\,f_{ds}$ and $\overline{I}_s = i_{qs} - j\,i_{ds}$. In this equation, $\overline{I}_s$ is to be replaced by

rotor flux $\overline{f}_r$. In the complex form, $\overline{f}_s$ and $\overline{f}_r$ can be expressed as functions of currents

as

$$\overline{f}_s = L_s\,\overline{I}_s + L_m\,\overline{I}_r \tag{3.28}$$

$$\overline{f}_r = L_r\,\overline{I}_r + L_m\,\overline{I}_s \tag{3.29}$$

Eliminating $\overline{I}_r$ from Equation (3.28), we get

$$\overline{f}_s = \frac{L_m}{L_r}\,\overline{f}_r + L_s'\,\overline{I}_s \tag{3.30}$$

where $L_s' = L_s L_r - L_m^2$. The corresponding expression of $\overline{I}_s$ is

$$\overline{I}_s = \frac{1}{L_s'}\,\overline{f}_s - \frac{L_m}{L_r L_s'}\,\overline{f}_r \tag{3.31}$$

Substituting Equations (3.31) in (3.27) and simplifying yields

$$\overline{T}_e = \frac{3}{2}\left(\frac{P}{2}\right)\frac{L_m}{L_r L_s'}\,\overline{f}_r \times \overline{f}_s \tag{3.32}$$

that is, the magnitude of the torque is

$$\overline{T}_e = \frac{3}{2}\left(\frac{P}{2}\right)\frac{L_m}{L_r L_s}\left|f_r\right|\left|f_s\right|\sin\gamma \tag{3.33}$$

where as γ is the angle between the fluxes, which is slip angle. Figure 3.2 shows the phasor (or vector) diagram for Equation (3.32), indicating the vectors $\overline{f}_s$, $\overline{f}_r$ and $\overline{I}_s$ for positive developed torque. If the rotor flux remains constant and the stator flux is changed incrementally by stator voltage $\overline{V}_s$ as shown, and the corresponding change of γ angle is $\Delta\gamma$, the incremental torque ΔT_e expression is given as

$$\Delta T_e = \frac{3}{2}\left(\frac{P}{2}\right)\frac{L_m}{L_r L_s}\left|f_r\right|\left|\overline{f}_s + \Delta\overline{f}_s\right|\sin\Delta\gamma \tag{3.34}$$
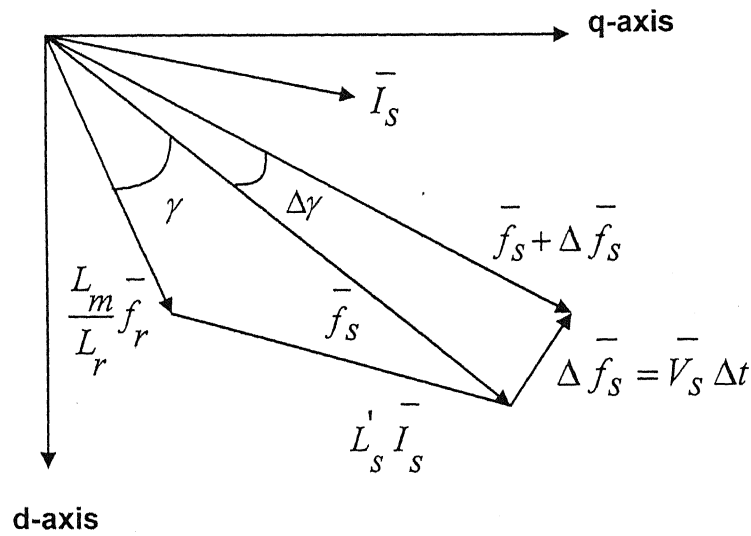
Fig. 3.2 stator flux, rotor flux, and stator current vectors on d-q stationary reference plane (stator resistance neglected)

3.5 Three-Level Space Vector Modulation

Multilevel voltage-fed inverters with space vector modulation have established their importance in high power and high performance industrial drive applications. Three-level voltage fed inverters are recently showing growing popularity for multi-megawatt industrial drive applications. The main reasons for this popularity are easy sharing of large voltage between the series devices and improvement of harmonic quality at the output compared to a two-level inverter. The space vector modulation of a three-level inverter provides the additional advantage of superior harmonic quality.
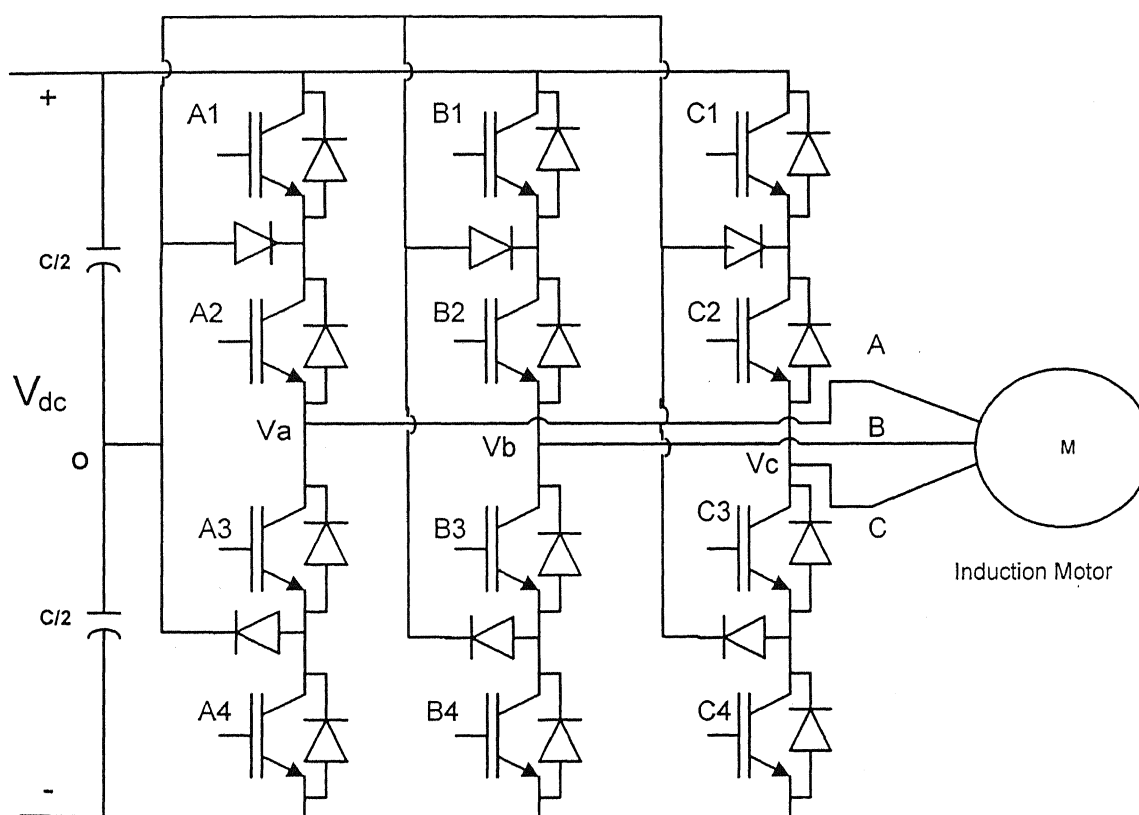
Fig. 3.3 Three-Level Inverter fed Induction Motor

However, space vector modulation of a three-level inverter is considerably more complex than that of a two-level inverter because of large number of inverter switching states. In addition, there is a problem of neutral point voltage balancing.

The structure of a three-level neutral point clamped inverter is shown in Fig. 3.3. A three-level inverter differs from a conventional two-level inverter in the sense that it is capable of producing three different levels of output phase voltage. When switches 1 and 2 are on, the output is connected to the positive supply bus. When switches 3 and 4 are on, the output is connected to the negative supply bus. When switches 2 and 3 are on, the output is connected to the supply neutral point via one of the two clamping diodes. With three possible output states for each of the three phases, there are a total of 27 possible switch combinations.
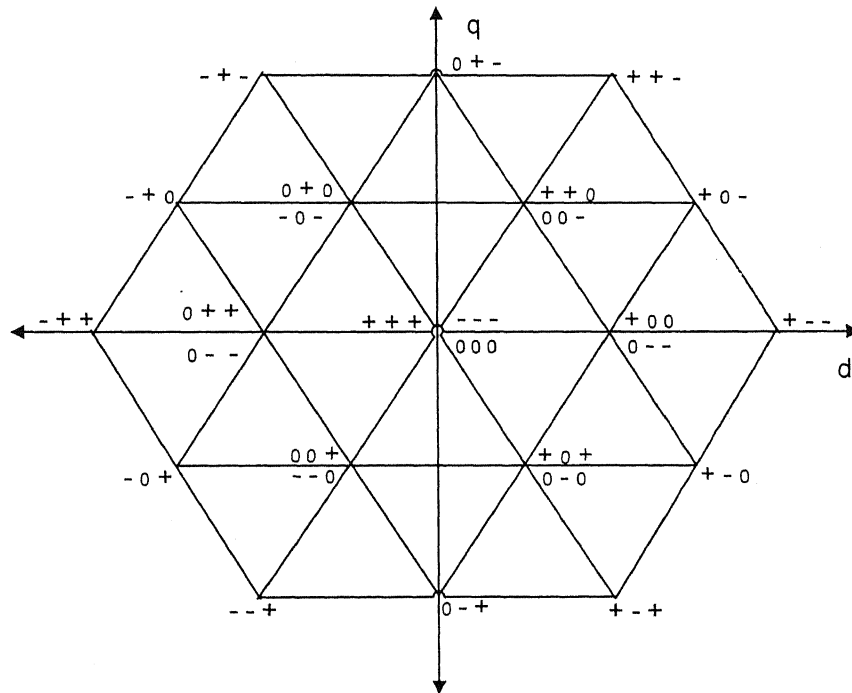
Fig. 3.4 Switching states of three-level inverter

The result of plotting each of the output voltages in a d-q reference frame is shown in Figure 3.4. Figure 3.4 shows that the 27 switch combinations result in a total of 19 unique voltage vectors since some of the combinations produce the same voltage vector. These different combinations relate to different ways of connecting the load to the DC bus that result in the same voltage being applied to the motor.

3.6 Theory of DTFC Involving Three – Level Inverter

In this section, the basic principle for the direct torque and flux control in a three-level inverter system is explained. Fig. 3.5 shows space-vector representation of three-level inverter output voltages, in which subscripts z, h, i and f denote zero, half, intermediate, and full voltages, respectively.
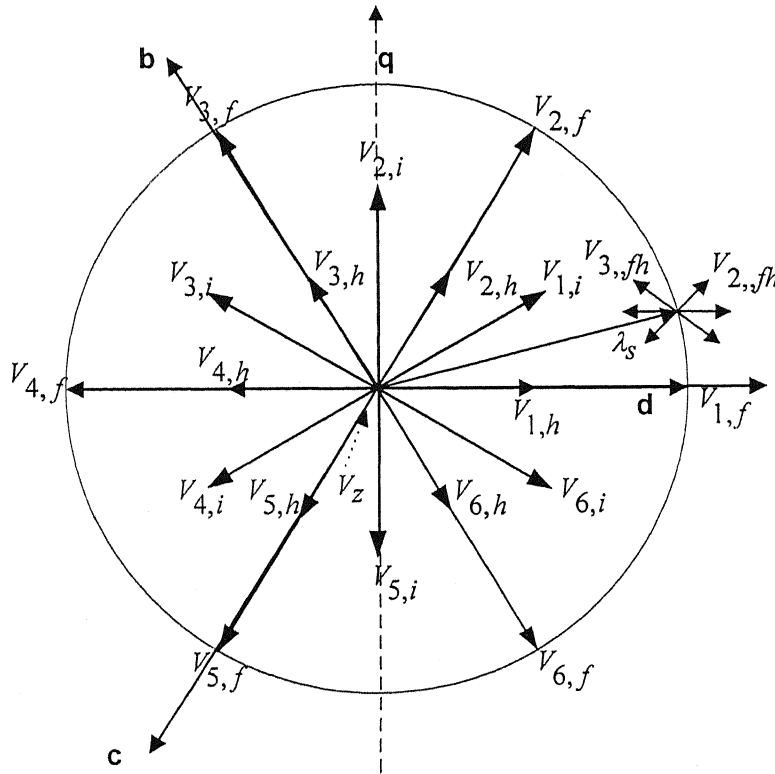
Fig. 3.5 Voltage vectors of three-level inverter

Since 27 possible choices for switching voltage vector selection exist in the three-level inverters, appropriate selection of the inverter switching voltage vector is more complex than that in the two-level inverters. Assuming that the stator flux vector is in the 1st sector, selection of the respective stator voltage vector is described in Fig. 3.5. The selection of $V_{3,f,h}$ and $V_{2,f,h}$ is able to increase the phase angle between the corresponding stator and rotor fluxes. As a consequence, the developed torque can be increased by the application of these voltages. It can be seen in Fig. 3.5 that the stator flux is increased by the selection of, $V_{2,f,h}$ and decreased by $V_{3,f,h}$. If the half voltage vector is selected, the lower slope of torque can be obtained.
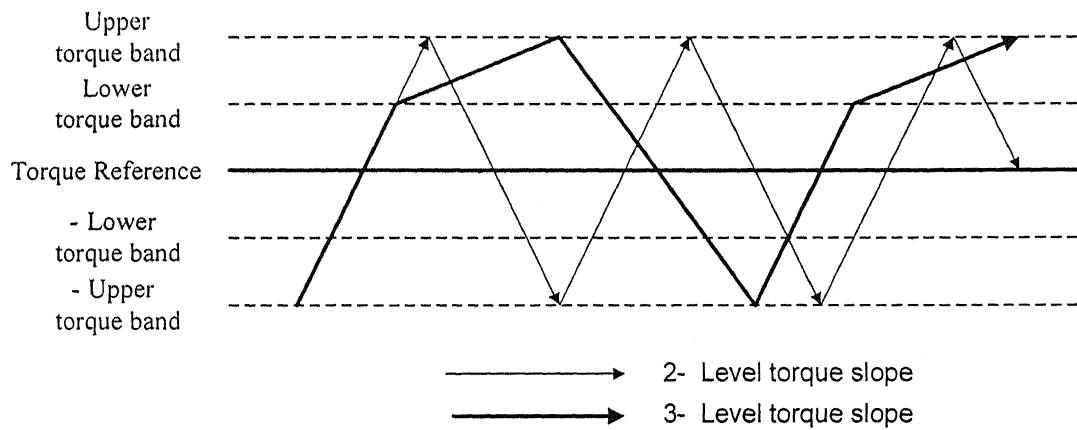
Fig. 3.6 Torque slope pattern of three-level inverter

Fig. 3.6 shows a double torque hysteresis band method applied for three-level inverter. It is seen in this figure that the torque control method for three-level inverter is provided with the lower torque bands additionally to the hysteresis bands for two-level inverters.

f_S in sector k		Torque		
		$\uparrow$	$\uparrow\uparrow$	$\perp$
Flux	$\uparrow$	$\upsilon_{k+1,h}$	$\upsilon_{k+1,f}$	υ_z
	$\downarrow$	$\upsilon_{k+2,h}$	$\upsilon_{k+2,f}$	υ_z

Table 3.1

Fig. 3.7 Switching lookup table

It is noted that positive lower hysteresis band is used for forward rotation of the induction motors and negative lower band is for reverse rotation. Provided that the induction motor is rotating in the forward direction, for instance, the appropriate full voltage vector is chosen to increase the developed torque when instantaneous torque goes down to the negative upper hysteresis band. When the controlled torque reaches the positive lower hysteresis band, the full voltage vector is replaced with the respective half voltage. If torque increases beyond the positive upper torque band, the zero voltage vector is applied to decrease the developed torque value. For the reverse rotation, considering that the reverse rotating field is required, the rules similar to the selection for the forward rotation can be applied. The resulting switching lookup table is shown in Figure 3.7.

When the above-mentioned DTFC switching method is applied for the low speed operation, it causes the demagnetization phenomenon of the stator flux, as shown in Fig. 3.8. This problem can be explained as follows. The demagnetization by nonzero-voltage vector is described in Fig. 3.8 (a), where the stator flux is placed in the $k+1^{th}$ sector. It is

seen in Fig. 3.8 (a) that, f_S, the stator flux in the region near the sector-to-sector boundary, happens to be decreased by the stator voltage vector $V_{k+2,f,h}$ which is selected to increase the stator flux magnitude by the basic switching lookup table of Fig. 3.7. It is noted that the voltage drop across the stator resistance takes significant proportion of the applied voltage, especially in the low-speed region.

3.7 Switching Strategy for Low – Speed Operation

The basic DTFC algorithm has some problems such as the stator flux drooping and the poor torque control, especially in the low-speed region. The flux drooping problem appears just after the position of the stator flux vector moves from one sector into the next sector. The application of the zero-voltage vector makes it difficult to decrease the developed torque in the low-speed operation.

The basic switching look up table described in the previous section cannot solve these problems occurring in the low-speed operation. Even if the flux demagnetization problems can be worked out by a rotation of the reference frame or the switching sector that are similar to methods for two-level inverters, a new method using the intermediate voltage vectors is more desirable for the three-level inverters. Moreover, the intermediate voltage vectors can be effective for preventing the torque control from being inactive. Fig. 3.9 shows only one sector of the 12 sectors that result from subdividing a six-sector plane of Fig. 3.5 into 12-sector plane. The every sector in Fig. 3.5 subdivided into the lower sub sector and the upper sub sector, each of which has a width of 30^0. It is assumed that the stator flux rotates in the counter clockwise direction.
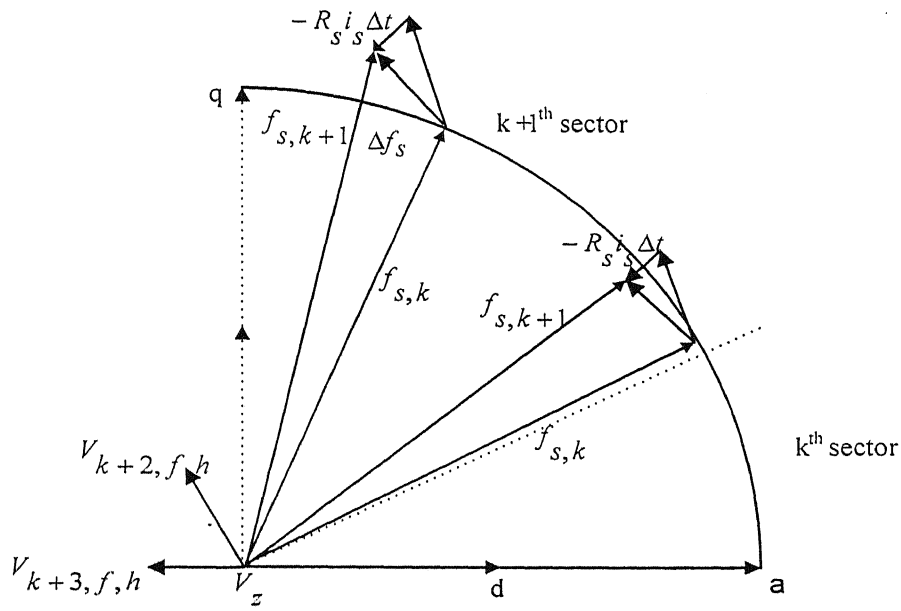
(a) Demagnetization by nonzero voltage vectors
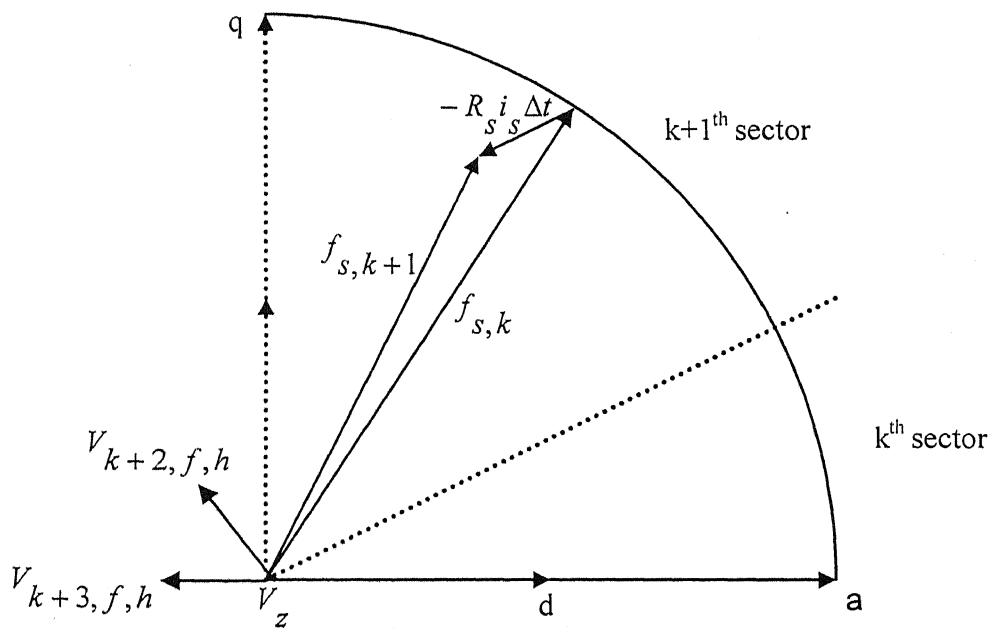
(b) Demagnetization by zero voltage vectors

Fig. 3.8 Demagnetization problem in low-speed operation
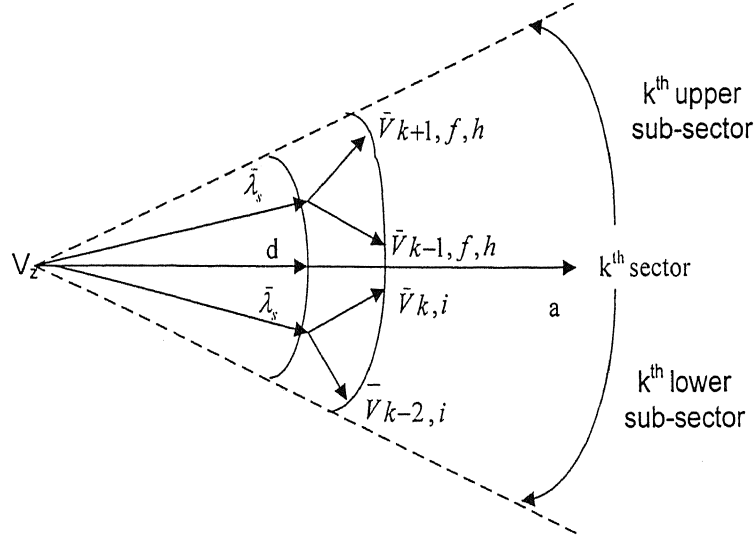
Fig. 3.9 Improved switching method

In the lower sub sector, the stator voltage vector $V_{k+1,f,h}$ which is determined

according to table Fig. 3.7, becomes ineffective in boosting the stator flux because the

full voltage vector is not able to sufficiently provide a flux vector component to increase

the corresponding stator flux. It can be seen in Fig. 3.9 that the respective intermediate

stator voltage $V_{k,i}$ can be more effective to increase the resultant stator flux. If the

intermediate voltage vector $V_{k,i}$ is selected instead of $V_{k+1,f}$, the demagnetization

problem can be resolved. When the stator flux moves into the upper sub sector passing

the lower sub sector, the voltage selected, $V_{k+1,f,h}$, is used to increase the developed

torque and the voltage vector $V_{k-1,f,h}$ instead of the zero voltage vector being used to

decrease the developed torque.
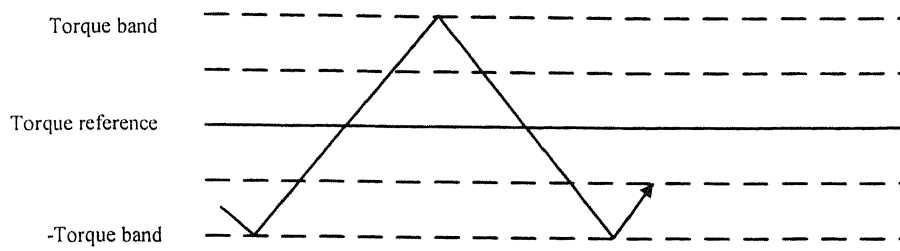
(a) Switching pattern for low half sector
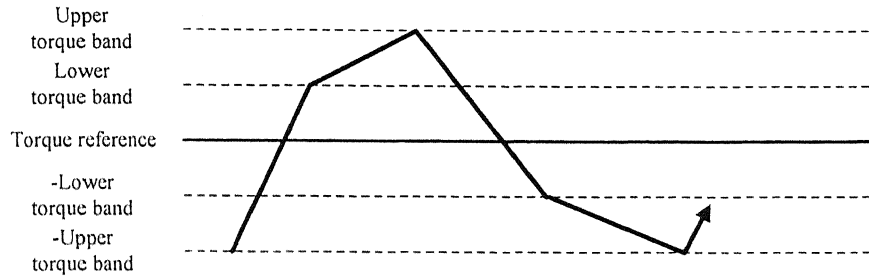
(b) Switching pattern for upper half sector

Fig. 3.10 Torque slope pattern in low-speed operation

f_S in sector k		Torque			
		$\uparrow$	$\uparrow\uparrow$	$\downarrow$	$\downarrow\downarrow$
Flux	Upper subsector	$\upsilon_{k+1,h}$	$\upsilon_{k+1,f}$	$\upsilon_{k-1,h}$	$\upsilon_{k-1,f}$
	Lower subsector	$\upsilon_{k,i}$		$\upsilon_{k-2,i}$	

Table 3.2
Fig. 3.11 Modified lookup table

To obtain the effectively magnetizing effect around the boundary between two sectors, especially at the low-speed region, a modified lookup table as shown in Fig. 3.11 is devised. The torque slope pattern change is shown in Fig. 3.10, where two and four torque slopes are applied in the lower subsector and the upper subsector, respectively.

3.8 Application of Synchronous Link Converter in DTFC of Induction Motor

The analysis and simulation of the synchronous link converter with resistive load has been discussed in chapter 2. When the synchronous link converter used as the front end converter in induction motor drive system, the power balance equation of the system is given as follows.

inverter input = motor input (by neglecting converter losses)

= rotor input + stator losses

$$V_{dc} * I_{dc} = T_e * \omega_r + (3/2) * I_{rms} * I_{rms} * R_s \qquad (3.35)$$

where ω_r is the motor speed, and T_e is electromagnetic torque developed by induction motor as given by Equation (3.24).

The load current for the synchronous link converter is given by

$$I_{dc} = \left(T_e * \omega_r + (3/2) * I_{rms} * I_{rms} * R_s\right) / V_{dc} \qquad (3.36)$$

In the motoring mode the inverter input current I_{dc} is positive, i.e. the power flow is from the source to the motor and the input power factor is maintained at unity as shown in simulation results. In the regenerative mode current I_{dc} is negative i.e. the induction motor act as a generator and the power is fed from the motor to the source. During this period source current and source voltage are out of phase (180°).

3.9 Four Quadrant DTFC Operation of Induction motor

To visualize the different steps of the simulation, a block diagram has been drawn as shown in Fig. 3.13. The source current reference is obtained by the dc link voltage error processed through a PI controller as given as

$$I_{s\_ref}(n) = I_{s\_ref}(n\_1) + K_{pr}\left(e_{dcn} - e_{dc(n-1)}\right) + K_{ir}e_{dc(n-1)}\Delta t \qquad (3.37)$$

The reference torque T_{e_ref} is generated by the speed error processed through the PI controller. The output of the PI controller is given as follows

$$T_{e\_ref}(n) = T_{e\_ref}(n\_1) + K_{p}\left(e_{wrn} - e_{wr(n-1)}\right) + K_{i}e_{wr(n-1)}\Delta t \qquad (3.38)$$

The model block takes the three-phase motor currents, the switching status of the inverter, the dc link voltage, and calculates the stator flux and the torque. The actual values of the electromagnetic torque T_e and actual flux f_s are compared with the reference torque T_{e_ref} and reference flux f_{s_ref} to give the torque and flux errors. Now the torque and flux errors are digitized by the five-level and two-level hysteresis comparators respectively. The outputs of the 5-level hysteresis torque comparator ct, 2-level flux comparator cf, and sector angle command θ_n is given to the optimum switching table which generates the required switching pulses for the inverter as the table shown in the Fig. 3.12.

cf	ct	Θ_1	Θ_2	Θ_3	Θ_4	Θ_5	Θ_6	Θ_7	Θ_8	Θ_9	Θ_{10}	Θ_{11}	Θ_{12}
1	2	$V_{2,f}$	$V_{2,i}$	$V_{3,f}$	$V_{3,i}$	$V_{4,f}$	$V_{4,i}$	$V_{5,f}$	$V_{5,i}$	$V_{6,f}$	$V_{6,i}$	$V_{1,f}$	$V_{1,i}$
1	1	$V_{2,h}$	$V_{2,i}$	$V_{3,h}$	$V_{3,i}$	$V_{4,h}$	$V_{4,i}$	$V_{5,h}$	$V_{5,i}$	$V_{6,h}$	$V_{6,i}$	$V_{1,h}$	$V_{1,i}$
1	0	V_z	V_z	V_z	V_z	V_z	V_z	V_z	V_z	V_z	V_z	V_z	V_z
1	-1	$V_{6,h}$	$V_{6,i}$	$V_{1,h}$	$V_{1,i}$	$V_{2,h}$	$V_{2,i}$	$V_{3,h}$	$V_{3,i}$	$V_{4,h}$	$V_{4,i}$	$V_{5,h}$	$V_{5,i}$
1	-2	$V_{6,f}$	$V_{6,i}$	$V_{1,f}$	$V_{1,i}$	$V_{2,f}$	$V_{2,i}$	$V_{3,f}$	$V_{3,i}$	$V_{4,f}$	$V_{4,i}$	$V_{5,f}$	$V_{5,i}$
0	2	$V_{3,f}$	$V_{3,i}$	$V_{4,f}$	$V_{4,i}$	$V_{5,f}$	$V_{5,i}$	$V_{6,f}$	$V_{6,i}$	$V_{1,f}$	$V_{1,i}$	$V_{2,f}$	$V_{2,i}$
0	1	$V_{3,h}$	$V_{3,i}$	$V_{4,h}$	$V_{4,i}$	$V_{5,h}$	$V_{5,i}$	$V_{6,h}$	$V_{6,i}$	$V_{1,h}$	$V_{1,i}$	$V_{2,h}$	$V_{2,i}$
0	0	V_z	V_z	V_z	V_z	V_z	V_z	V_z	V_z	V_z	V_z	V_z	V_z
0	-1	$V_{5,h}$	$V_{5,i}$	$V_{6,h}$	$V_{6,i}$	$V_{1,h}$	$V_{1,i}$	$V_{2,h}$	$V_{2,i}$	$V_{3,h}$	$V_{3,i}$	$V_{4,h}$	$V_{4,i}$
0	-2	$V_{5,f}$	$V_{5,i}$	$V_{6,f}$	$V_{6,i}$	$V_{1,f}$	$V_{1,i}$	$V_{2,f}$	$V_{2,i}$	$V_{3,f}$	$V_{3,i}$	$V_{4,f}$	$V_{4,i}$

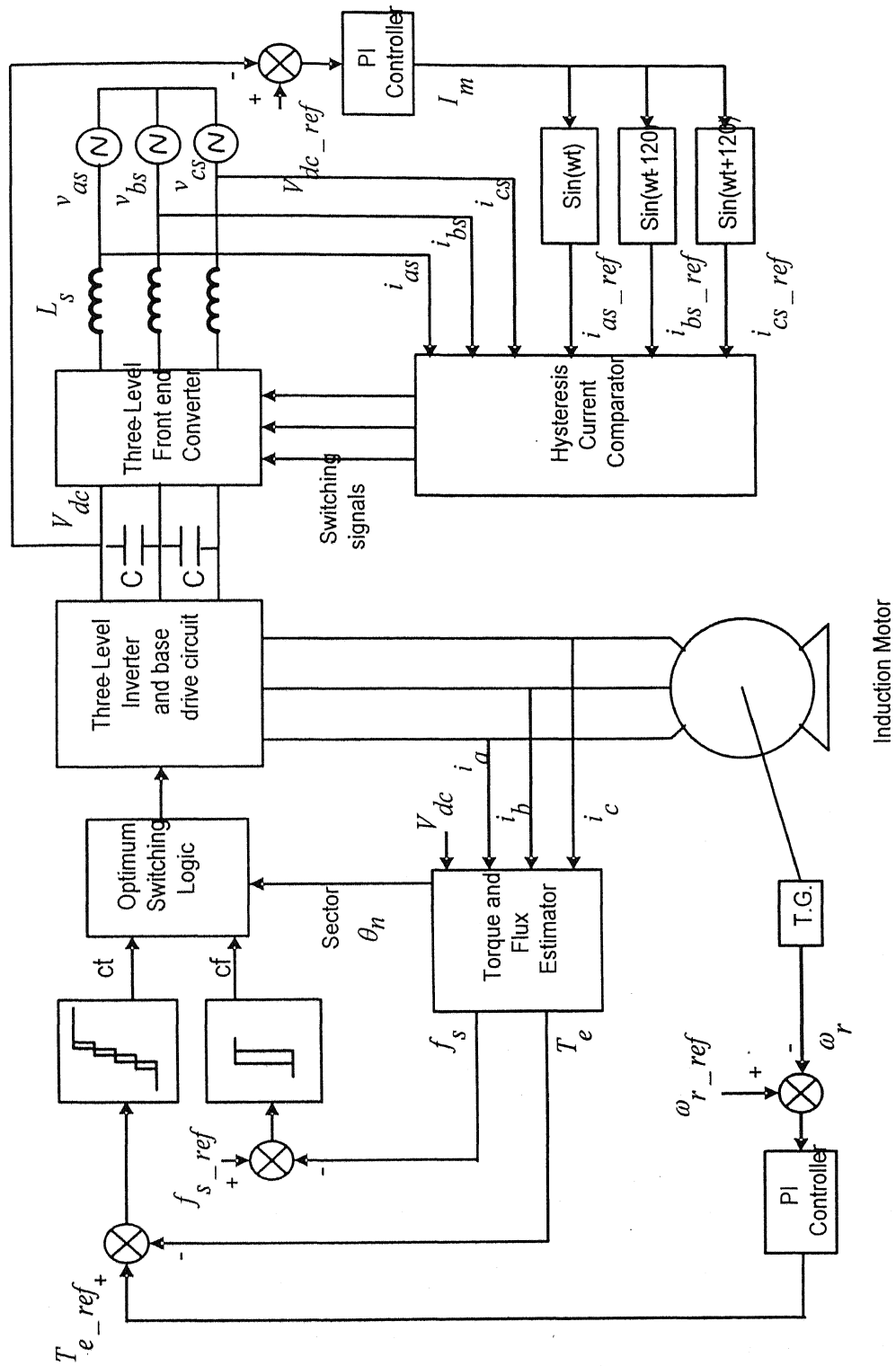Fig. 3.12 Modified Switching Table

Fig. 3.13 Block diagram of DTFC with SLC as front end converter

3.10 Simulation Results

The flow chart of the computer simulation is shown in Fig.3.14, and the program listing in C language is given in the Appendix D. The inputs to the program are motor parameters like stator and rotor resistances, inductances, moment of inertia of the coupled drive system, reference flux, reference speed, and reference dc link voltage. The simulation plots are given in next few pages.

Fig 3.15 (a) shows the demagnetization of the stator flux under low speed operation (5% of base speed) by using conventional look up table. It can also be observed in Fig. 3.16 (a), polar plot of dq-axes stator flux. As from the Fig. 3.15 (b) and 3.16 (b) we can conclude that the flux drooping is almost removed and stator flux follows a circular trajectory even in the low speed region.

Fig. 3.17 to Fig. 3.27 show the various wave forms under no load operation at 85% of the rated speed of the motor. Fig. 3.20 shows the dc link voltage obtained by using three-level synchronous link converter. Fig. 3.21 shows that unity power has been achieved by using synchronous link converter and Fig. 3.22 shows that the source currents are sinusoidal.

Fig. 3.28 to Fig. 3.39 shows the motor currents, flux, speed and torque responses at the starting on no load, and various responses to step change in speed from standstill to 750 rpm at starting, speed reversal from 750 rpm to – 750 rpm at 1.75 second and again the speed reversal from reverse motoring (-750 rpm) to forward motoring (750 rpm) at 3 second. Speed reversal from forward motoring at 750 rpm to reverse motoring -750 rpm takes around 0.25 second. Motor current is found to be in limits during starting and during speed reversal. Motor currents and d, q-axes fluxes are nearly sinusoidal. From

Fig. 3.36 it can be seen that there is a drop in the DC link voltage during transition of speed. It is clear from Fig. 3.37 that unity power factor has been achieved under forward motoring operation. Fig 3.38 shows that unity power factor is still maintained under reverse motoring operation. It can be observed that the power generated under reverse motoring operation is dissipated in the SLC.

Fig. 3.40 to Fig. 3.50 shows motor currents, flux, speed and torque responses on application and removal of a load of 2 N-m at 1.5 second and 4 second respectively. Torque response is found to be almost instantaneous. Speed of the motor follows the reference speed with a dip and a raise corresponding to change in load. Finally speed settles at the reference speed. Motor current is found to be in limits on application and removal of a load torque also motor currents and dq-axes fluxes are nearly sinusoidal. Fig. 3.48 shows that there is drop and raise in DC link voltage at the instants of change in torque. It can be observed that unity power is maintained under load condition from Fig. 3.49. The source currents are being maintained approximately sinusoidal. No change in flux is observed with change in load and therefore independent control of torque and flux is achieved.

3.11   Conclusion

The analysis of direct torque and flux control of an induction motor has been made in this chapter. Synchronous link converter is used as the front-end converter for bi-directional power flow and to get unity power factor at the source side. The machine parameters are assumed to be constant at all operating conditions. The torque response depends upon the time differential of the slip angle and upon the capability of voltage source inverter to meet the required large transient power. Hysteresis current controlled

scheme is used for synchronous link converter. An advanced DTFC algorithm with improved low-speed operation of induction motors for high-power three-level applications has been presented in this chapter. The simulation results of induction motor drive under direct torque and flux control show excellent results in both steady state and transient conditions.
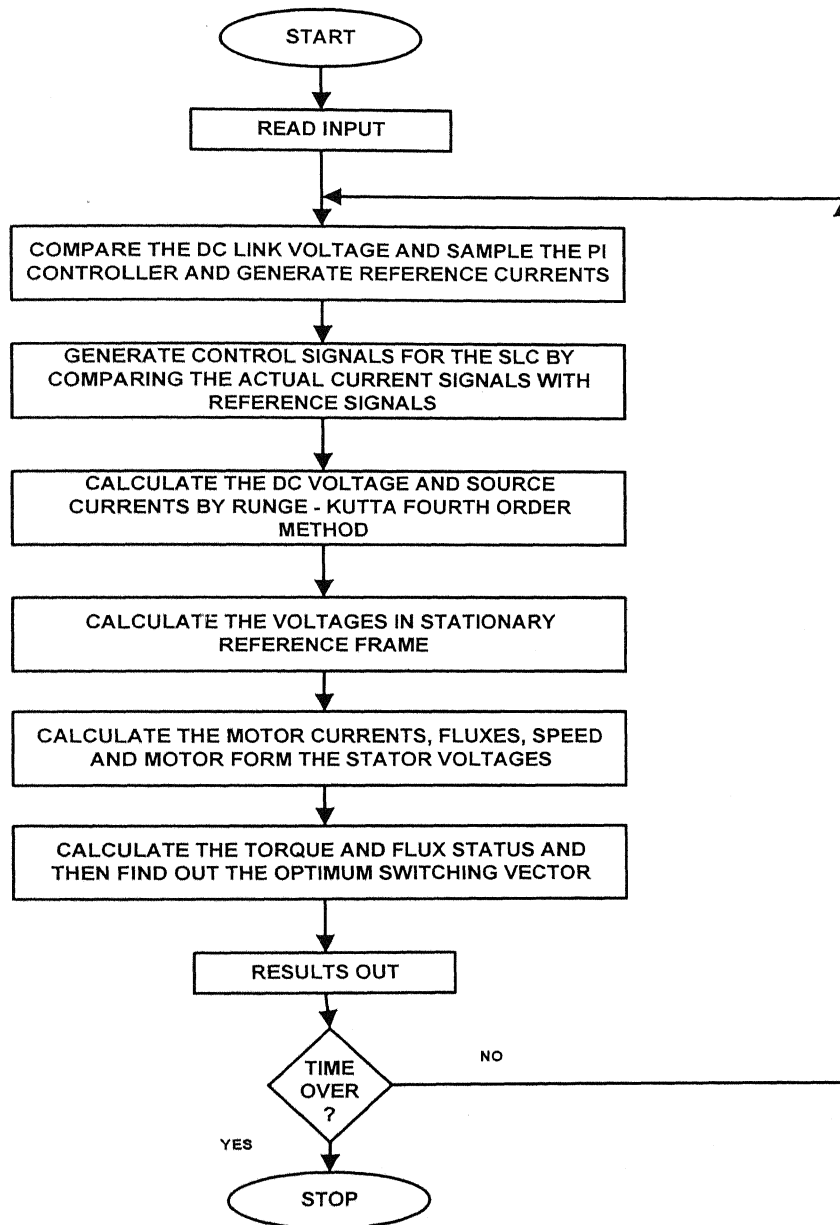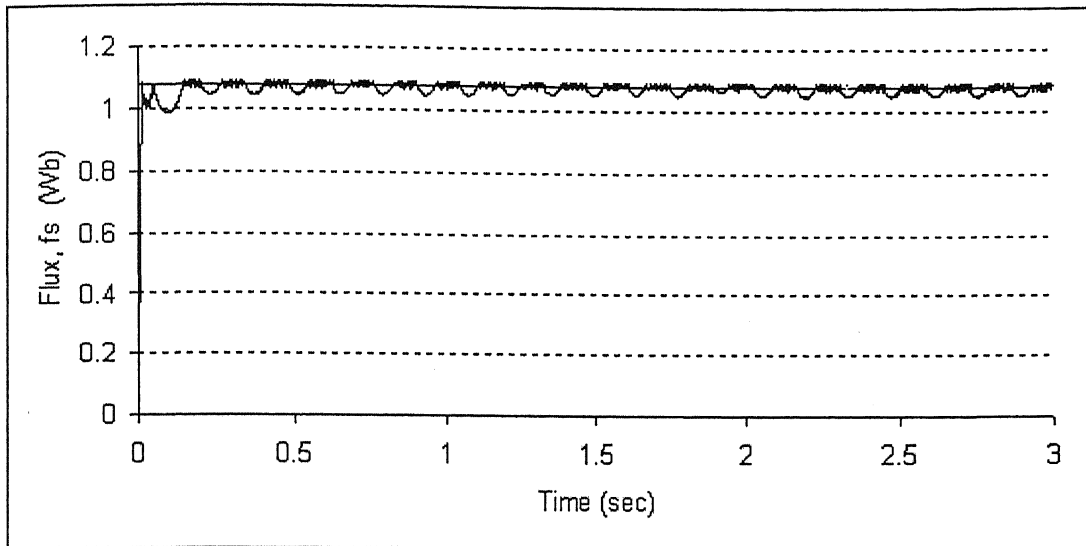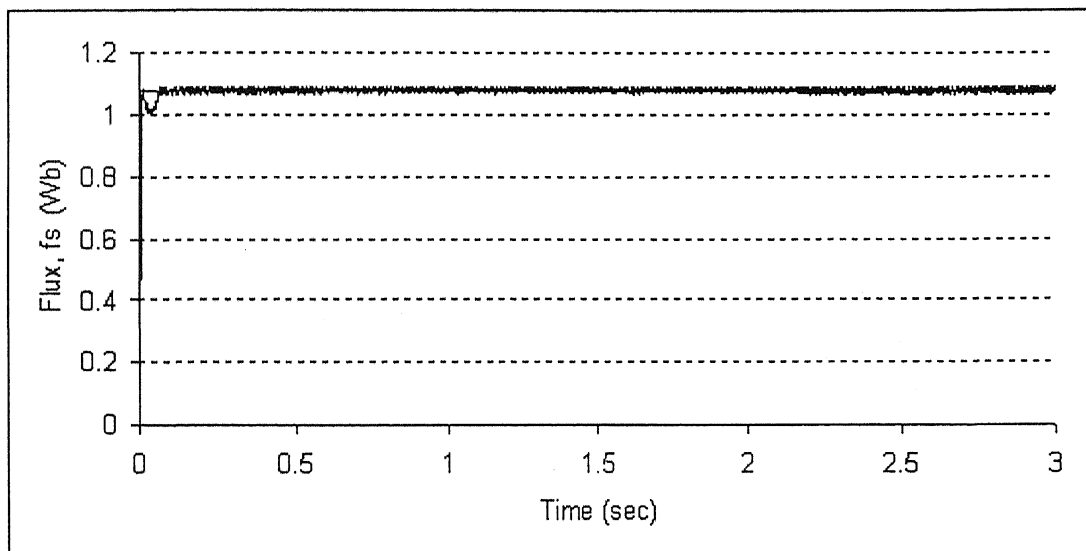

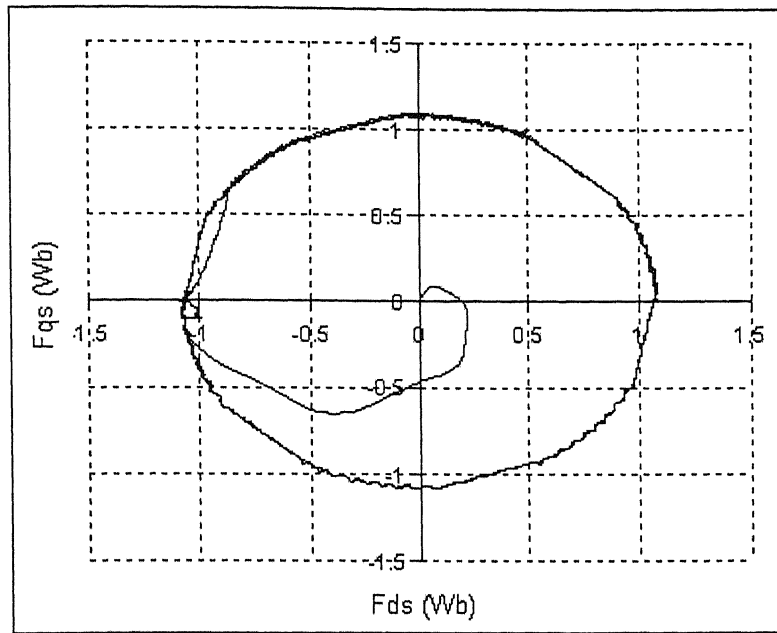Fig. 3.14 Flow chart for the Four Quadrant operation of DTFC

(a) Using conventional lookup table

(b) Using modified lookup table

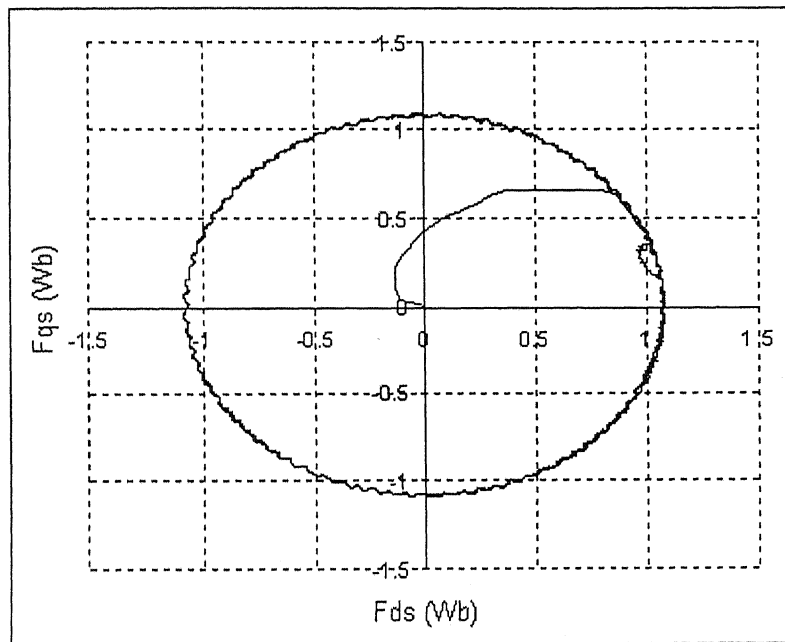Fig. 3.15 Stator flux under low speed (5% of rated speed) operation

(a) Using Conventional lookup table

(b) Using modified look up table

Fig. 3.16 Polar plot of d-axis and q-axis stator flux for 5% of rated speed operation
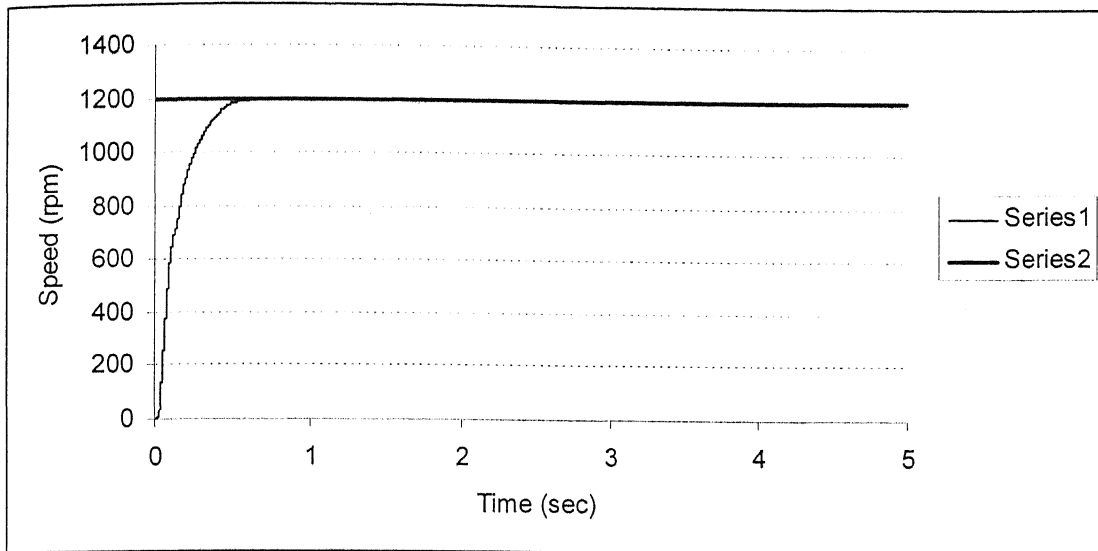
Actual speed (Series 1), Reference speed (Series 2)

Fig.3.17 No load Operation of the motor with 85% of rated speed
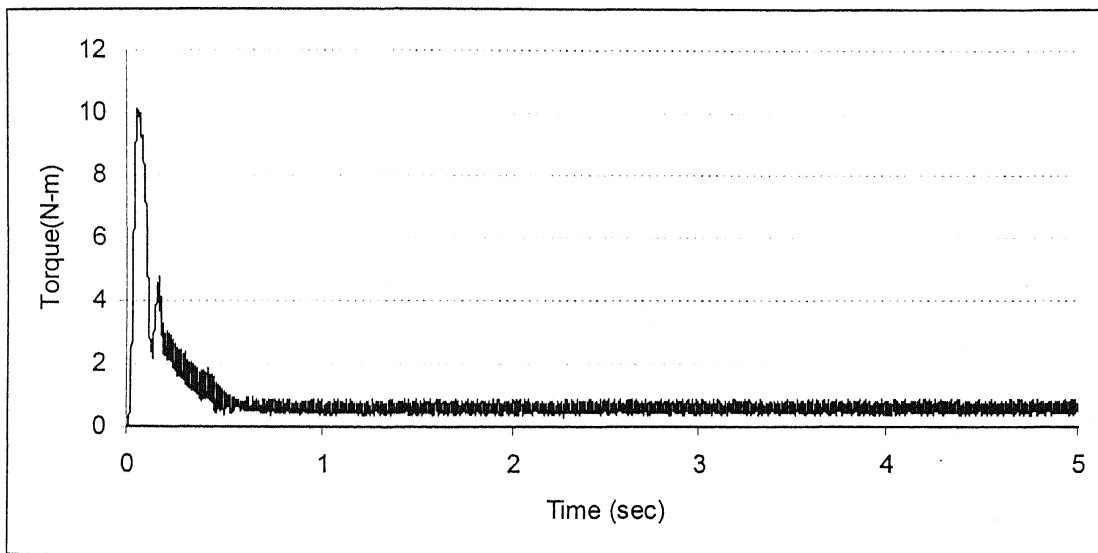
Fig. 3.18 Torque under no load at 85% of rated speed
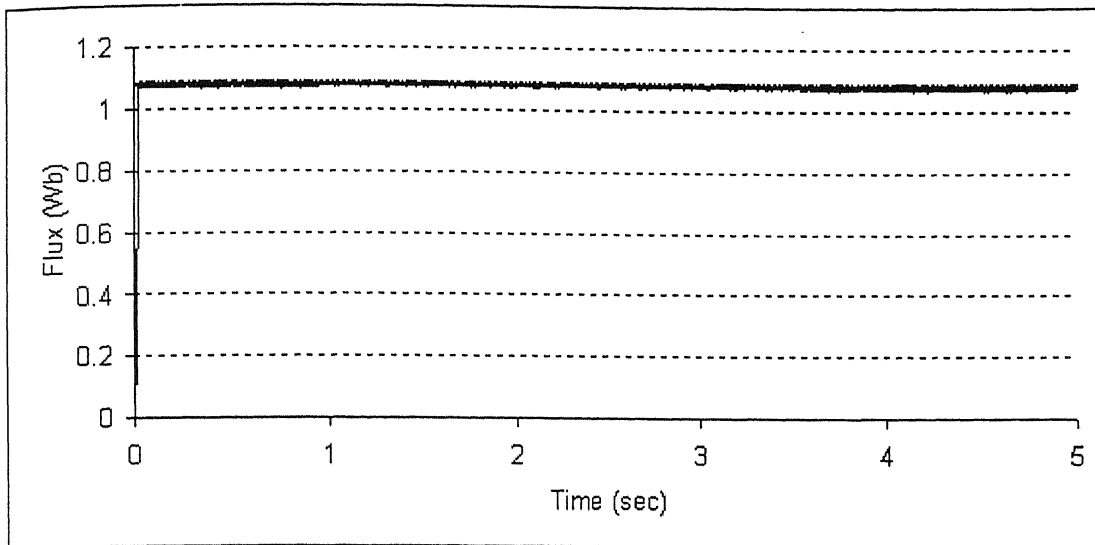
Fig. 3.19 Stator Flux under no load and at 85 % of rated speed

(Normal operating condition)
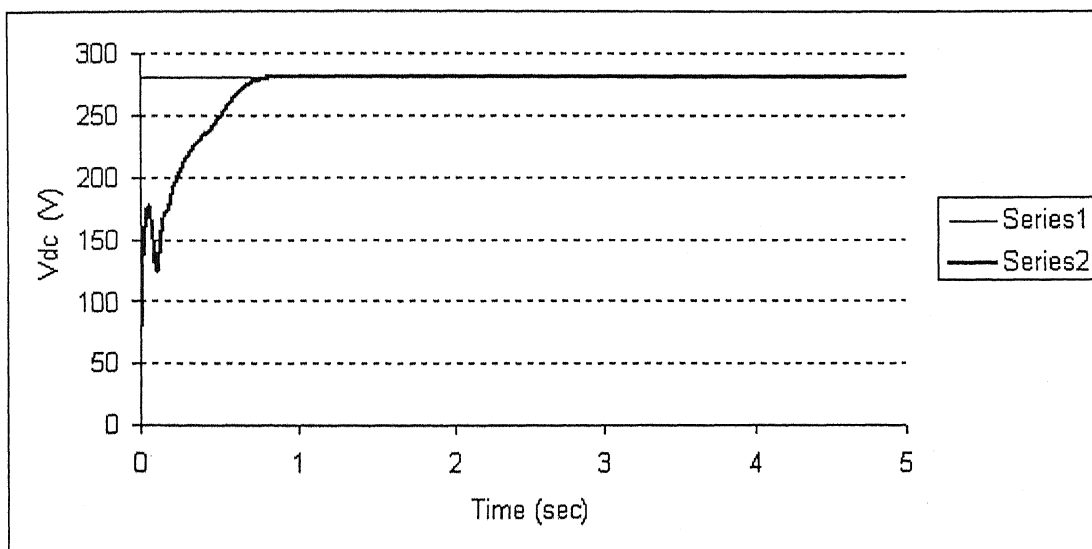
Reference voltage (Series 1), Actual voltage (Series 2)

Fig. 3.20 DC link Voltage at 85 % of rated speed operation
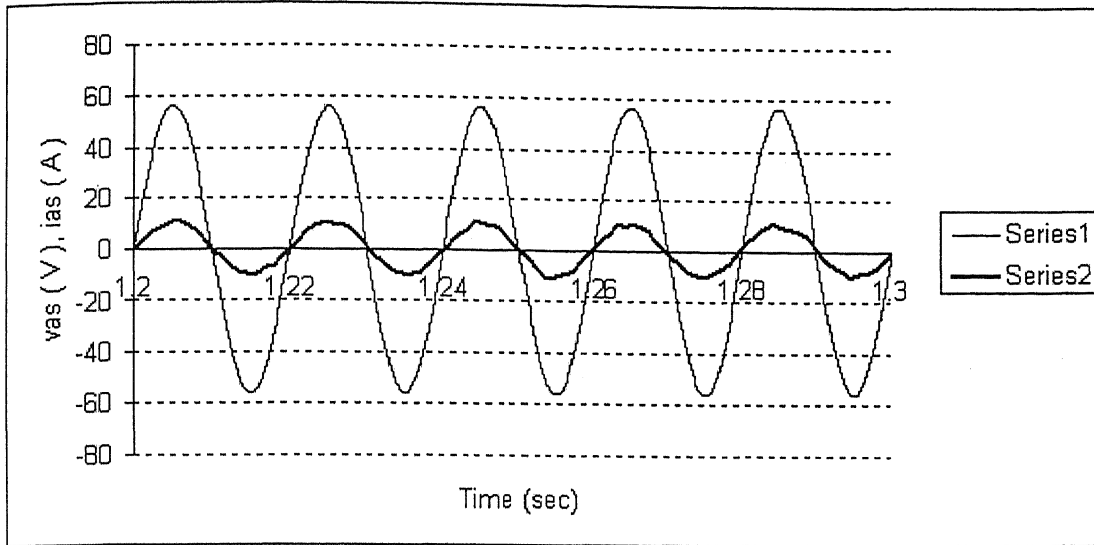
X-axis 1div = 0.02 sec (time)

Y-axis 1div = 20 A (source current, i_{as})--- (Series 1)

Y-axis 1div = 100 V (source voltage, v_{as})--- (Series 2)

Fig. 3.21 Source Voltage and Source current at 85% of rated speed operation of the motor
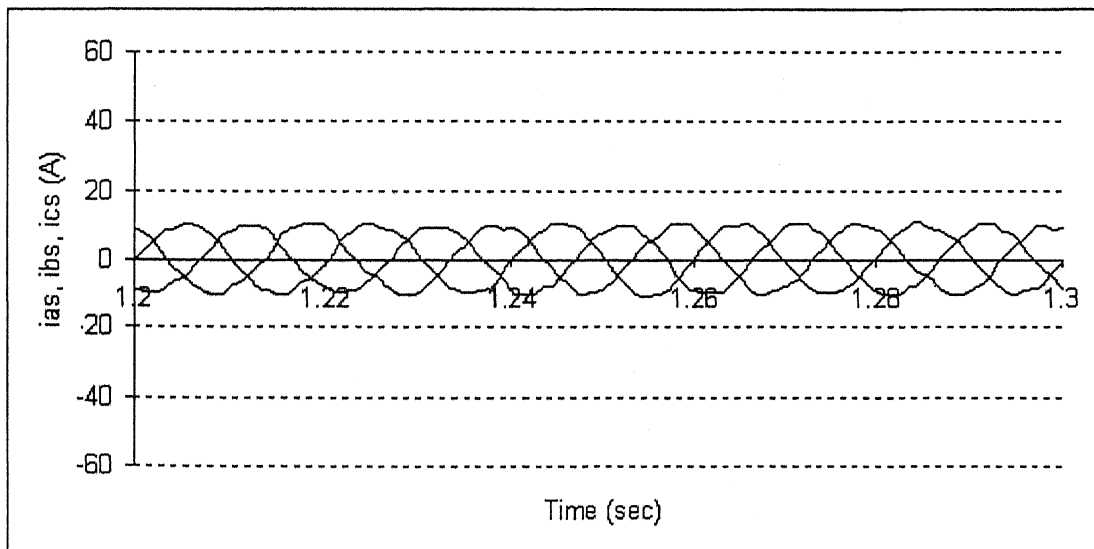
Fig 3.22 Source phase currents i_{as}, i_{bs}, i_{cs} under steady state operation
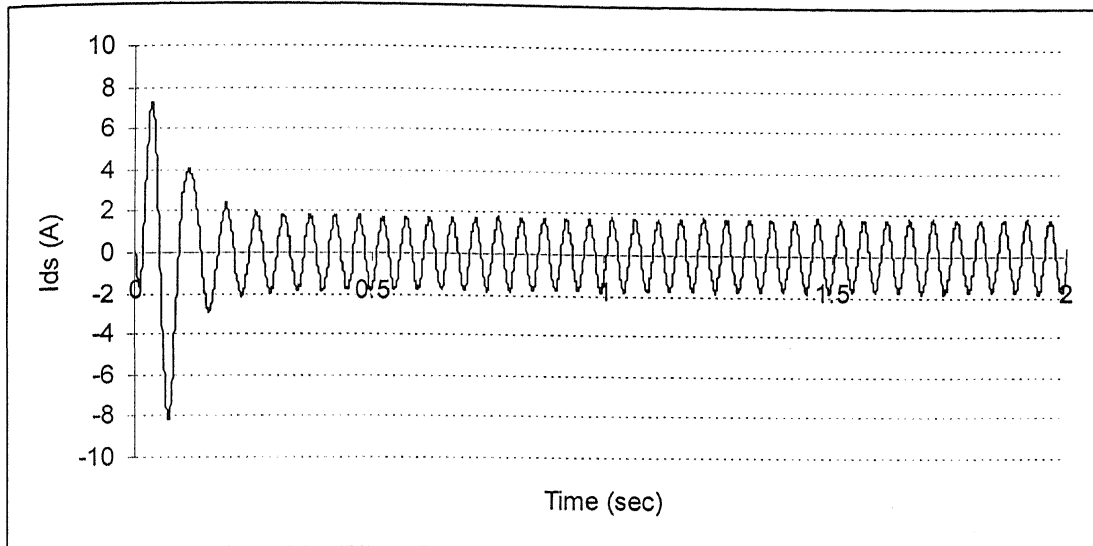
Fig 3.23 d-axis stator current or motor phase current i_a under normal operating condition
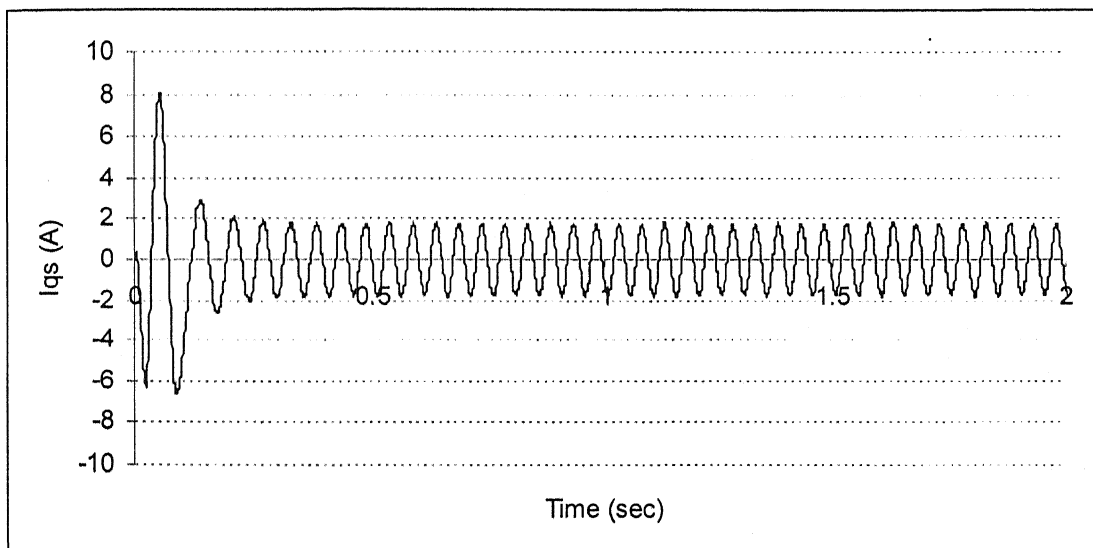
Fig 3.24 q-axis stator current under normal operating condition
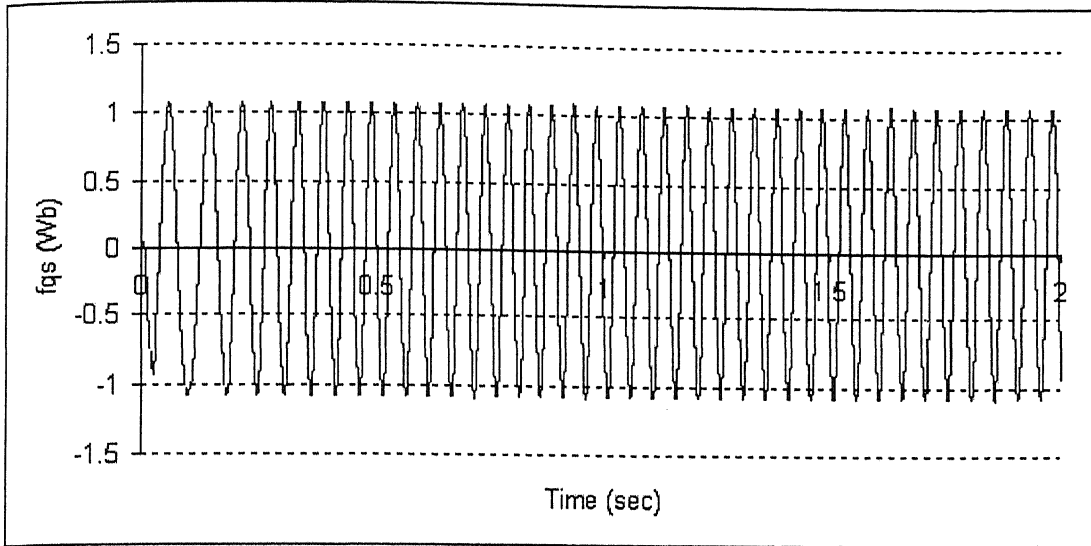
Fig. 3.25 q-axis Stator flux under normal operating condition
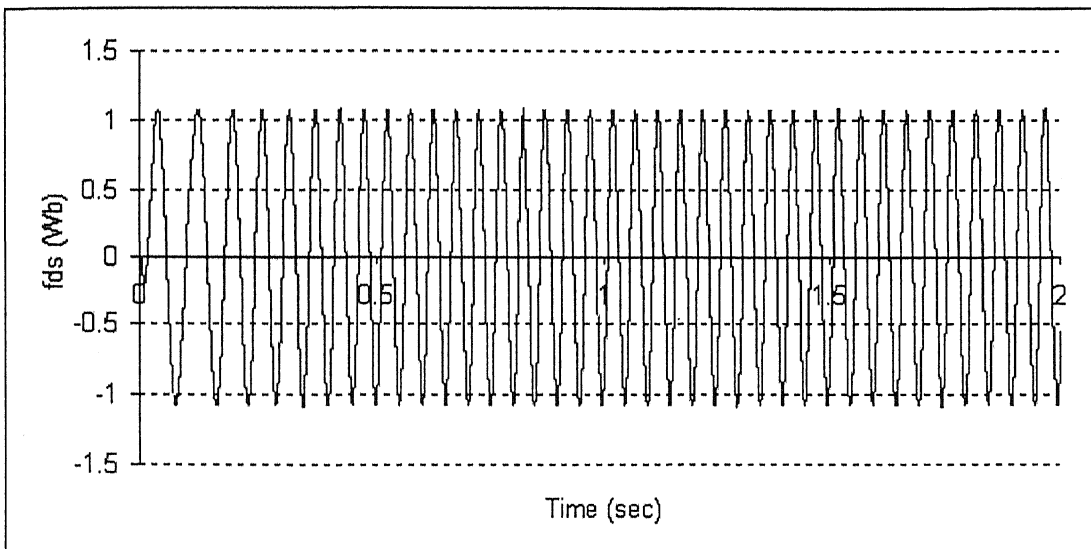
Fig. 3.26 d-axis Stator flux under normal operating condition
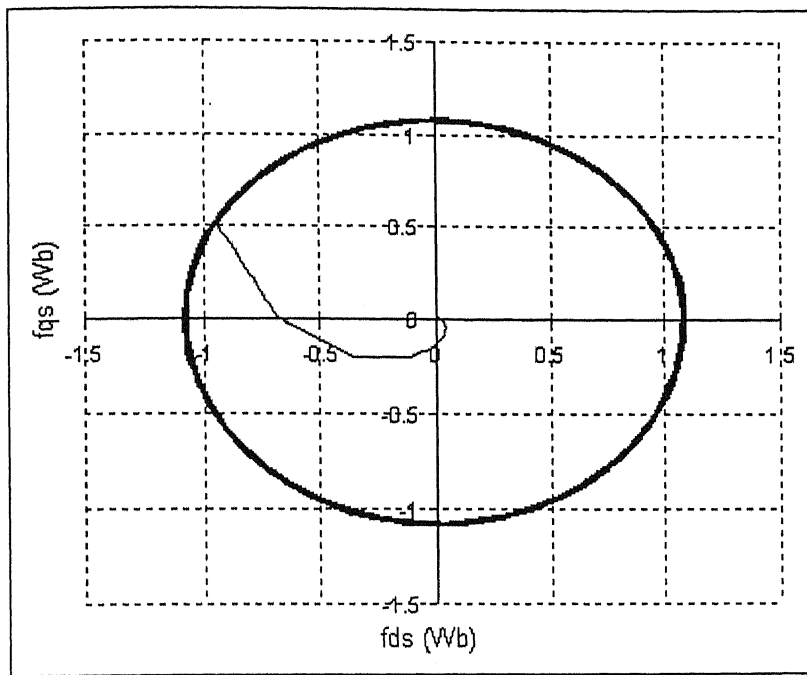
Fig. 3.27 Polar plot of d-axis and q-axis stator flux for 85% of rated speed operation
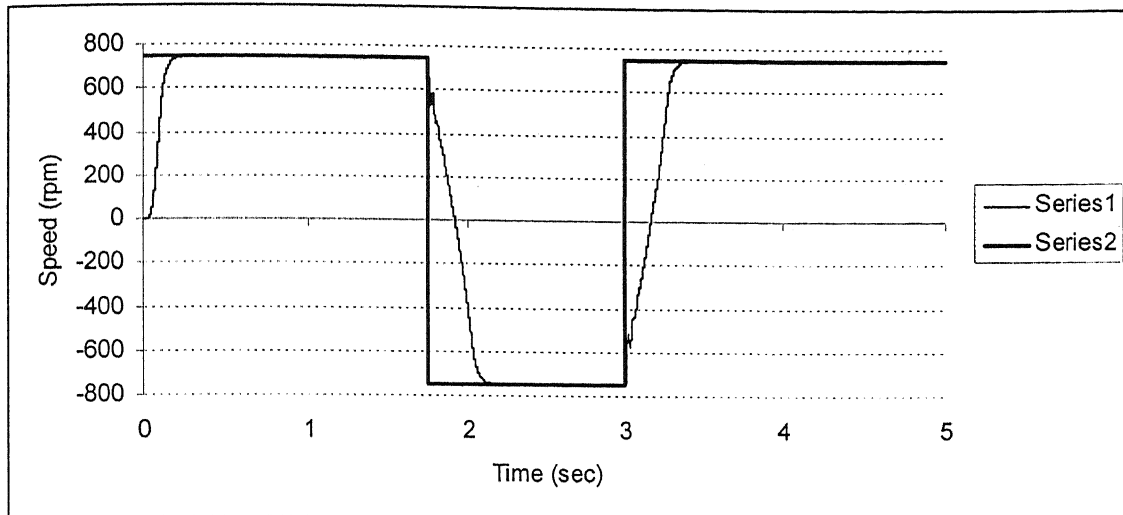
Reference speed (Series 1), Actual speed (Series 2)

Fig. 3.28 Forward motoring and reverse motoring Operation of DTFC
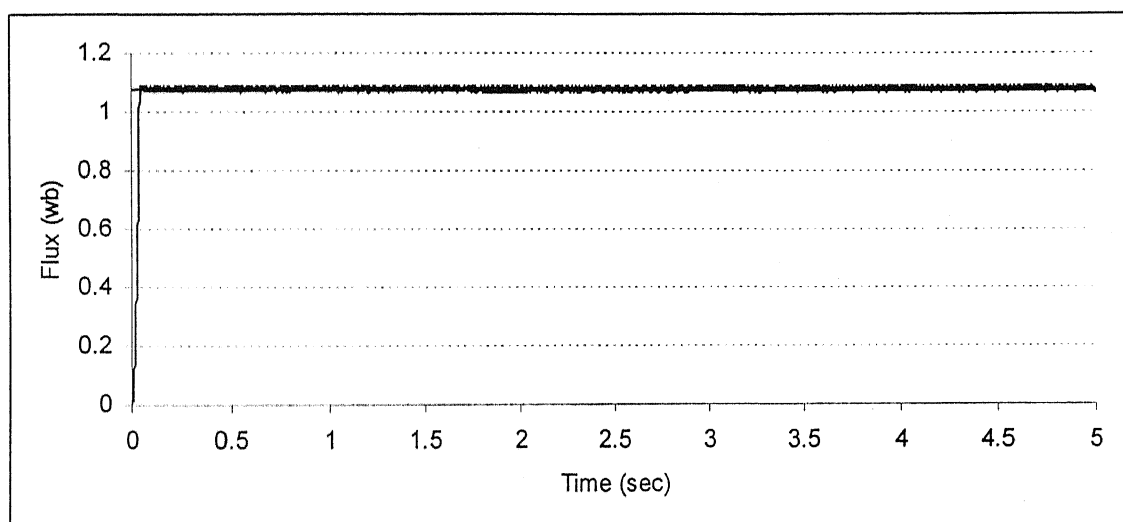
Fig. 3.29 Stator flux during speed reversal
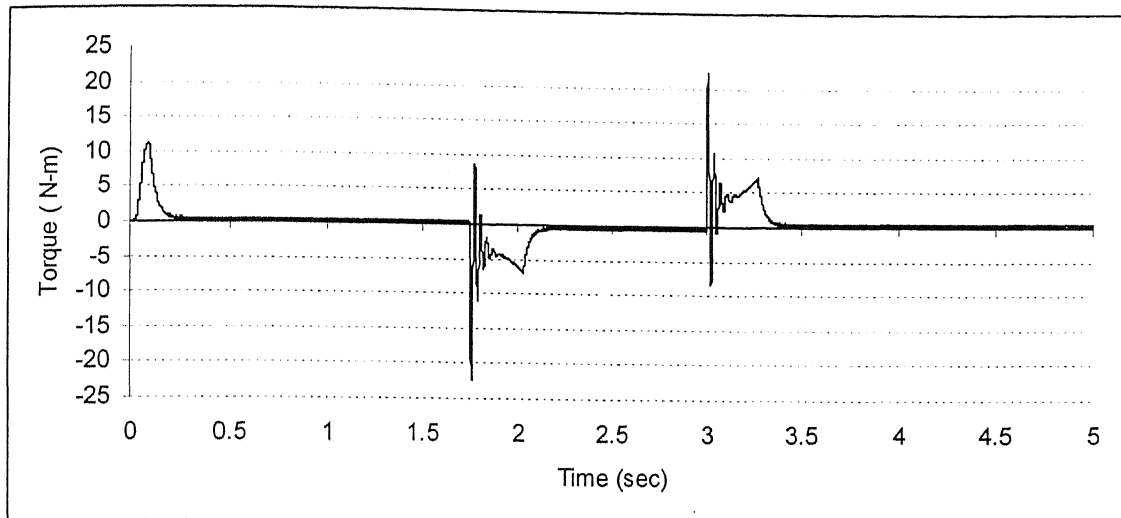
Fig. 3.30 Torque Response under speed changes
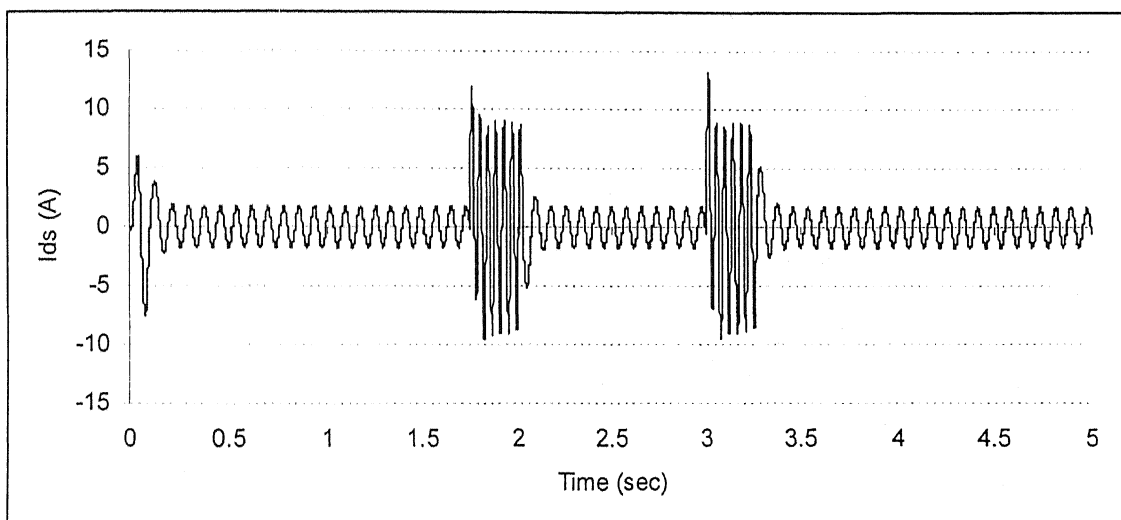
Fig.3.31 d-axis or a-phase motor current during speed changes
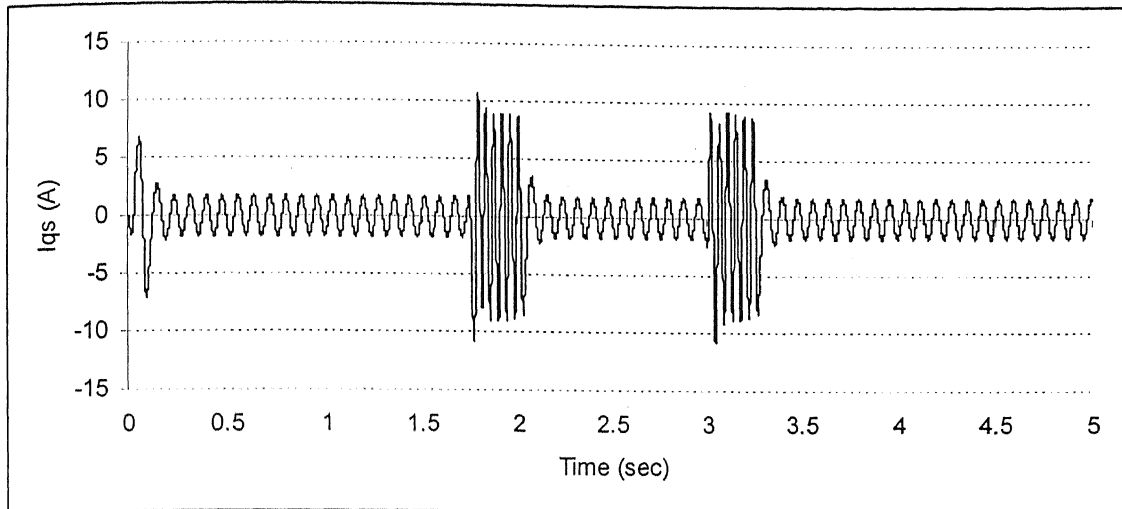
Fig.3.32 q-axis motor current during speed changes
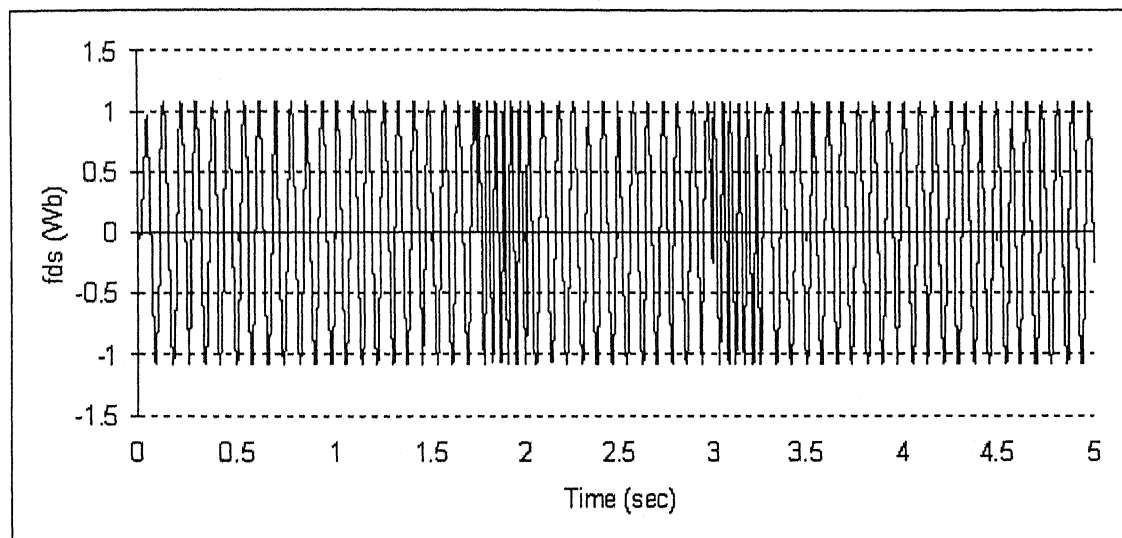
Fig.3.33 d-axis stator flux during speed changes
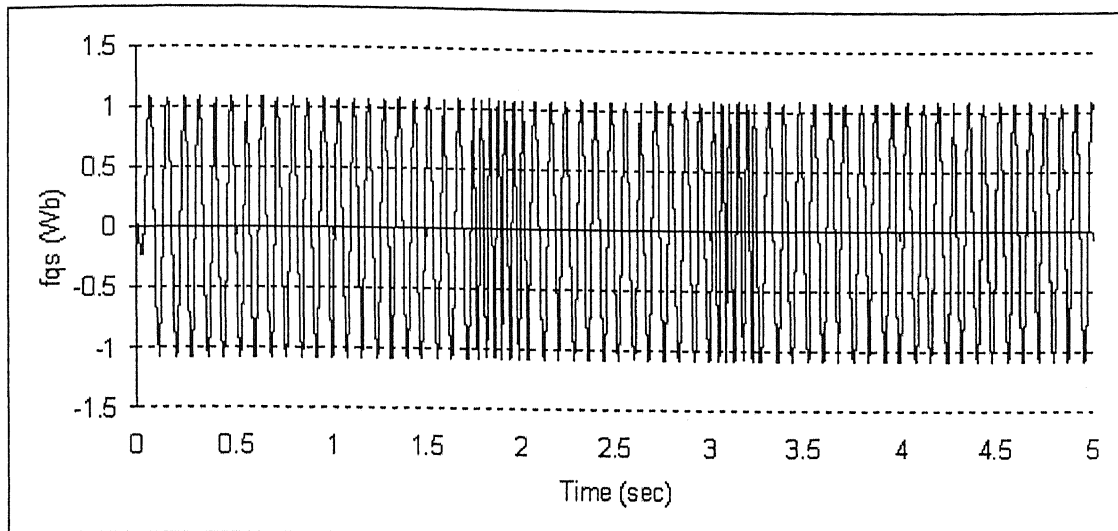
Fig.3.34 q-axis stator flux during speed changes
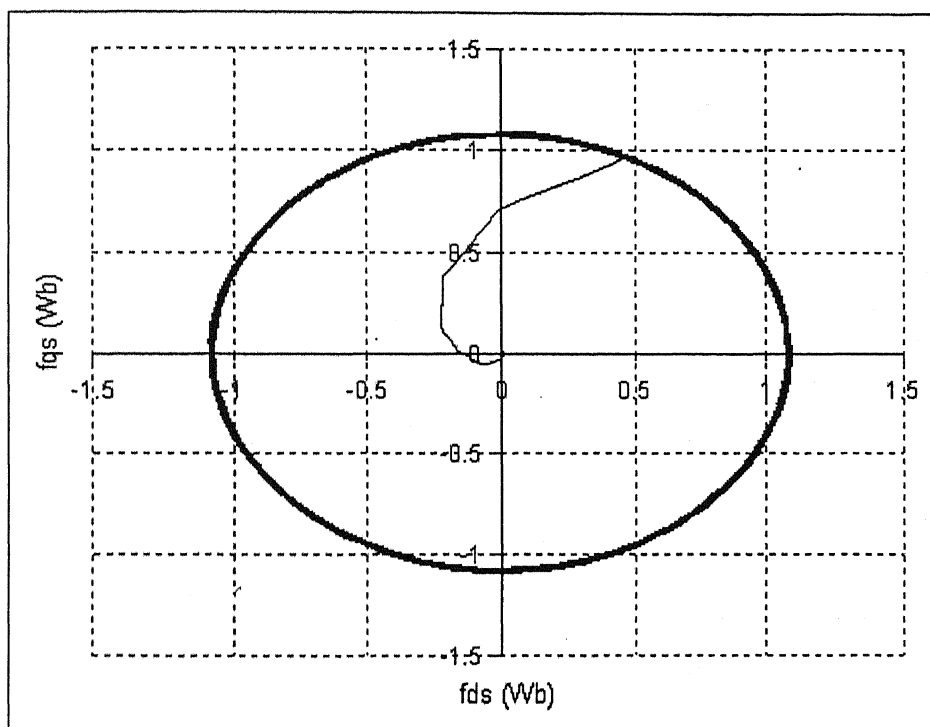
Fig.3.35 Polar plot of d and q axis stator flux under speed changes
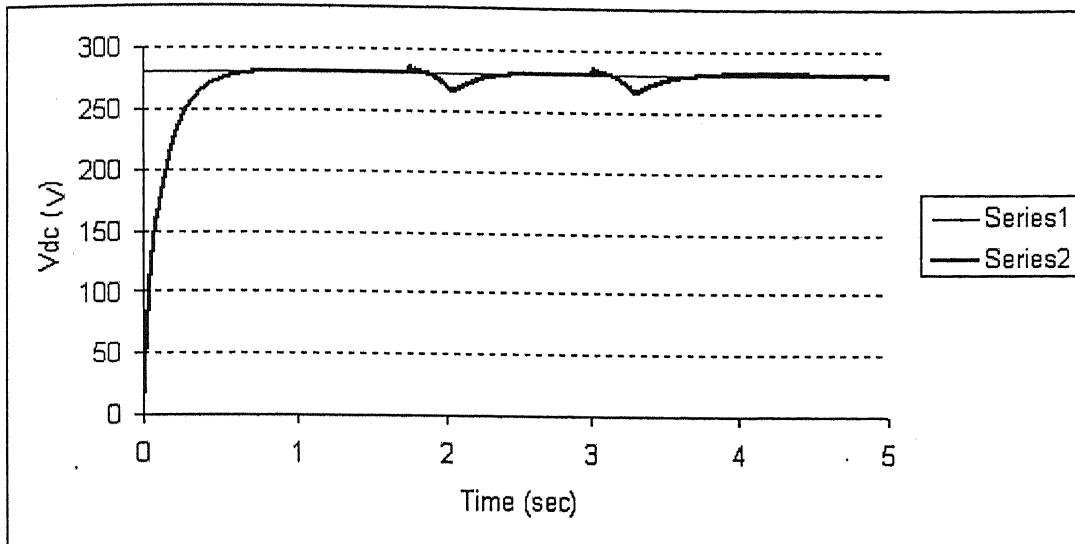
Reference voltage (Series 1), Actual voltage (Series 2)

Fig. 3.36 DC link Voltage under step change in speed
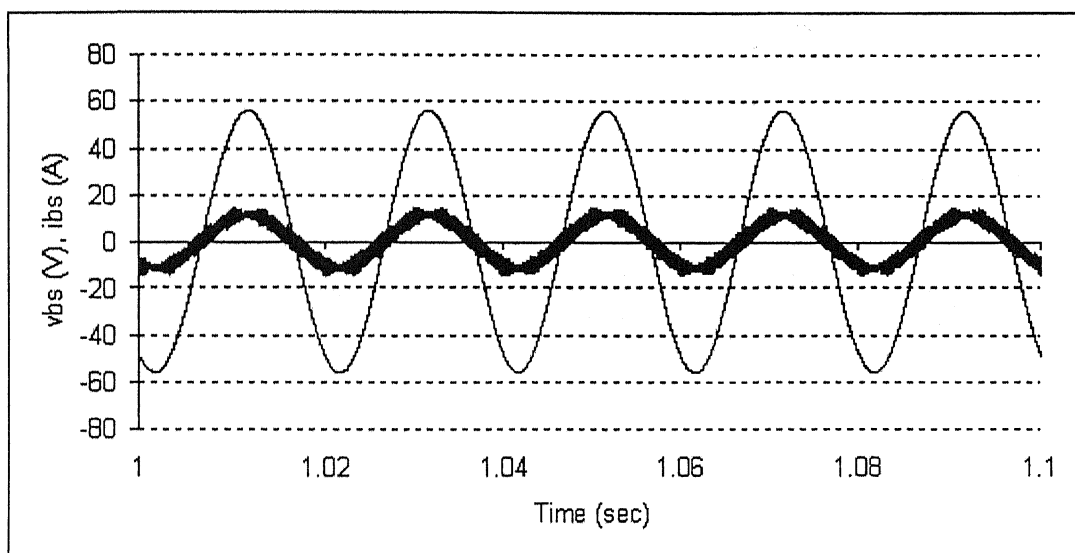
Y-axis 1div = 20 A (source current i_{bs})

Y-axis 1div = 100 V (source voltage, v_{bs})

Fig. 3.37 Source Voltage and Source current (phase 'b') at 750 rpm (forward motoring)
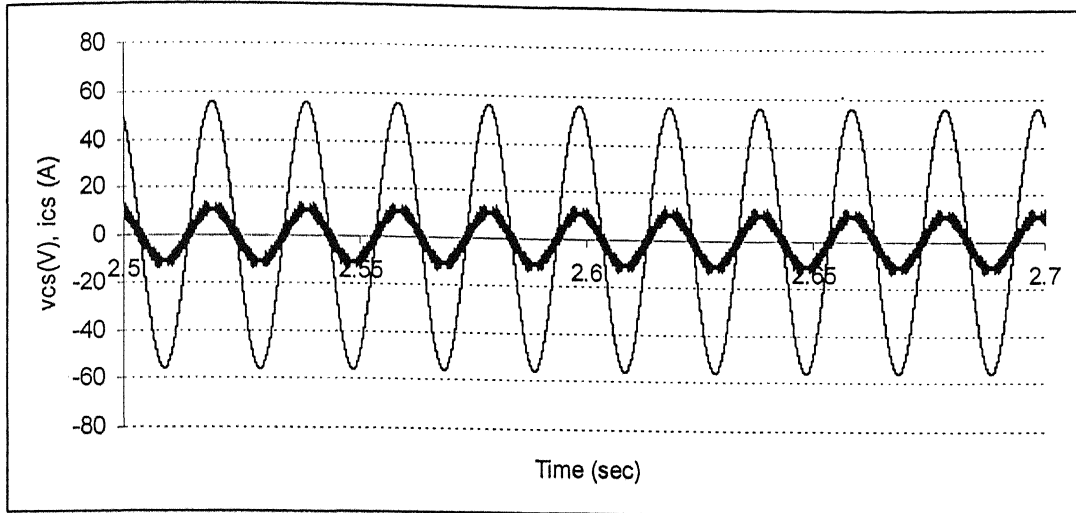
Y-axis 1div = 20 A (source current i_{cs})

Y-axis 1div = 100 V (source voltage, v_{cs})

Fig. 3.38 Source Voltage and Source current (phase 'c') at -750 rpm (reverse motoring)
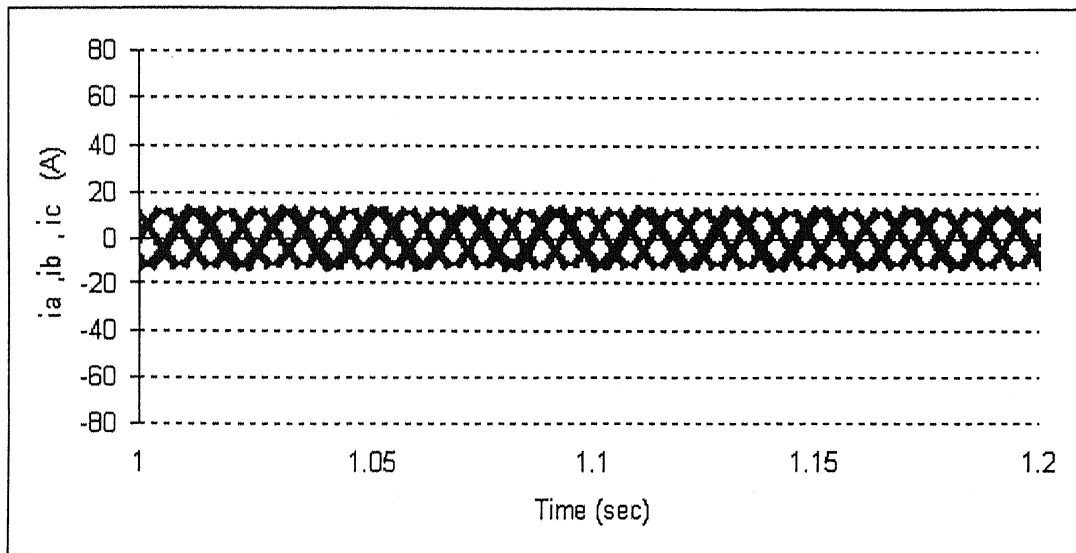
Fig 3.39 Source phase currents i_{as}, i_{bs}, i_{cs} at 750 rpm of forward motoring operation
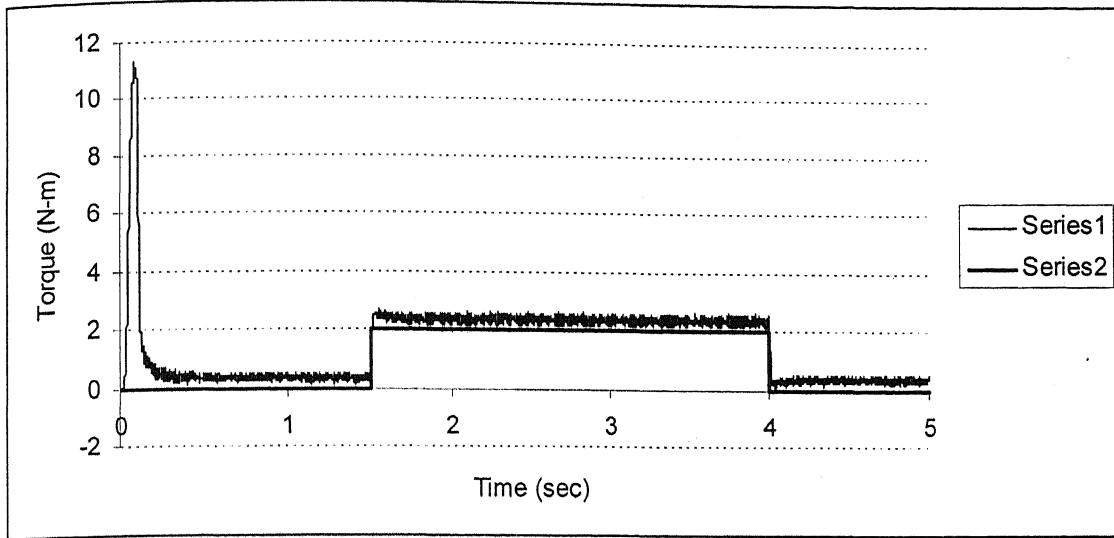
Actual torque (Series 1), Reference torque (Series 2)

Fig.3.40 Step change in load torque at 705 rpm speed
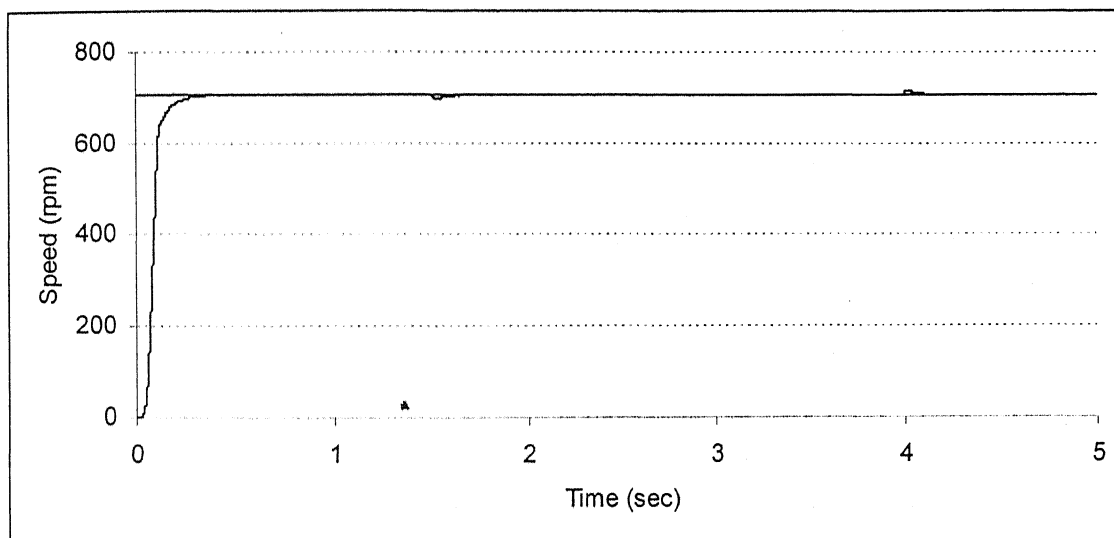
Fig.3.41 Speed during step change in load torque
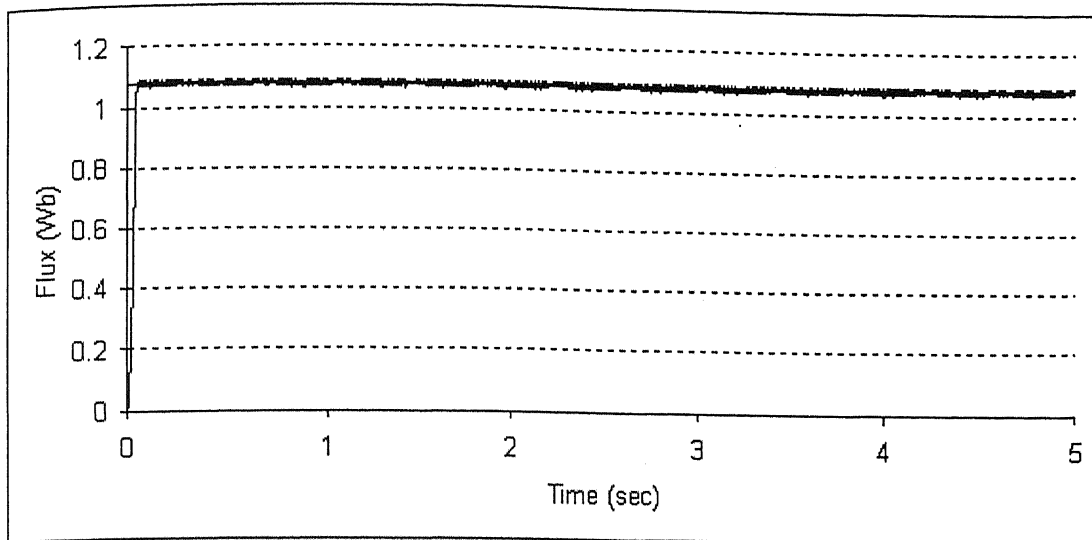
Fig.3.42 Stator flux during step change in load torque
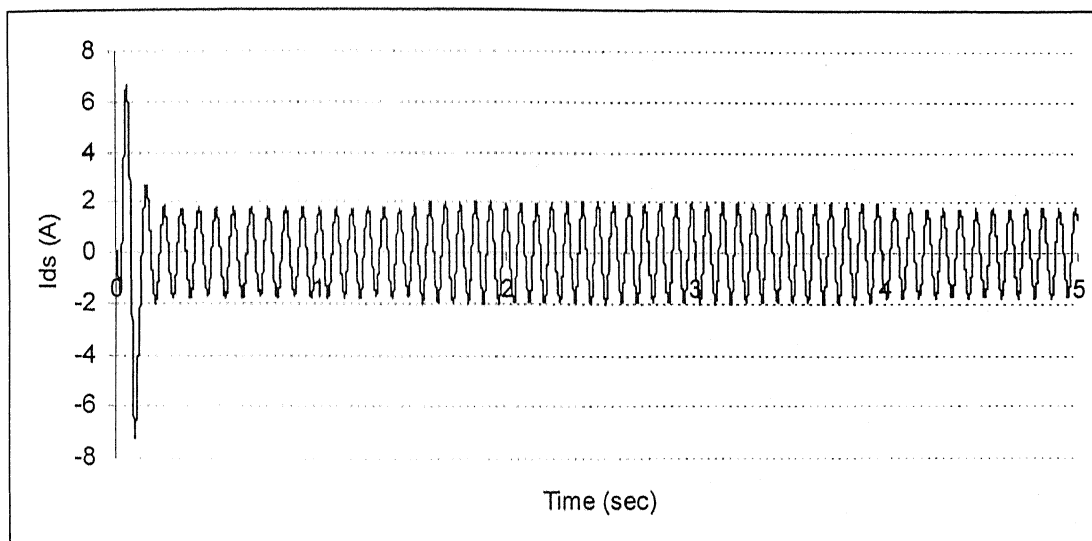
Fig. 3.43 d-axis stator current during change in load torque
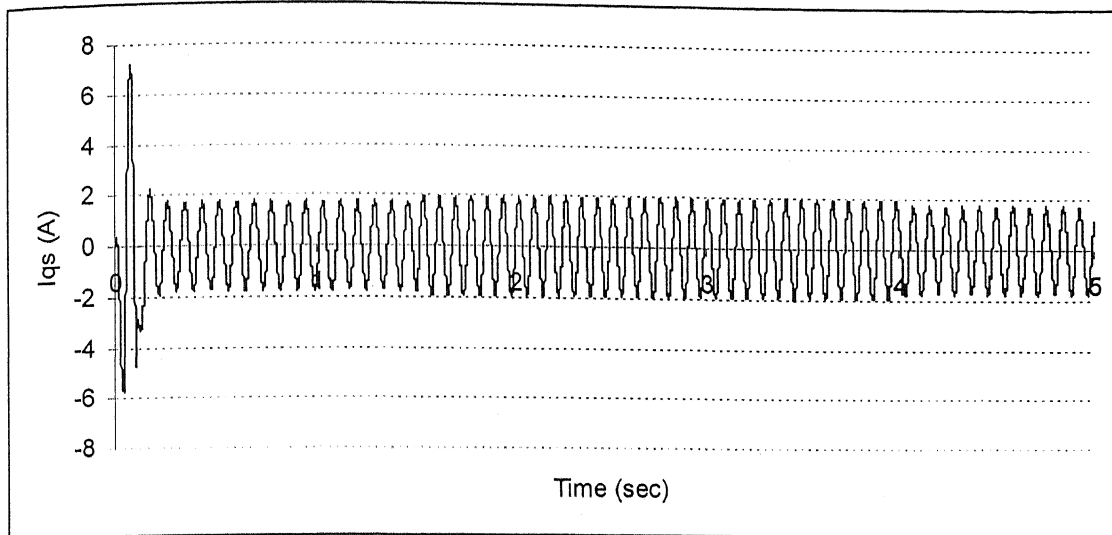
Fig. 3.44 q-axis stator current during change in load torque
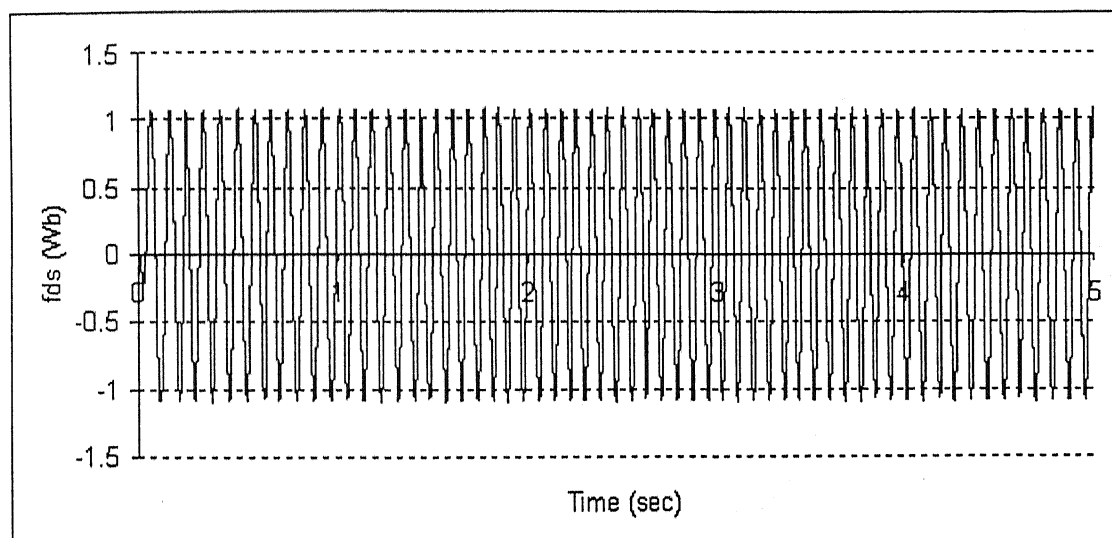
Fig. 3.45 d-axis stator flux during change in load torque
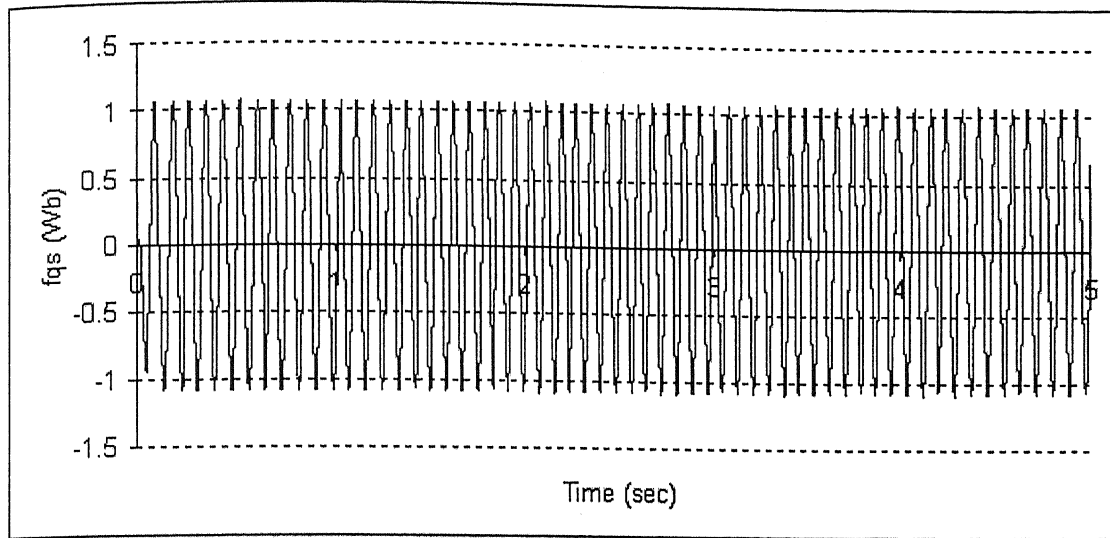
Fig. 3.46 q-axis stator flux during change in load torque
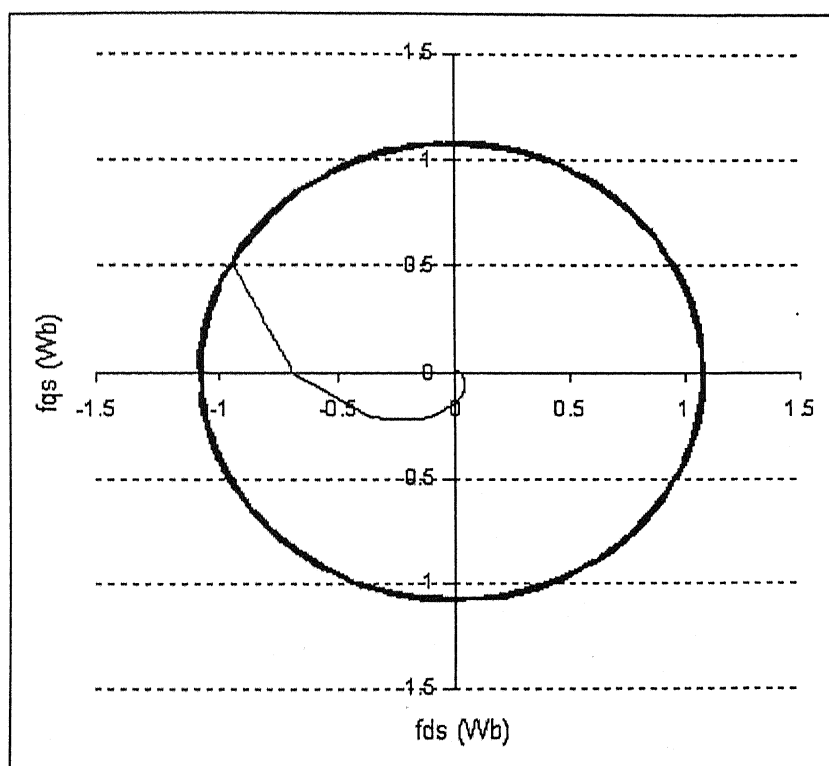
Fig.3.47 Polar plot of d and q axis stator flux under change in load torque
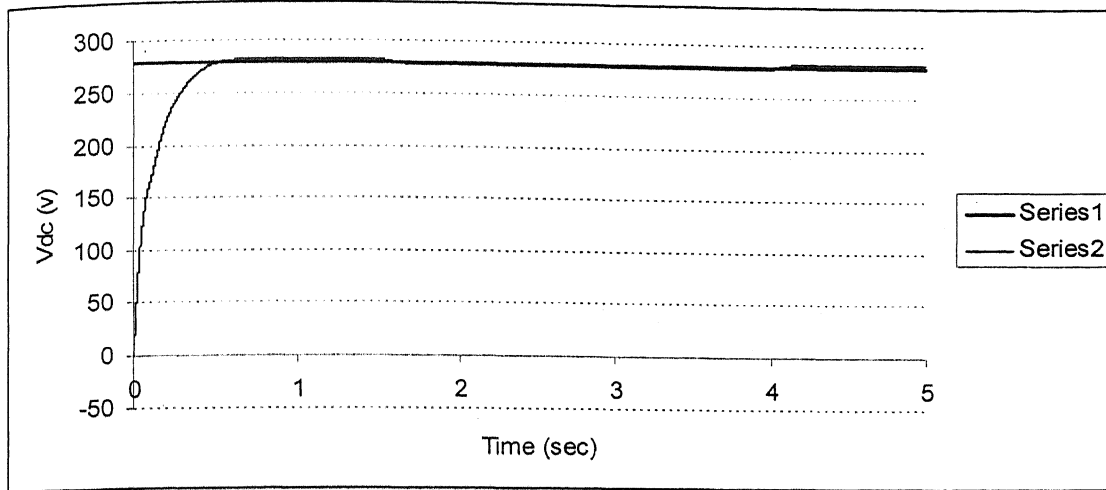
Actual voltage (Series 2), Reference voltage (Series 1)

Fig.3.48 DC link voltage during step change in load torque
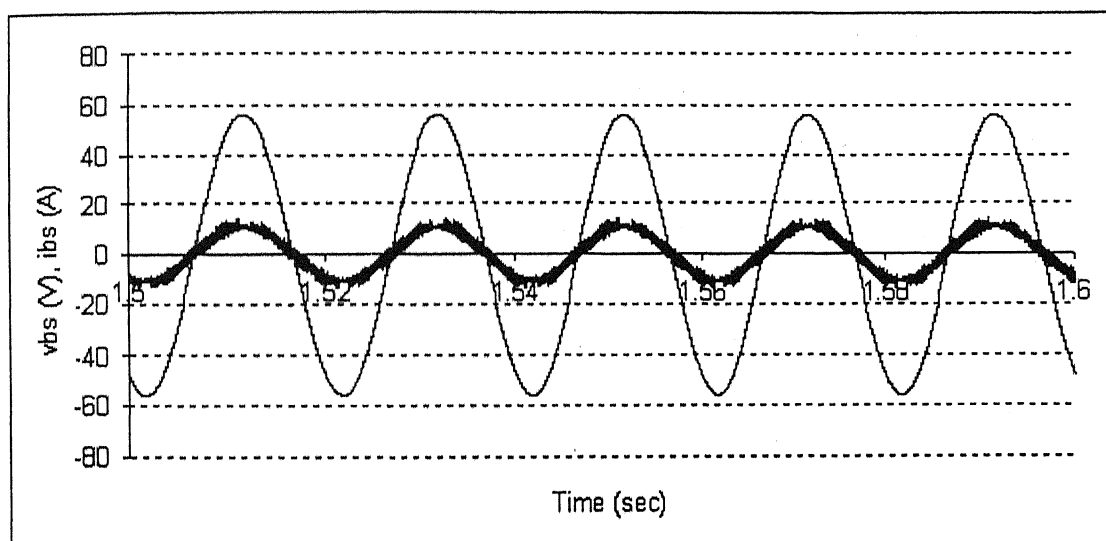
Y-axis 1div = 20 A (source current, i_{as})

Y-axis 1div = 100 V (source voltage, v_{as})

Fig. 3.49 Source Voltage and Source current (phase 'b') under loaded condition
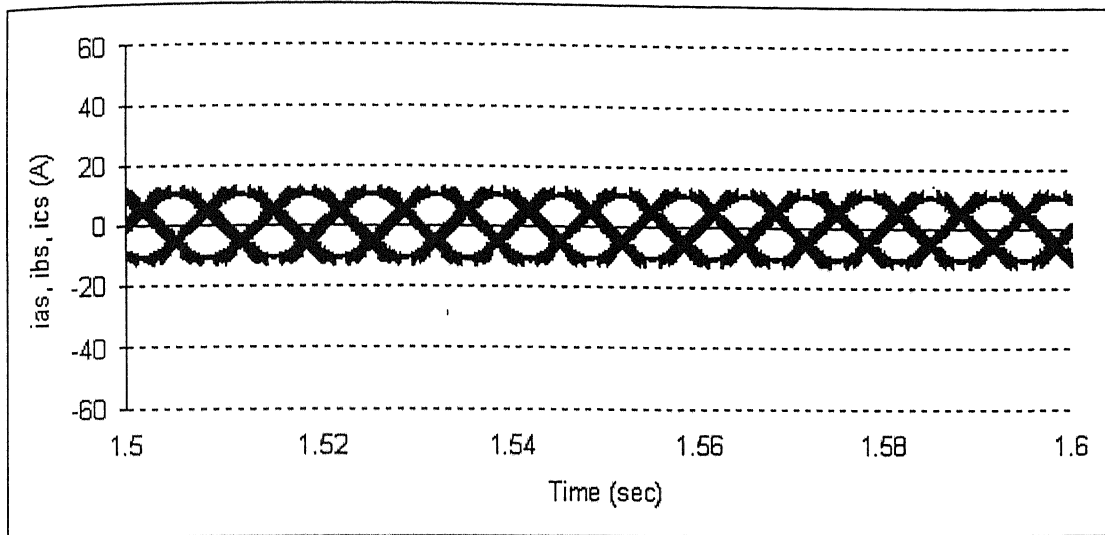
Fig 3.50 Source phase currents i_{as}, i_{bs}, i_{cs} under loading condition

(Steady state)

Chapter 4

PC-based Implementation of the Induction Motor Drive System

4.1 Introduction

This chapter describes the experimental setup of PC-based hardware implementation of the "Direct Torque and Flux Control" of induction motor using three-level VSI, as discussed in chapter 3. In chapter 3, simulation studies have been made for DTFC of induction motor drive system. After obtaining the simulation results, it is important to validate the control algorithm under real time applications. This chapter gives a detailed description of experimental setup. Section 4.2 gives a detailed description of the experimental setup and the circuits used. Section 4.3, describes the PC – based implementation of the control circuit and section 4.4, PC – based control of the proposed DTFC scheme. Experimental results are given at the end of the chapter while section 4.6, ends this chapter with the necessary conclusions.

4.2 Experimental Set – up

The lay out of the PC – based implementation is given in Fig. 4.1. The practical implantation is carried out in such a way that the hardware circuits are minimized.

The DC link voltage is supplied with a 3- phase rectifier. The 3–phase rectifier is fed from a 400 V, 3 phase AC supply through an auto transformer. Two 2200 µF

capacitors are connected in series across output of the rectifier. Mid point of the two capacitors is treated as neutral.

A motor generator set is used for the experiment. The detailed rating of the motor generator set is given in Appendix A. The parameters of the machine are calculated by no-load and blocked rotor tests. Moment of inertia is found out from retardation test.
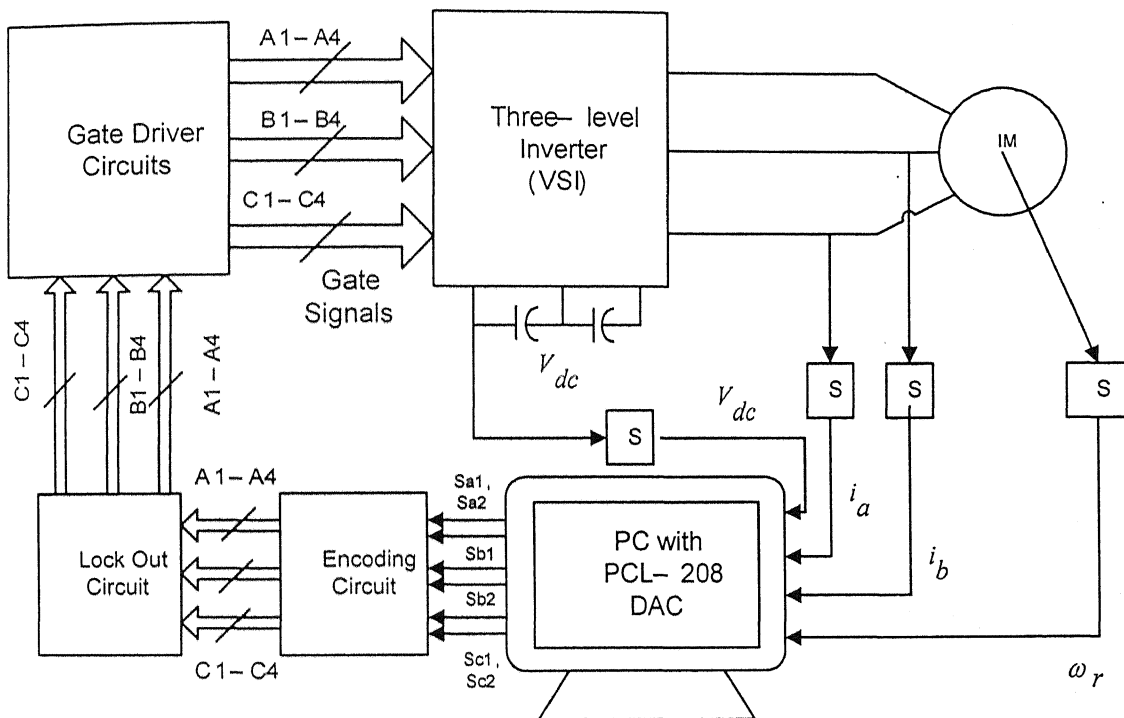
Fig. 4.1 Schematic diagram of the PC – Based implementation

For inverter switches, Mitsubishi IGBT modules (2 IGBTs in each module) with a voltage rating of 1200 V and current rating of 50 A, have been used. A high performance Mitsubishi driver circuit is used to drive IGBT. Actually it is a hybrid IC (M57959L) with a circuit designed for driving n-channel IGBT modules in any gate amplifier application. This device operates as an isolation amplifier for these modules and provides

the required electrical isolation between the input and output with an opto -coupler. Short circuit protection is provided by a built in de-saturation detector. The pin diagram and connection details for these drivers are given in the table 4.1 and Figures 4.2, and 4.3 respectively.

Table 4.1: Pin Configuration of the Hybrid IC M57959L

Pin 1: connected to collector of IGBT through a diode (1N4007) to protect against malfunction of over current protection (Detect pin)

Pin 2: Not connected

Pin 3: Not connected

Pin 4: + 15 V supply (V_{CC})

Pin 5: Drive output given to the Gate of the IGBT

Pin 6: - 9 V supply (V_{EE})

Pin 7-12: Not connected

Pin 13: Drive Signal i/p (-)

Pin 14: Drive Signal i/p (+)
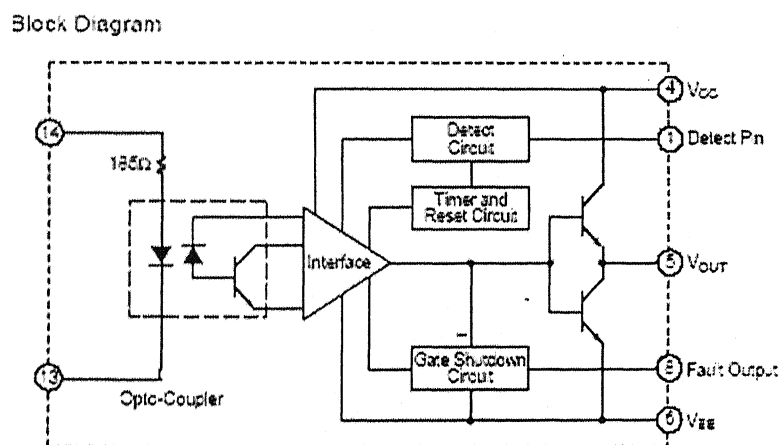
Fig. 4.2 Functional Block Diagram of IC M57959L

It can be noted that to build a three-level inverter 12 IGBTs are required. So there is a need of 12 IGBT driver circuits. Each Driver circuit requires +15 V and – 9 V dc voltages. 12 Power supplies range of (+15 V) –0–(-9 V) are developed by using thee isolated transformers of rating 230 V / 20-0-15 V (four secondary) and bride rectifiers.
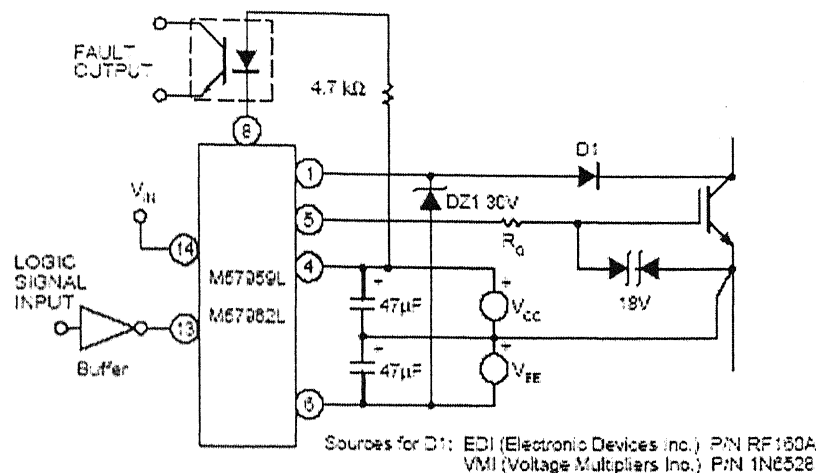
Fig. 4.3 Application diagram of M57959L

Three lock out circuits are fabricated to get the required blocking period for each leg of the inverter. Each lock out circuit consists of two dual mono-stable multivibrators IC74123, four AND gate IC 7408, and an HEX inverter IC 7404. The lock out circuit provides a time delay of approximately 5 μs between the changes of state in a leg. There are 3 possible states in a leg of three-level inverter is shown in table 4.2. The logic diagram of lock out circuit is shown in Fig. 4.4.

A1	A2	A3	A4	Sa1	Sa2
1	1	0	0	0	0
0	1	1	0	0	1
0	0	1	1	1	0

Table 4.2 Logic for lock out circuit and Encoding Circuit
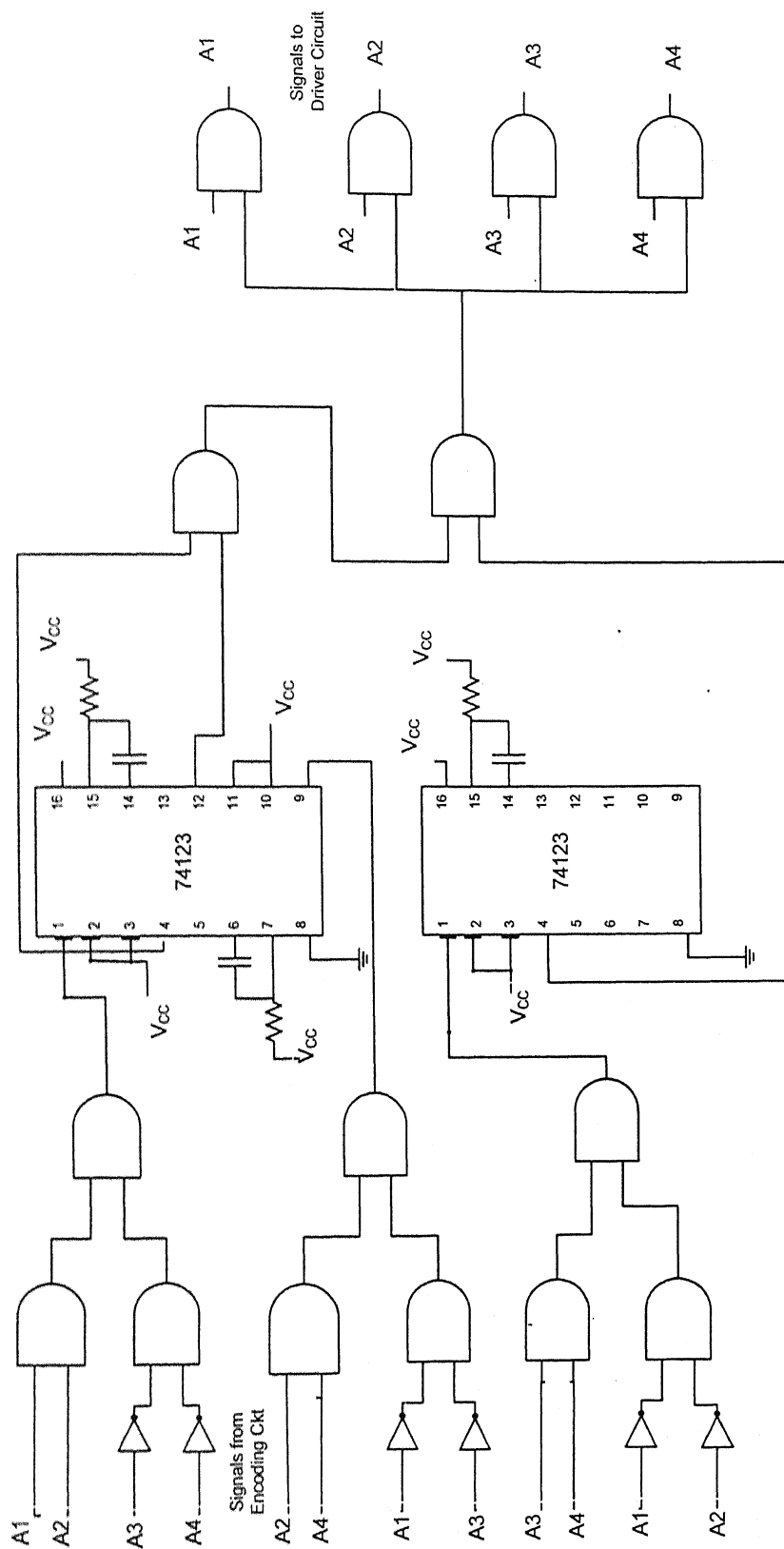
Fig. 4.4 Logic diagram for Lock circuit for one phase

Each phase requires 4 control signals as there are four switches for each phase. An encoder circuit is designed to decrease the no. of output control signals from PC. The logic can be obtained by drawing a k-map from table 4.2. Only two signals are given from PC for each phase and they are encoded to four signals. Sa1 and Sa2 are the two signals corresponding to switching signals A1, A2, A3, and A4 given from Digital output connector of PCL 208. The logic diagram for single phase encoding circuit is shown in Fig. 4.5.
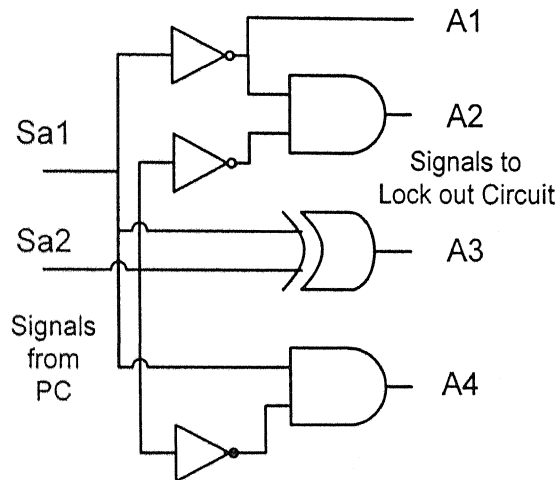
Fig. 4.5 Encoding Circuit for one phase

Encoding circuit for three phases has been designed on single PCB to minimize the no. of components. Encoding circuit consists of one NOT gate IC 7404, one EXOR gate IC 7486 and two AND gate ICs 7408. Inputs for encoding circuit are given from Digital output from PCL – 208. Output of encoding circuit is given to lock out circuit.

With the building up of the encoding circuit, lock out circuit and driver circuit, the inverter part is ready. The dc link voltage is sensed by using a voltage sensor (Model LV - 25P). Two phase currents are sensed by using two current sensors (Model LA 50P). The details of the voltage and currents are given in Appendix C. An ac tachogenerator is

coupled with the induction motor to sense the speed of the motor. A potential divider circuit and a suitable filter are used to scale down the speed corresponding to suitable dc voltage. All the voltage, current and speed sensors are calibrated to determine the conversion of actual and measured quantity. With the building blocks hardware part of the implementation is over.

4.3 PC – based Implementation of the Control Circuit

The control circuit mainly consists of a PC operating at a clock frequency of 266 MHz. The control algorithm executed in a real time on the PC. The calculations are performed inside the PC. A high speed Data Acquisition Card (PCL – 208) has been interfaced with the PC for the data transfer between PC and external hardware. The detailed specification of the card is given in Appendix B. In the actual experimental setup, the drive is controlled by a software program. In the PC-based control scheme the data, like motor currents, motor speed, and dc link voltage signals are given to the digital computer through the A/D converter of high speed data acquisition card (PCL – 208). The switching status for inverter are generated by calculations performed inside the computer and control pulses, for inverter gate circuits are computed by the digital output ports of the data acquisition card.

4.4 PC – based Control of the Proposed DTFC Scheme

The PC-based real time program is given in Appendix D. the program is in C language. In the control program, analog signals like motor phase currents, motor speed, and dc link voltage are sensed. In fact the sensed analog signals are converted into digital

signals by the in-built A/D converter of the DAC card. In the algorithm the converted digital values will again be converted to analog values. The converted analog values after multiplication with sensor gains will give the actual values of the voltage, currents, and speed present at that time. These actual analog values will be used by the DTFC algorithm to calculate the sector number and the status of the flux and torque. From the knowledge of these three variables, namely flux status, torque status and sector angle the required voltage vector and hence switching signals for inverter are selected from the switching table. Finally the PC will send out six switching signals Sa1, Sa2; Sb1, Sb2; and Sc1, Sc2; two for each phase, required to operate the machine in direct torque and flux control strategy.

4.5 Experimental Results

The experiment is done on a 3-pahse, 1.1 kW, 415 V, 2.6 A, 1410 rpm and 50 Hz, star connected squirrel cage induction motor which is mechanically coupled with a 230 V, 1500 rpm dc machine for loading purpose. Typical data of machine parameters are given in Appendix 'A'. Typical experimental results are presented and they are compared with the simulation results to validate the design methodology.

4.5.1 Under no load condition

Fig. 4.6 - 4.8 show the simulation and experimental results under no load condition. Fig 4.6 shows that for the step change of speed the stator flux is constant and is equal to the reference value of 1.07 Wb. Fig. 4.7 shows that the torque developed when

there is a step change in speed in the starting. Fig. 4.8 shows the current waveform under step change in speed. Fig. 4.7 and Fig. 4.8 have been compared with simulation results.

4.5.2 Speed reversal

Simulated and experimental waveforms of the speed response, the flux response, motor phase current and torque response for the step change in speed from 280 rpm (forward motoring) to -280 rpm (reverse motoring) and vise versa are shown in Fig. 4.9 to 4.11. The speed response is found to be fast. During the transient period, the motor phase current is high as shown in Fig. 4.11. The flux is constant during the transient and is equal to the reference value 1.07 Wb. The torque response is shown in the Fig. 4.10 during speed reversal. This shows the de-coupling of the torque and flux and establishes that the operation is similar to that of separately excited dc machine.

4.5.3 Step change in torque command

The load on induction motor is applied by connecting a resistive load to the dc generator, which is coupled to the motor. To bring about a step change in torque command, dc generator coupled to the induction motor was loaded by switching on the field supply while the resistive load is connected to the dc generator. In Fig. 4.12, it is shown that as the load is applied on motor, flux is constant and is at reference value. Fig. 4.13 shows that the speed is almost constant at its reference value when there is an application of load torque. Fig. 4.14 shows the current waveform under step change in load torque.

4.6 Conclusion

Experimental setup for the direct torque and flux control of induction motor is explained in this chapter. Data transfer between PC and hardware is achieved by PCL – 208 data acquisition card. Control signals are generated in side the computer. Instead of conventional designed control circuits, a high performance M59759L hybrid drives ICs are used for amplification of control pulses and to provide isolation between low power control and high power control and high power IGBT inverter circuit, thus making inverter design compact. The simulation and experimental results are compared in this chapter and experimental results are matched with simulated results. The experimental results for both steady state and transient conditions were found satisfactory. The torque response is almost instantaneous and speed of the motor is fast. From the result it is seen that the machine is under decoupled control, where torque and flux can be controlled directly and independently.
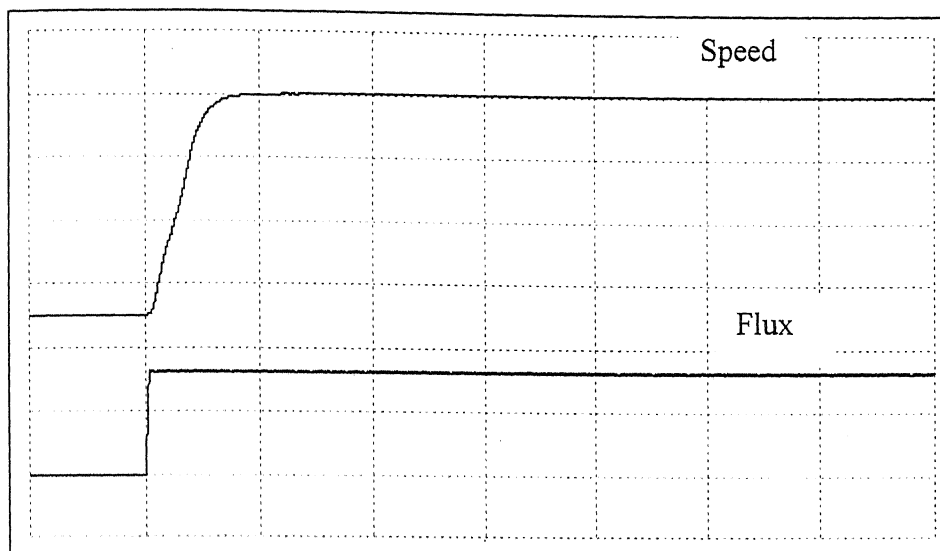
X-axis 1 div = 0.25 sec (time)
Y-axis 1 div = 80rpm (Motor speed)
1 div = 0.65wb (Stator flux)

Fig. 4.6(a) Simulated Waveform
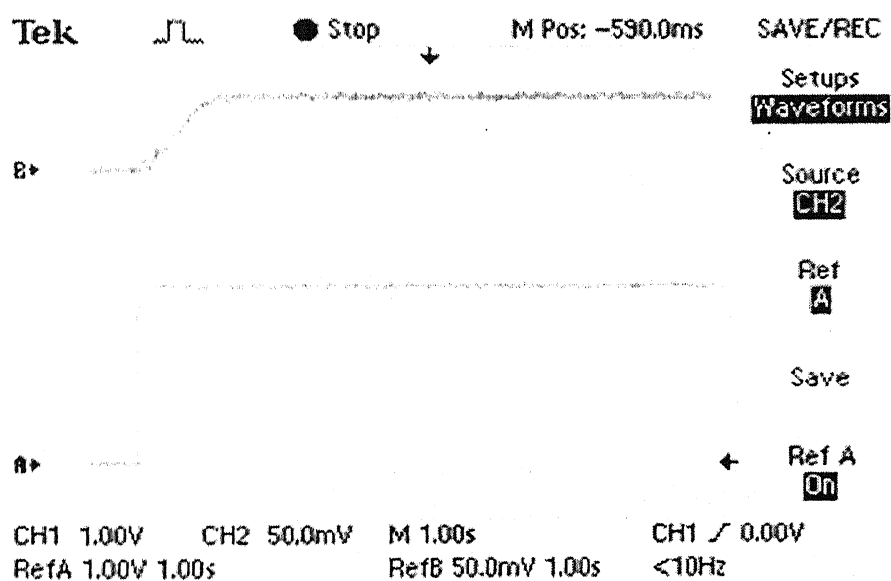
X-axis: 1div = 1 sec (time)
Y-axis: 1div = 2Wb (stator flux, Channel 1)
: 1div = 230 rpm (Motor Speed, Channel 2)
(There is a, +2.5V offset in D/A converter's output, Channel 1)

Fig. 4.6 Flux response during step change of speed from 0 rpm to 280 rpm
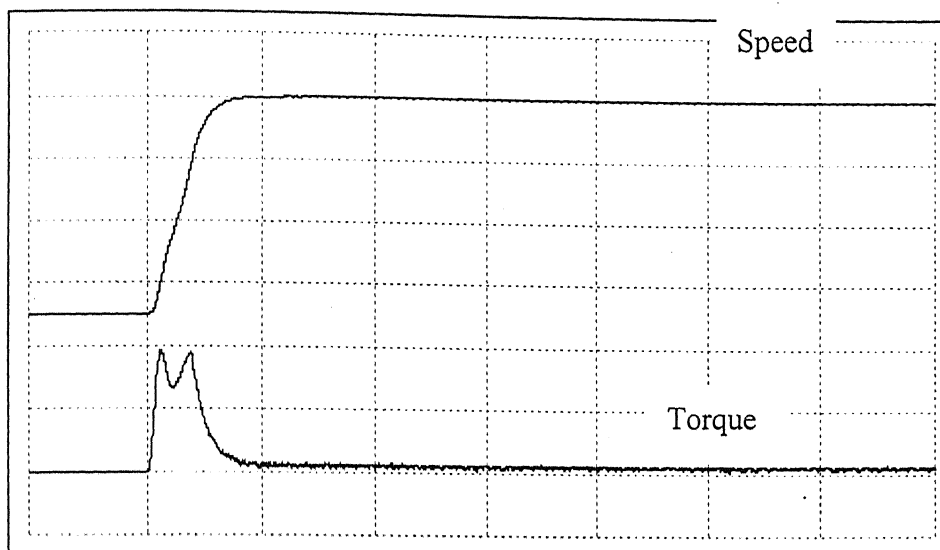
X-axis 1 div = 0.25 sec (time)
Y-axis 1 div = 80rpm (Motor speed)
1 div = 2 N-m (Torque developed)

Fig. 4.7(a) Simulated Waveform
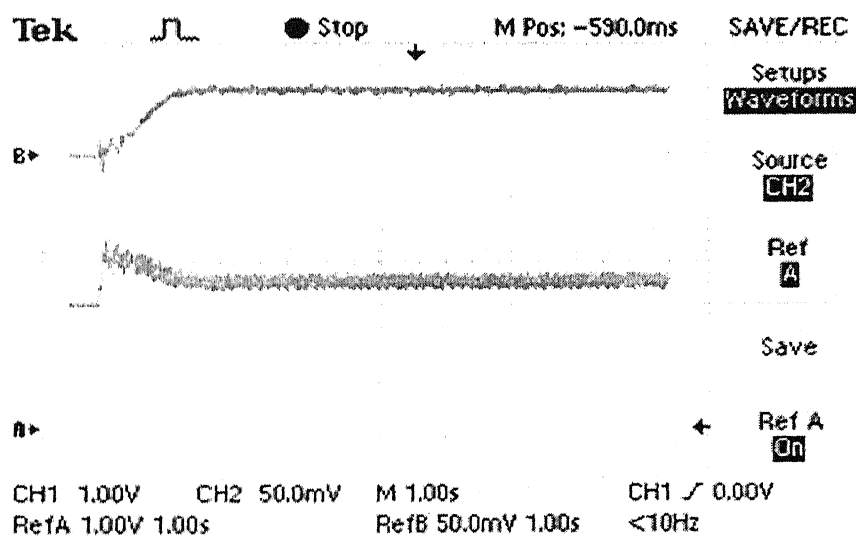
X-axis: 1div = 1 sec (time)
Y-axis: 1div = 5N-m (Torque developed, Channel 1)
: 1div = 230 rpm (Motor Speed, Channel 2)
(There is a, +2.5V offset in D/A converter's output, Channel 1)

Fig. 4.7 Torque response during step change in speed from 0 rpm to 280 rpm
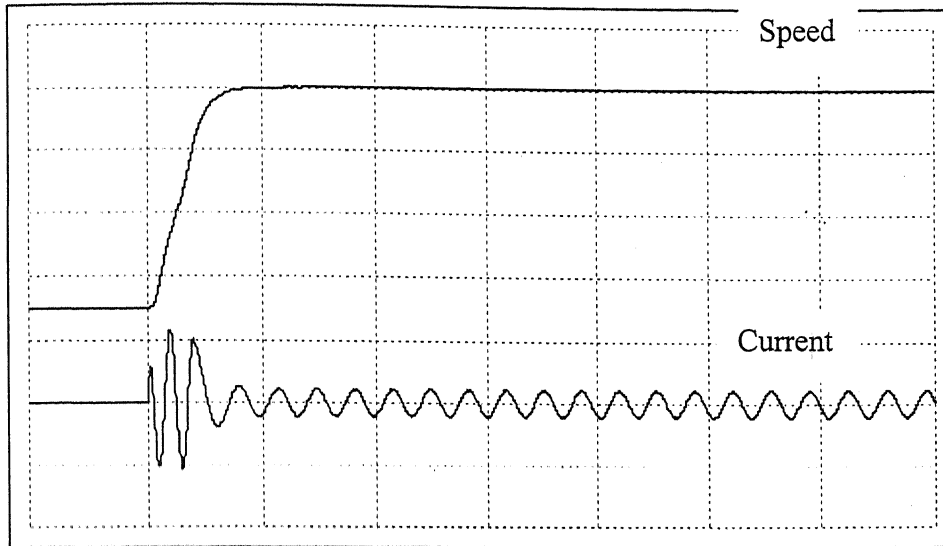
Speed

Current

X-axis 1 div = 0.25 sec (time)
Y-axis 1 div = 80rpm (Motor speed)
1 div = 4.5 A (Motor phase 'a' current)

Fig. 4.8 (a) Simulated Waveform
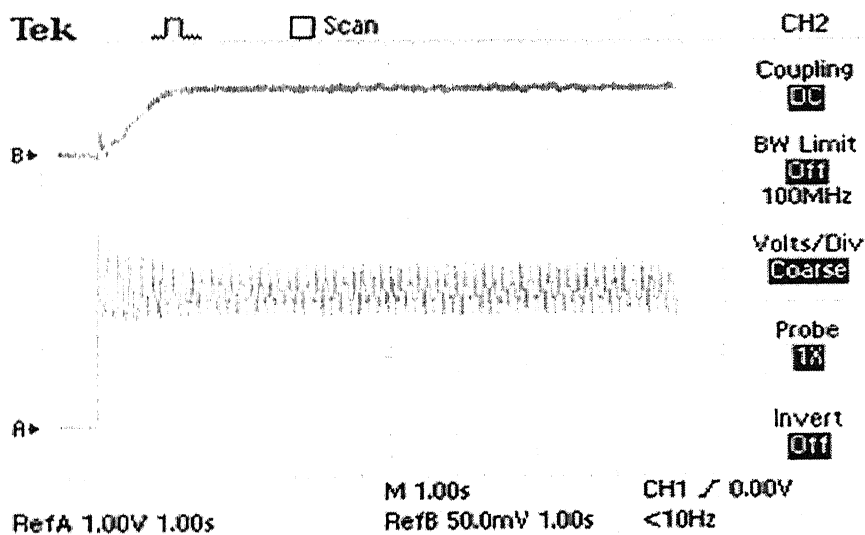
Tek   ⎍⎍   ☐ Scan   CH2

Coupling
DC

BW Limit
Off
100MHz

Volts/Div
Coarse

Probe
1X

Invert
Off

M 1.00s   CH1 ╱ 0.00V
RefA 1.00V 1.00s   RefB 50.0mV 1.00s   <10Hz

X-axis: 1div = 1 sec (time)
Y-axis: 1div = 1A (Motor phase 'a' current, Channel 1)
: 1div = 230 rpm (Motor Speed, Channel 2)
(There is a, +2.5V offset in D/A converter's output, Channel 1)

Fig. 4.8 Motor phase 'a' current during step change in speed from 0 rpm to 280 rpm
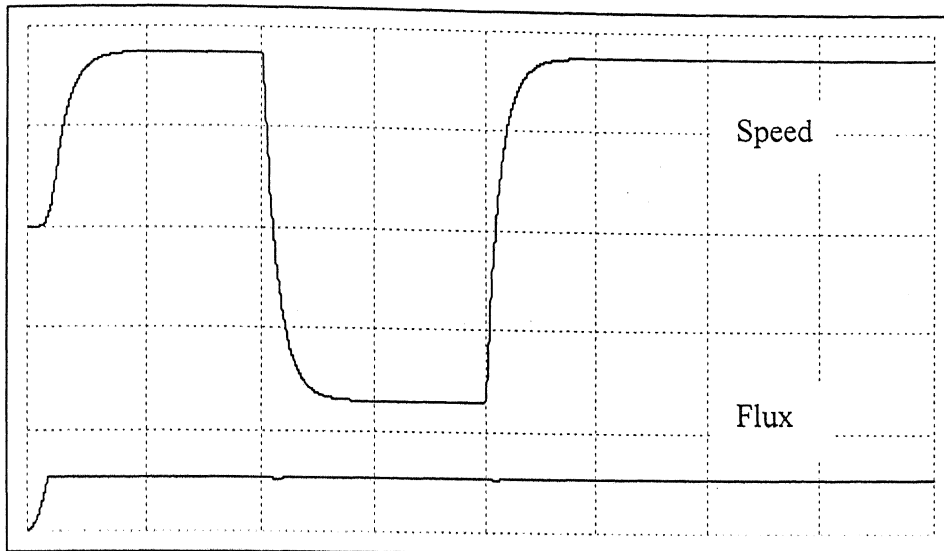
X-axis 1 div = 0.25 sec (time)
Y-axis 1 div = 160rpm (Motor speed)
1 div = 2wb (Stator flux)

Fig. 4.9 (a) Simulated Waveform
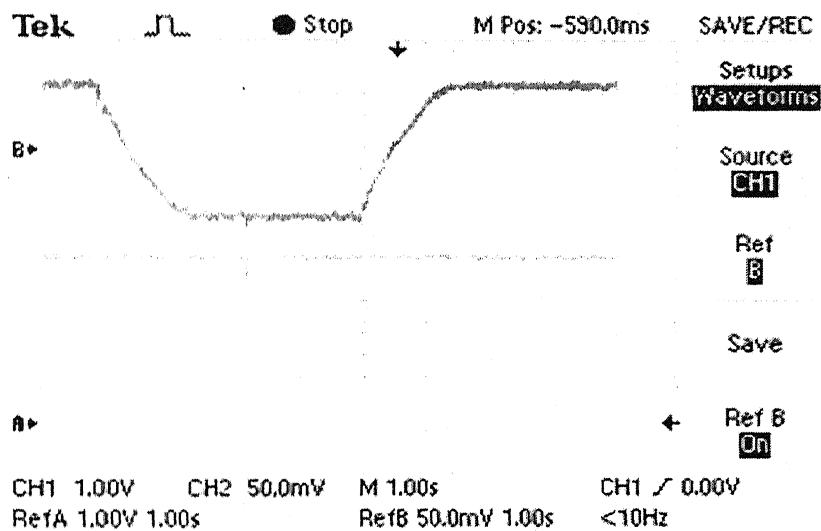
X-axis: 1div = 1 sec (time)
Y-axis: 1div = 2Wb (Stator Flux, Channel 1)
      : 1div = 230 rpm (Motor Speed, Channel 2)
(There is a, +2.5V offset in D/A converter's output, Channel 1)

Fig. 4.9 Stator flux response when step change in speed from 280 rpm (forward motoring) to -280 rpm (reverse motoring) and vise versa.

X-axis 1 div = 0.25 sec (time)
Y-axis 1 div = 400 rpm (Motor speed)
1 div = 7.25 N-m (Torque developed)

Fig. 4.10(a) Simulated Waveform
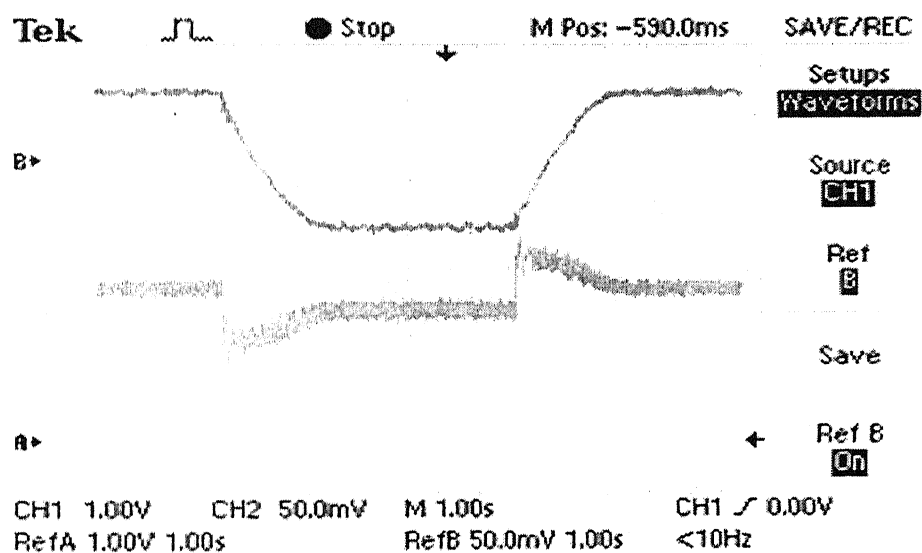
X-axis: 1div = 1 sec (time)
Y-axis: 1div = 5 N-m (Torque developed, Channel 1)
: 1div = 230 rpm (Motor Speed, Channel 2)
(There is a, +2.5V offset in D/A converter's output, Channel 1)

Fig. 4.10 Torque response when step change in speed from 280 rpm (forward motoring)
to -280 rpm (reverse motoring) and vise versa.
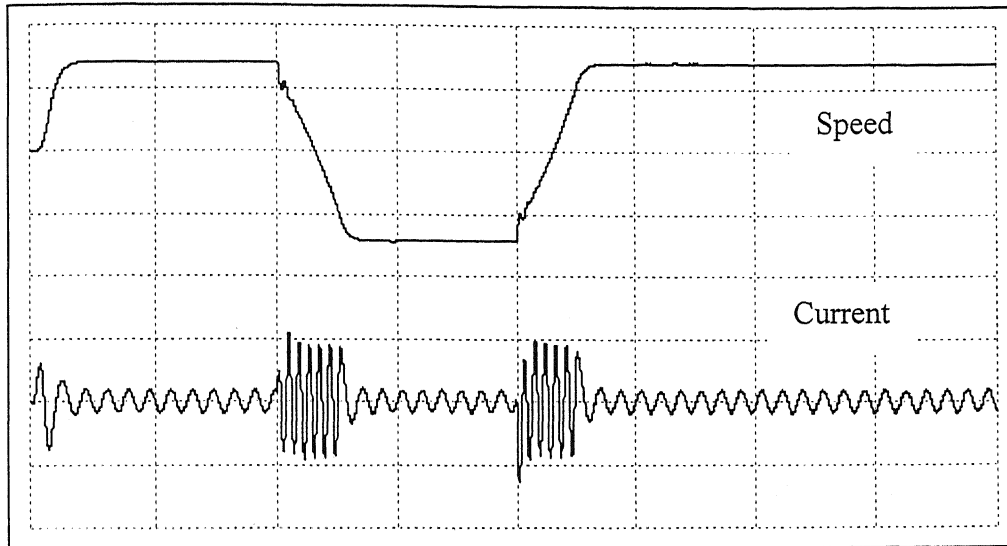
X-axis 1 div = 0.5 sec (time)
Y-axis 1 div = 450rpm (Motor speed)
        1 div = 4.5 A (Motor phase 'a' current)

Fig. 4.11(a) Simulated Waveform
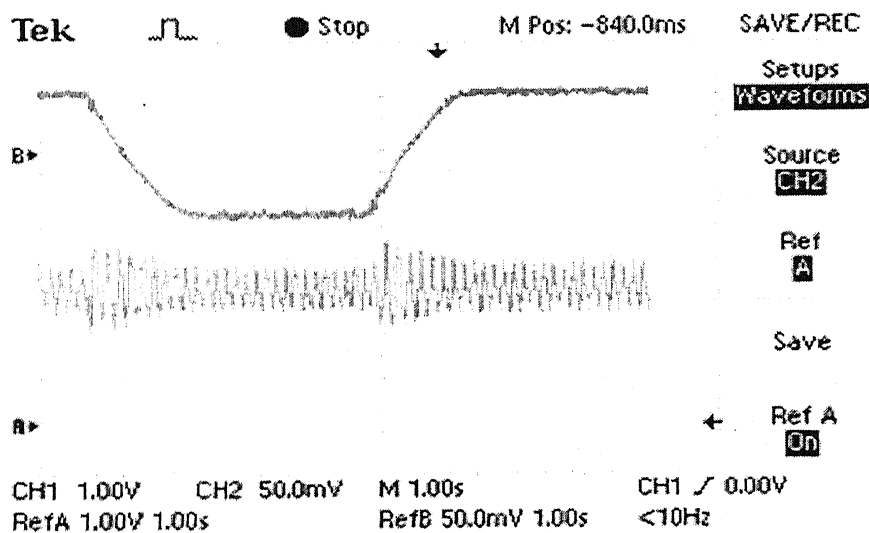
X-axis: 1div = 1 sec (time)
Y-axis: 1div = 1A (Motor phase 'a' current, Channel 1)
       : 1div = 230 rpm (Motor Speed, Channel 2)
(There is a, +2.5V offset in D/A converter's output, Channel 1)

Fig. 4.11 Motor phase 'a' current when step change in speed from 280 rpm (forward
     motoring) to -280 rpm (reverse motoring) and vise versa. ·
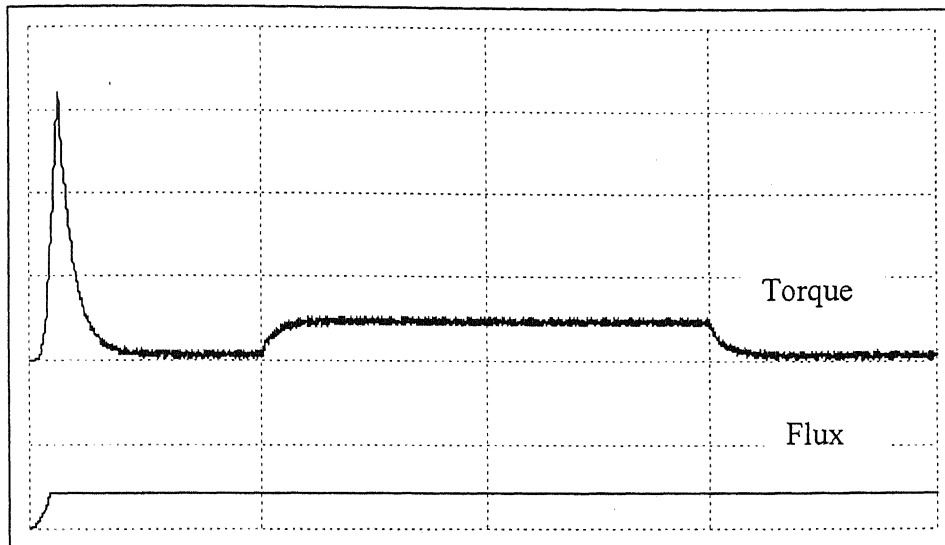
X-axis 1 div = 0.5 sec (time)
Y-axis 1 div = 2.5 N-m (Torque developed)
1 div = 2.5wb (Stator flux)

Fig. 4.12(a) Simulated Waveform
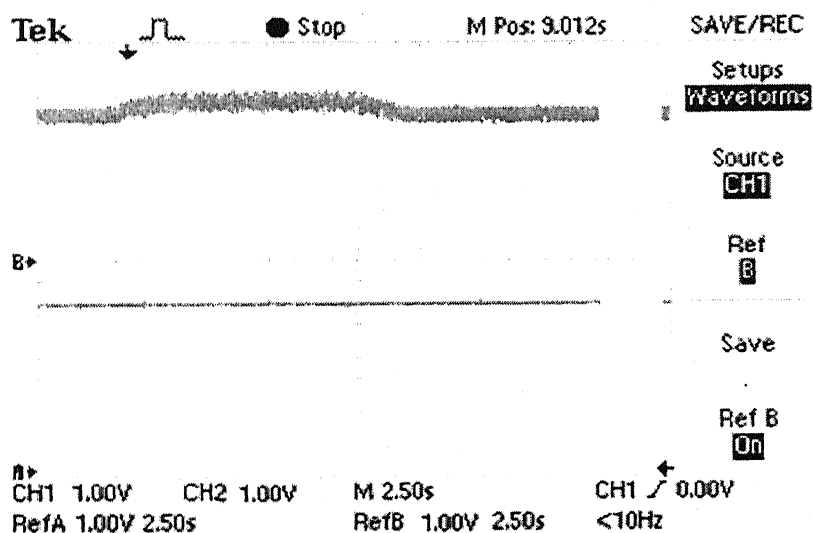
X-axis: 1div = 2.5 sec (time)
Y-axis: 1div = 2Wb (Stator flux, Channel 1)
: 1div = 5 N-m (Torque developed, Channel 2)
(There is a, +2.5V offset in D/A converter's outputs, Channel 1 & 2)

Fig. 4.12 Stator flux response under step change in load
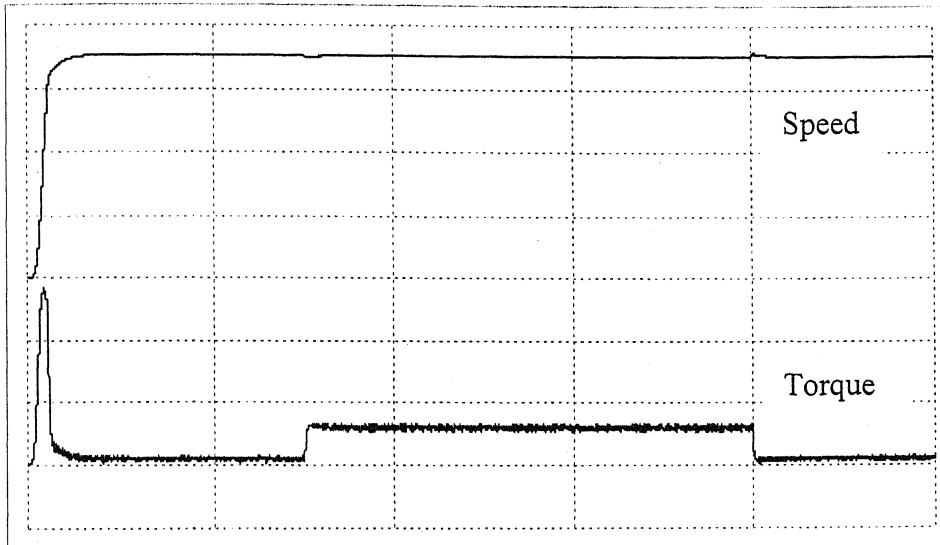
X-axis 1 div = 1 sec (time)
Y-axis 1 div = 4 N-m (Torque developed)
1 div = 200 rpm (Motor Speed)

Fig. 4.13(a) Simulated Waveform
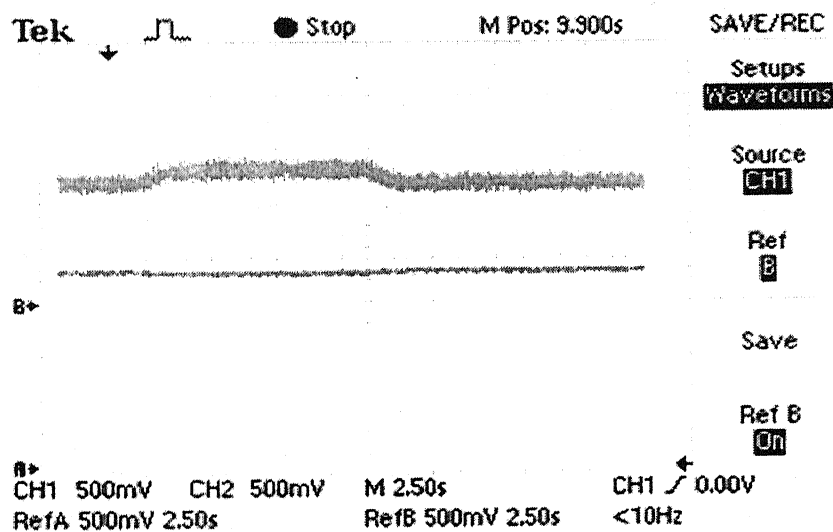
X-axis: 1div = 2.5 sec (time)
Y-axis: 1div = 5 N-m (Torque developed, Channel 1)
: 1div = 350 rpm (Motor Speed, Channel 2)
(There is a, +2.5V offset in D/A converter's output, Channel 1)

Fig. 4.13 Speed response under step change in load
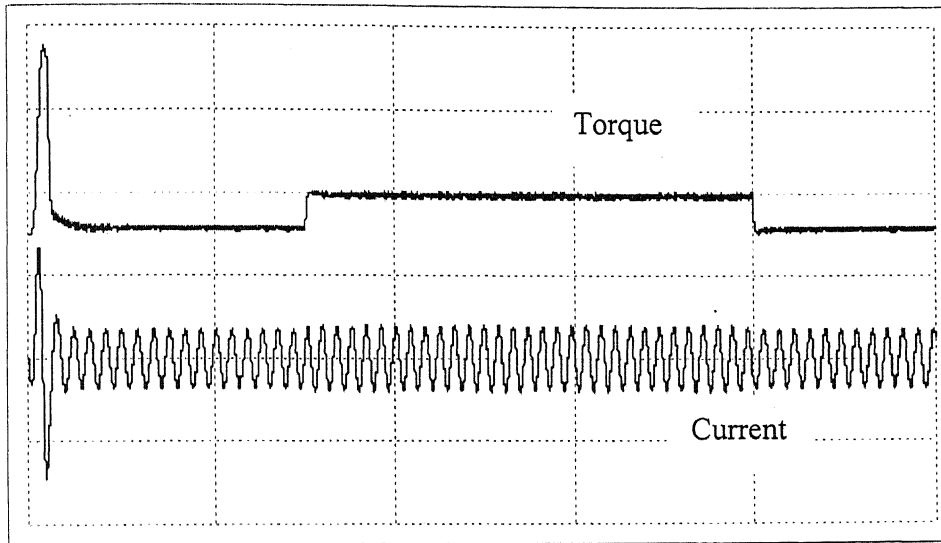
Torque

Current

X-axis 1 div = 1 sec (time)
Y-axis 1 div = 4 N-m (Torque developed)
1 div = 3 A (Motor phase 'a' current)

Fig. 4.14(a) Simulated Waveform

Tek   JL   ● Stop   M Pos: 3.012s   SAVE/REC

Setups
Waveforms

Source
CH1

Ref
B

Save

Ref B
On

CH1 500mV   CH2 1.00V   M 2.50s   CH1 ∫ 0.00V
RefA 500mV 2.50s   RefB 1.00V 2.50s   <10Hz
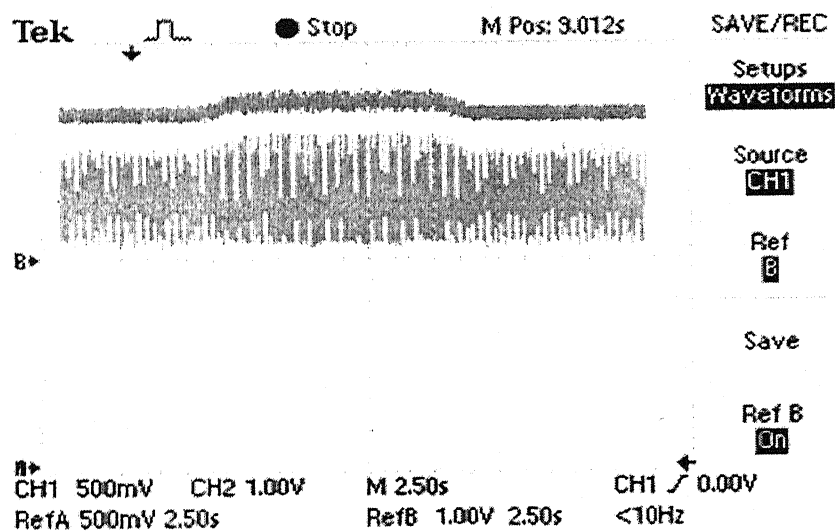
X-axis: 1div = 2.5 sec (time)
Y-axis: 1div = 0.5 A (Motor phase 'a' current, Channel 1)
: 1div = 5 N-m (Torque developed, Channel 2)
(There is a, +2.5V offset in D/A converter's outputs, Channel 1 & 2)

Fig. 4.14 Motor phase 'a' current under step change in load
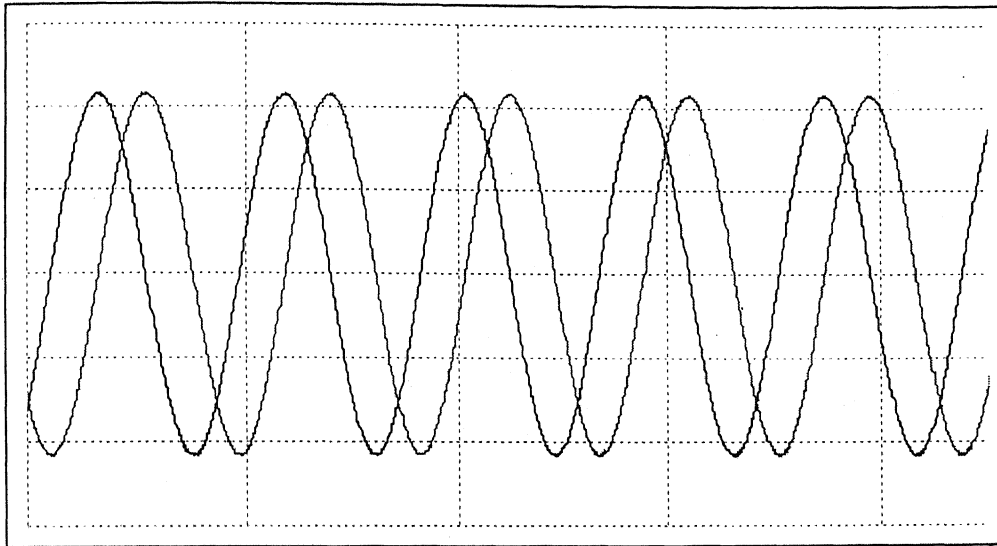
X-axis 1 div = 0.2 sec (time)
Y-axis 1 div = 0.5wb (Stator flux)

Fig. 4.15(a) Simulated Waveform
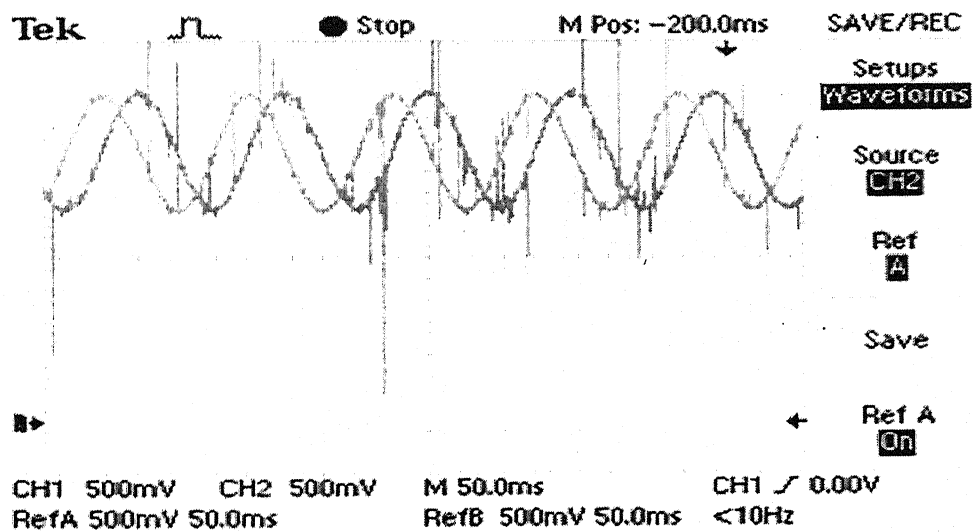
X-axis: 1div = 50 ms (time)
Y-axis: 1div = 1Wb (d and q-axis stator flux)
(There is a, +2.5V offset in D/A converter's outputs, Channel 1 & 2)

Fig. 4.15 d and q-axis fluxes, under steady state running condition.

A View of Experimental set-up of DTFC of an Induction Motor Drive System
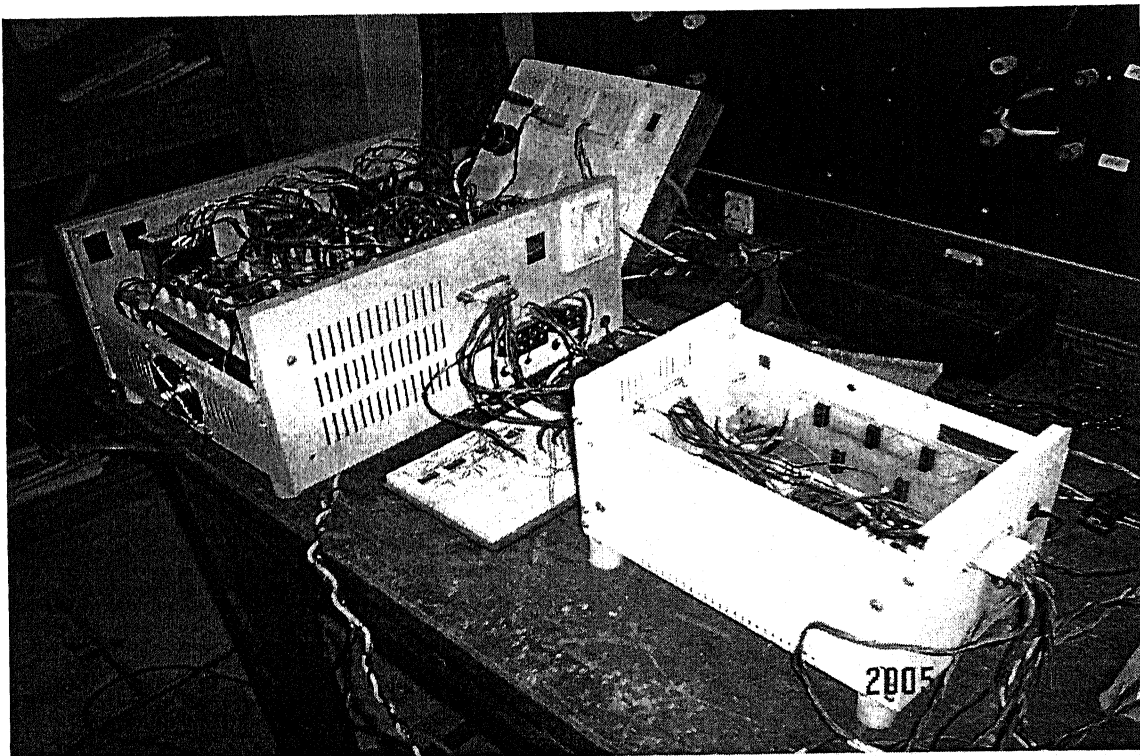
A View of Three-Level Inverter with Lock-out Circuit
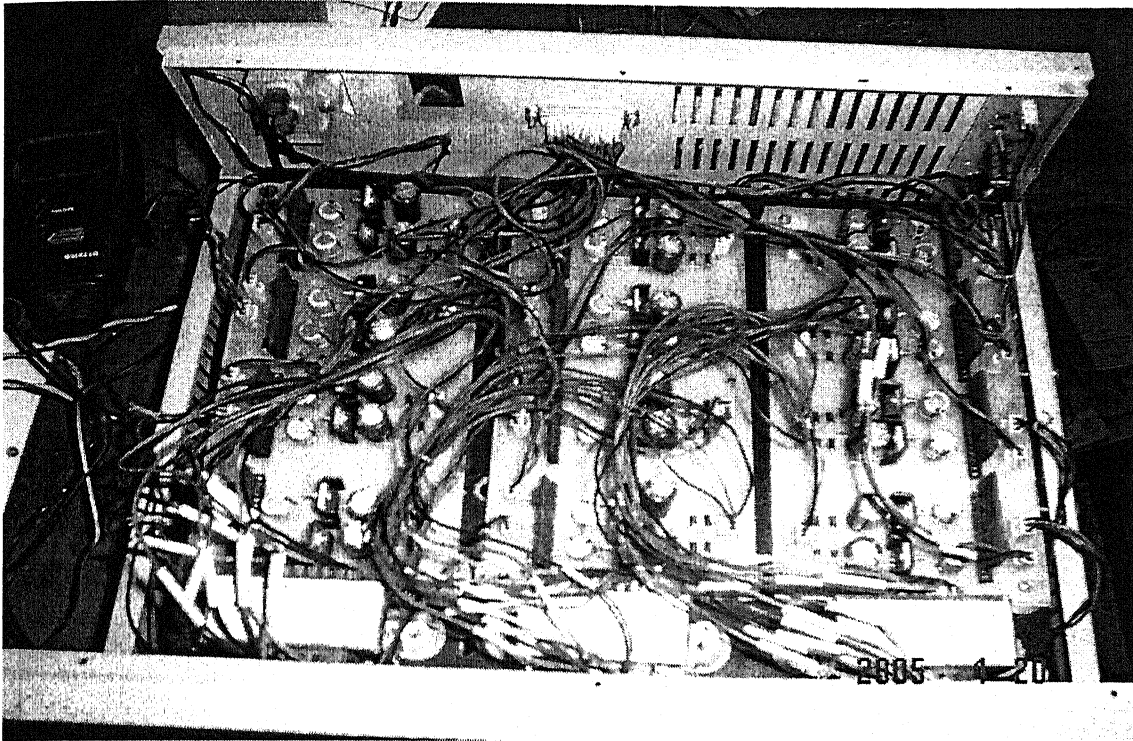
A Inside View of Three-Level Inverter
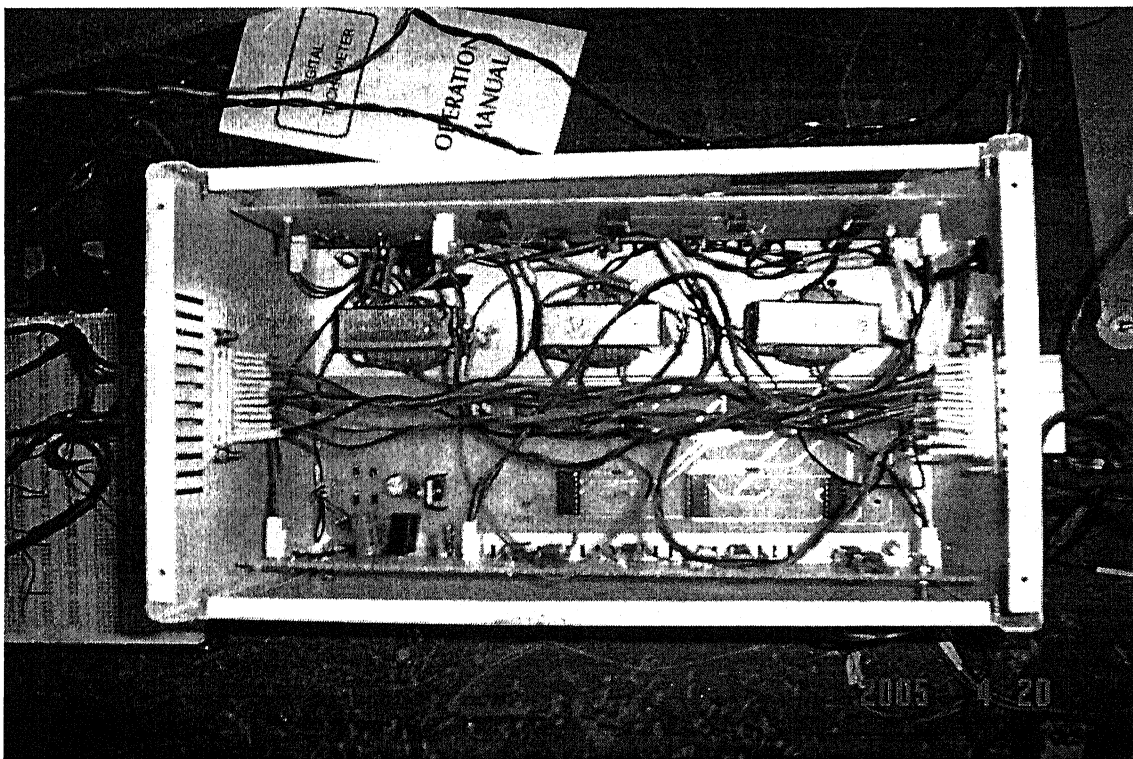
A Inside View of Lockout Circuit

A View of DTFC control of Induction Motor Drive System under operation
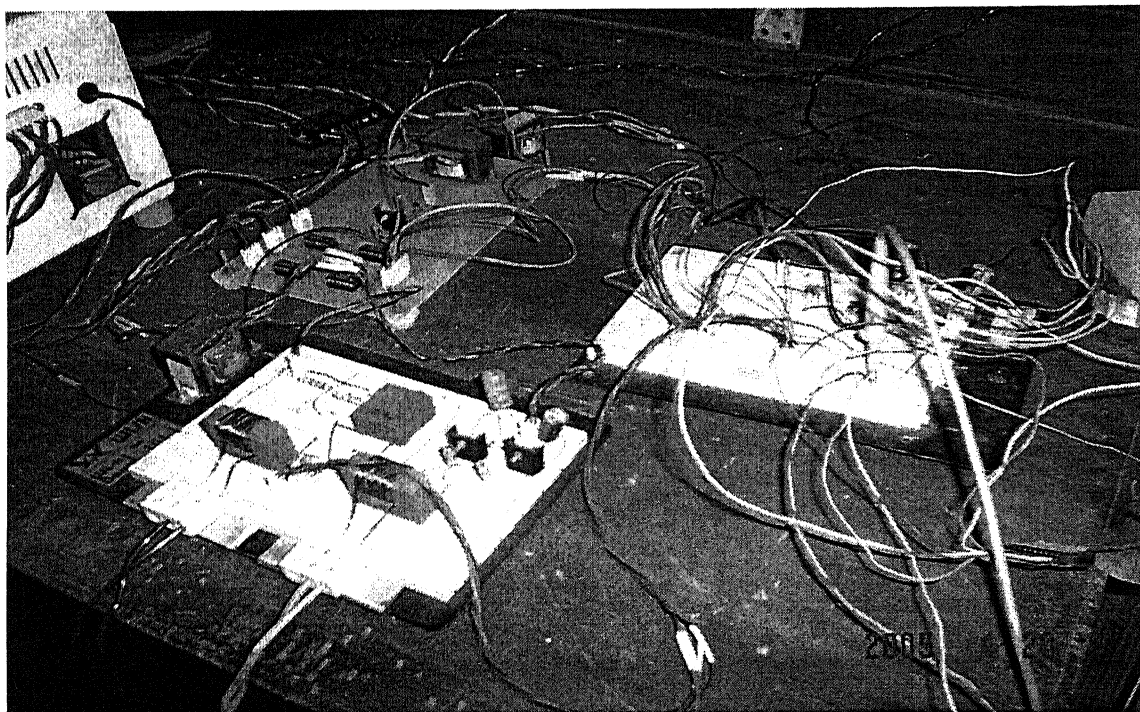
A Close View of Sensor Circuits and Encoder Circuit

Chapter 5

Conclusions

5.1 Contributions of the Present Thesis work

Initially, simulation of four-quadrant direct torque and flux control of induction motor has been presented. The results show that the harmonics in the source current is less, and power factor is unity. Subsequently, PC-based implementation of a direct torque and flux controlled three-level inverter fed induction motor has been presented for high power applications. The dynamic response of the drive is fast with direct and independent control of torque and flux. From the simulation results it can be seen that the low speed performance of the induction motor has been improved using modified look up table.

The salient contributions of the present thesis work can, thus, be summarized as follows.

1. Simulation of three-level synchronous link converter.

2. Modeling and simulation of a utility friendly direct torque and flux controlled induction motor drive system.

3. PC-based hardware implementation of the proposed, direct torque and flux control scheme, for three-level inverter-fed induction motor.

5.2 Scope for the Future Work

In the present work hysteresis current control scheme is used for SLC. For high power application, hysteresis current control scheme cannot be used. This is due to the switching limitation of high power devices. Constant frequency pulse width modulated control scheme is suitable for high power application.

Direct torque control (DTFC) of induction machines has been actively researched in the area of AC machine drives for a number of years. DTFC method described in this work relies on the hysteresis principle in which both torque values and stator flux magnitudes are regulated within pre-specified numerical ranges. The performance of such a scheme depends on the error band set between the desired and measured torque values. In general the narrower this band, the superior the torque performance, however the higher the switching frequency. The flux and torque hysteresis bands are the only gains to be adjusted in DTFC, and the switching frequency and the current waveform are greatly influenced by them. Therefore, the magnitude of the hysteresis band should be determined based on reasonable guidelines which can avoid excessive switching frequency and current harmonics in the whole operating region.

In the present thesis, the reference torque is generated by using the motor speed signal obtained from a mechanical transducer mounted on the rotor shaft. However, this transducer makes the system less robust and reduces the system reliability. An improved drive system can be designed by estimating the speed to avoid the use of speed sensor.

In the proposed scheme, change in parameters is not taken into consideration. If the parameter variation is also considered the accuracy of the results can be improved. Thus if an adaptive motor model is taken the problem of change in characteristics with a change in machine parameters can be tackled and results can be improved.

Two major problems that are usually associated with DTFC drives are: 1) switching frequency that varies with operating conditions and 2) high torque ripple. To solve these problems, a constant switching frequency torque controller has to be used instead of the conventional hysteresis-based controller.

References

[1] J. W. Finch, D. J. Arkinson, "General principles of modern induction motor control", *University of Newcastle upon tyne,* UK, pp. 364-369.

[2] F. Blaschke, "The principle of field orientation as applied to the new transvector closed loop control system for rotating field machines,", *Siemens review,* vol. 34, pp. 212-220, May 1972.

[3] Yen-Shin Lai, "Machine modeling and universal controller for vector-controlled induction motor drives", *IEEE Trans. on Energy Conversion,* vol. 18, no. 1, pp.23 -32, March 2003.

[4] S. P. Das, "Design, simulation and implementation of a current controlled VSI-fed induction motor with indirect field orientation," *M.Tech. Thesis* IIT kharagpur 1991.

[5] A. N. Thakur, S. P. Das, N. K. De, A. K. Chattopadhyay, "Hybrid implementation of indirect vector controlled induction motor and comparison with slip regulated v/f control," in *proc. NSC,* IIT Kanpur 1993.

[6] S. Yamamura, "AC Motors for High Performance Applications", *Newyork: Mercel Dekker,* 1986.

[7] R. Stephan, "Field oriented and field acceleration control for induction motors. Is there a difference?", *Proc. IECON,* pp. 567-572, 1991.

[8] I. Ludtke, M. G. Jayne, "Direct torque control of induction motors", *The Institute of Electrical Engineers,* 1995.

[9] I. Takahashi, T. Nogushi, "A New Quick-Response and High-Efficiency Control Strategy of an Induction Motor", *IEEE Trans. Industry Applications,* vol. IA-22, pp. 820-827, October 1986.

[10] K. B. Lee, J. H. Song, I. Choy, J. Y. Yoo, "Improvement of low-speed operation performance of DTC for three-level inverter-fed induction motors", *Industrial Electronics, IEEE Trans.* on vol. 48, Issue 5, pp. 1006 – 1014, Oct. 2001.

[11] I. Takahashi, Y. Ohmori, "High-performance direct torque control of an induction motor", *IEEE Trans. on Industry Applications,* vol. 25, Issue 2, pp. 257 – 264, March-April 1989.

[12] Y. A. Chapuis, D. Roye, J. Davoine, "Principles and Implementation of Direct Torque Control by Stator Flux Orientation of an Induction Motor", *Applied Power Electronics Conf. and Exposition,* vol.1, Tenth Annual Issue 0, pp.185 - 191, March 1995.

[13] M. P. Kazmierkowski, A. B. Kasprowicz, "Improved direct torque and flux vector control of PWM inverter-fed induction motor drives", *IEEE Trans. on Industrial Electronics,* vol. 42, Issue 4, Aaugust 1995.

[14] J. Faiz, M. B. B. Sharifian, A. Keyhani, A. B. Proca, "Sensorless direct torque control of induction motors used in electric vehicle", *IEEE Trans. on Energy Conversion,* vol. 18, Issue 1, March 2003.

[15] K. K. Shyu, L. J. Shang, H. Z. Chen, K. W. Jwo, "Flux Compensated Direct Torque Control of Induction Motor Drives for Low Speed Operation*", IEEE Trans. on Power Electronics,* vol. 19, Issue 6, pp. 1608-1613, November 2004.

[16] D.Cdi, G.Grd, G. Serra, A. Tmi, "Effects of Flux and Torque Hysteresis Band Amplitude in Direct Torque Control of Induction Machines", *Industrial Electronics, Control and Instrumentation,* vol. 1, pp. 299 – 304, 1994.

[17] M. Jayne, I. Ludtke, L. Yiqiang, T. Arias, "Evaluation of Vector and Direct Torque Controlled Strategies for Cage Rotor Induction Motor Drives", *Power Electronics and Motion Control Conference,* The Third International vol.1, pp. 452-457, Aug. 2000.

[18] K. K. Shyu, L. J. Shang, H. Z. Chen, and K. W. Jwo, "Flux Compensated Direct Torque Control of Induction Motor Drives for Low Speed Operation", *IEEE Trans. on Power Electronics,* vol. 19, no. 6, November 2004.

[19] A. Tripathi and S. P. Das, "A pc-based hardware and software design for a direct torque and flux controlled induction motor drive system," *IEEE Proc. International Conference on Industrial Technology* 2000, vol. 2, pp. 26-31, 2000.

[20] R. Krishnan and A. S. Bharadwaj, "A review of parameter sensitivity and adaptation in indirect vector controlled induction machine drive systems", *IEEE Trans. on Power Electronics,* vol. 6, Issue 4, pp.695-701, Oct. 1991.

[21] H. P. Pham, H. L. Huy, "Direct Torque Control with Switching Frequency Limitation for Three-Level Inverter-Fed Induction Motors*", Industrial Electronics Society,* The 29th Annual Conference of the IEEE vol. 3, pp. 2783-2788, Nov. 2003.

[22] R. Krishnan, *Electric motor drives modeling, analysis, and control,* Prentice-Hall, New Jersey, 1996.

[23] X. Hu and L. Zhang, "A Predictive direct torque control scheme for a three-level VSI- fed induction motor drive", Ninth International Conference on *Electrical Machines and Drives,* Conference Publication No. 468,pp. 334-338,1999

[24] Y. Liu, X. Wu, and L. Huang, "Implementation of three-level inverter using a novel space vector modulation algorithm", *IEEE Conference Proc. on Power Sytem Technology,* vol. 1, pp.606-610, Oct. 2002.

[25] V. Perelmuter, "Three-level inverters with direct torque control", *IEEE Transactions on industrial Application,* vol. 3, pp. 1368-1374, 2000.

[26] G. Escobar, J. Leyva-Ramos, J. M. Carrasco, E. Galvan, R. C. Portillo, M. M. Prats, L. G. Franquelo, "Modeling of a Three Level converter used in synchronous rectifier application", *Power Electronics Specialists Conference, IEEE* 35th Annual vol. 6, pp. 4306 - 4311, 2004.

[27] A. D. Cheok, S. Kawamoto, T. Matsumoto, and H. Obi, "High Power AC/DC Converter and DC/AC Inverter for High Speed Train Applications", *TENCON 2000 Proceedings,* vol. 1, pp. 423 – 428, Sept. 2000.

[28] B. K. Bose, *Modern Power Electronics and AC drives,* 2002.

[29] W. P. Robbins, N. Mohan, T. M. Undeland, *Power electronics converters, applications, and design,* John Willey & Sons Asia, Singapore, 1995.

[30] A. M. Trzvnadlowski, *Introduction to Modern Power Electronics,* John Willey & Sons.

Appendix A

Specifications of a 3 – phase Induction Motor

Ratings

Power	:	1.1 kW
Voltage	:	415 L-L
Current	:	2.6 A
Speed	:	1410 rpm
Moment of Inertia of motor-generator set (j)	:	0.012 kg-m^2

Stator Parameters

Resistance (rs)	:	8.2 Ohm
Leakage inductance (lls)	:	0.026 H
Magnetizing inductance (lm)	:	0.377 H

Rotor Parameters (ref. to stationary)

Resistance (rr)	:	4.3 Ohm
Leakage inductance (llr)	:	0.026 H

Specifications of DC machine

Ratings

Power	:	1 hp
Voltage	:	230 V
Current	:	4.5 A
Speed	:	1500 rpm

Appendix B

Specifications of PCL – 208 Data Acquisition Card

PCL – 208 is a high performance, high speed multifunction data acquisition card for the IBM PC/XT/AT or compatibles. The high end specifications of this full size card and complete software support make it deal for wide range of applications in the industrial and laboratory environment, like data acquisition, process control, automatic testing and factory automation.

Main Features:

- Switch selectable 16 single-ended or 8 analog input channels.

- An industrial standard 12 bit successive approximation converter (ADC 674) to convert analog inputs. The maximum A/D sampling rate is 60 kHz in DMA mode.

- Switch selectable versatile analog input ranges.

   Bipolar: +/- 0.5 V, +/- 1 V, +/-2.5 V, +/- 5 V, +/- 10 V.

   Unipolar: +1 V,+2 V,+5 V,+10 V.

- Provides three A/D trigger modes: software trigger, Programmable pacer trigger and external trigger pulse trigger.

- A/D converted data can be transferred by program control, interrupt handler routine or DMA transfer.

- An INTEL 8254 programmable Timer/Counter provides pacer output (trigger pulse) at the rate of 2.5 MHz to 71 minutes/pulse to the A/D. The timer time base

is switch selectable to 10 MHz or 1 MHz. One 16-bit counter channel is reserved for user configuration applications.

➢ Two 12-bit monolithic multiplying D/A output channels. Output range of 0 to +5 V can be created by using the onboard -5 V reference. This precision reference is derived from the A/D converter reference. External AC or DC reference can also be used to generate other D/A output ranges.

➢ TTL/DTL compatible 16 digital input & 16 digital output channels.

A/D & D/A Converter Specifications

Analog Input Specifications

o Channels : 16 Single-ended or 8 Differential switch selectable.

o Resolution : 12 bits.

o Input range : Unipolar: +1 V,+2 V,+5 V,+10 V.

Bipolar: +/- 0.5V, +/- 1V, +/-2.5V, +/- 5V, +/- 10V.

All input ranges are switch selectable.

o Over voltage : Continuous +/- 30 V Max.

o Conversion Type : Successive Approximation.

o Conversion Speed : 60 kHz max.

o Accuracy Speed : 0.01 % of reading +/- 1 bit.

o Linearity : +/- 1 bit.

o Trigger Mode : Software trigger, onboard programmable timer or external trigger.

o Data transfer : Program control, Interrupt control or DMA.

Analog Output Specifications:

- Channels : 2 channels.
- Resolution : 12 bits.
- Output range : 0 to +5 V with fixed -5 V refernce.

  +/- 10 V with external DC to AC reference.
- Reference voltage : Internal: -5 V (+/- 0.05 V).

  External: DC or AC, +/- 10 V max.
- Conversion Type : 12 bit monolithic multiplying (DAC 7541)
- Linearity : +/- 1/2 bit.
- Output Drive : +/- 5ma max.
- Settling Time : 5 microseconds.

General Specifications:

- Power Consumption : +5 V : typ.700 mA, max. 1A.

  +12 V : typ.140 mA, max. 200 mA.

  -12 V : typ.14 mA, max. 20 mA.
- I/O Connector : 20 pin flat cable connector for all Analog/Digital

  I/O ports.
- I/O Base Address : Requires 16 consecutive address locations. Base

  address is definable by the DIP switches for address

  lines A9 - A4.

Specifications used in Experimental Work:

- 16 Single-ended Analog input channels
- Bipolar +/- 10 V, -5 V internal reference.

Appendix C

Voltage and Current Sensors

Technical Specifications of Voltage Sensors, Current Sensors, are tabulated in the following tables.

Table C.1: Voltage Sensor: Model LV 25 – P

Primary nominal current	:	10 mA
Secondary nominal current	:	25 mA
Conversion ratio	:	2500:1000
Overall accuracy at 25^0 C	:	±0.9 %
Supply Voltage	:	±12 V (±5 %)
Isolation test voltage	:	2.5 kV (rms) / 50 Hz / 1 min
Linearity	:	<0.2 %
Response time	:	<40 μs
Operating Temperature	:	0^0 C to 70^0 C
Current consumption	:	10 mA + output current
Primary Internal Resistance	:	250 Ω (at 70^0 C)
Secondary Internal Resistance	:	110 Ω (at 70^0 C)
Weight	:	22 gm
Operating Range	:	10 to 500 V

Polarity Marking: A positive output current is obtained on terminal M when positive voltage is applied in terminal +HT of the primary circuit.

Primary resistor R1 : The transducer's optimum accuracy is obtained with the nominal primary current. As far as possible, R_1 should be calculated so that the nominal voltage to be measured corresponding to primary current of 10 mA.

Table C.2: **Measuring Resistances**

Voltage rating	R_M (min)	R_M (max)
With ±12 V and ±10 mA max	30 Ω	190 Ω
With ±12 V and ±14 mA max	30 Ω	100 Ω

Table C.3: **Connection Pins**

Pin +	:	Supply Voltage +15 V
Pin M	:	Measuring point
Pin -	:	Supply Voltage -15 V
Pin +HT	:	Primary Voltage +
Pin –HT	:	Primary Voltage –

Table C.4: **Current Sensor: Model LA 55 – P**

Primary nominal current	:	50 A
Secondary nominal current	:	50 mA
Conversion ratio	:	1:1000
Overall accuracy at 25^0 C	:	±0.65 %
Supply Voltage	:	±12 V (± 5%)
Isolation test voltage	:	2.5 kV (rms) / 50 Hz / 1 min
Linearity	:	<0.15 %
Response time	:	<1 µs
Operating Temperature	:	-25^0 C to 85^0 C
Current consumption	:	10 mA + output current
Weight	:	18 gm

Table C.5: **Measuring Resistances (85^0 C)**

Voltage rating	R_M (min)	R_M (max)
With ±12V and ±50mA max	60 Ω	95 Ω
With ±12V and ±70mA max	60 Ω	60 Ω

Table C.6: **Connection Pins**

Pin +	:	Supply Voltage +15 V
Pin M	:	Measuring point
Pin -	:	Supply Voltage -15 V

Appendix D

1. Simulation program

```c
#include<stdio.h>
#include<conio.h>
#include<stdlib.h>
#include<math.h>
#define pi 3.1415
void main()
{
int   p=4,f=50,x=100;
float vrated=415.0,vqs=0.0,vds=0.0,pm;
float wrm;
float h=0.00001;
float lm=0.57,lr=0.632,ls=0.632,rs=1.0,rr=3.46;
float lls,llr,lm1;
float j=0.02,b=0.01;
float ids=0.0,iqs=0.0,idr=0.0,iqr=0.0,is=0.0,wr=0.0,wr1=0.0;
float fds=0.0,fqs=0.0,fdr=0.0,fqr=0.0,fs=0.0;
float fds1=0.0,fqs1=0.0,fdr1=0.0,fqr1=0.0;
float wre=0.0,wre0=0.0;
float wr_ref,wrm_ref=0.0,wr_rated,wc;

float fqm=0.0,fdm=0.0;
float te=0.0,tmx,tmn,ted,te_ref=0.0,tl=0.0,tl_rated=24.536;
float fref,fh,fl;
float tetae=0.0,ki=.08,kp=.3222,ht1,ht2,hf;

float sim_time=5.0,t,ti,k;
int   i,ct=0,cf=0,tetan=0,v;

float k1[4],k2[4],k3[4],k4[4],k5[4];

// Variables for SLC
float vdc_ref=280.0,vdc=0.0,vm=280.0,vas=0.0,vbs=0.0,vcs=0.0;
float vdc1=0.0,vdc2=0.0,nr=1410.0;
float van=0.0,vbn=0.0,vcn=0.0,vao=0.0,vbo=0.0,vco=0.0;
float Ias_ref=0.0,Ibs_ref=0.0,Ics_ref=0.0,Ias=0.0,Ibs=0.0,Ics=0.0;
float Im=0.0,Idc1=0.0,Idc2=0.0;
float lsr=.00024,Rr=35.5,c=0.008,kpr=.2,kir=1.195,il=0.0;
float v_err=0.0,err0=0.0,err1=0.0,sa1=0.0,sa2=0.0,sb1=0.0,sb2=0.0,sc1=0.0,sc2=0.0;
float wrs=2.0*pi*50.0;
float hi=0.2;
float kc1[4],kc2[4],kc3[4],kc4[4],kc5[4];
```

```c
float Ia1=0.0,Ib1=0.0,Ic1=0.0,vd1=0.0,vd2=0.0;

/* Lookup Table */
const int lookuptable[2][5][12]={
{
        {52,53,62,63,12,13,22,23,32,33,42,43},
        {51,53,61,63,11,13,21,23,31,33,41,43},
        {8,7,8,7,8,7,8,7,8,7,8,7},
        {31,33,41,43,51,53,61,63,11,13,21,23},
        {32,33,42,43,52,53,62,63,12,13,22,23},
},
{

        {62,63,12,13,22,23,32,33,42,43,52,53},
        {61,63,11,13,21,23,31,33,41,43,51,53},
        {7,8,7,8,7,8,7,8,7,8,7,8},
        {21,23,31,33,41,43,51,53,61,63,11,13},
        {22,23,32,33,42,43,52,53,62,63,12,13}

}
};


FILE *fp1,*fp2,*fp3,*fp4,*fp5,*fp6,*fp7,*fp8,*fp10,*fp11,*fp12,*fp13,*fp14,*fp15,*fp16;

fp1=fopen("3torq1.txt","w");
fp2=fopen("3spd1.txt","w");
fp3=fopen("3Iqs1.txt","w");
fp4=fopen("3fqs1.txt","w");
fp5=fopen("3flux1.txt","w");
fp6=fopen("3fds1.txt","w");
fp7=fopen("3fqds1.txt","w");
fp8=fopen("3Ids1.txt","w");
//fp9=fopen("3Comd.txt","w");
fp10=fopen("3test1.txt","w");
fp11=fopen("3VIas1.txt","w");
fp12=fopen("3VIbs1.txt","w");
fp13=fopen("3VIcs1.txt","w");
fp14=fopen("3Vdc1.txt","w");
fp15=fopen("3Iabcs1.txt","w");
fp16=fopen("3Vdc121.txt","w");

clrscr();
printf("Program is running... ");


lls=ls-lm;
llr=lr-lm;
```

```
lm1=1/((1/lm)+(1/lls)+(1/llr));

fref=sqrt(2.0/3.0)*(vrated/wrs);
ht1=0.01*tl_rated;
ht2=0.02*tl_rated;
hf=0.01*fref;
wr_rated=nr*2.0*pi/60.0;

tmx=2.0*tl_rated;
tmn=-2.0*tl_rated;

for (t=0.0;t<=sim_time;t+=h)
{
if (t< 0.5)
wr_ref=0.05*wr_rated;
if(t>=.50)
wr_ref=0.5319*wr_rated;
 if ((t>=1.75)&&(t<3.0))
 wr_ref=-0.5319*wr_rated;
 //tl=5.0;
 if(t>=3.0)
wr_ref=0.5319*wr_rated;
 //tl=0.0;

 wre=wr_ref-wr;
 te_ref=te_ref+kp*(wre-wre0)+ki*h*wre;
 if(te_ref>=tmx)
 te_ref=tmx;
 if(te_ref<=tmn)
   te_ref=tmn;
 wre0=wre;
 ted=te_ref-te;

if(ted>=0.0 && ted<ht1 && ct==0)
 ct=0;
else if(ted>=ht1 && ted <ht2 && ct==0)
 ct=1;
else if(ted>=ht2)
 ct=2;
else if(ted>=ht1 && ted<ht2 && ct==2)
 ct=2;
else if(ted<ht1 && ted>=0.0 &&ct==2)
 ct=1;
else if(ted<=0.0 && ct==1)
 ct=0;
else if(ted<=0.0 && ted>-ht1 && ct==0)
```

```
      ct=0;
   else if(ted <= -ht1 && ted>-ht2 && ct==0)
    ct=-1;
   else if(ted<=-ht2)
    ct=-2;
   else if(ted<= -ht1 && ted>-ht2 && ct==-2)
    ct=-2;
   else if(ted>-ht1 && ted<=0.0 &&ct==-2)
    ct=-1;
   else if(ted<0.0 && ted>=-ht1 && ct==-1)
    ct=-1;
   else if(ted>=0.0 && ct==-1)
    ct=0;
// else printf("ct=%d\n",ct);

   fh=fref+hf;
   fl=fref-hf;
   if(fs<=fl)
     cf=1;
   if(fs>=fh)
     cf=0;

// Calculation of flux vector

   if(tetae>=0.0 && tetae<pi/6.0)
     tetan=1;
    else if(tetae>=pi/6.0 && tetae<pi/3.0)
     tetan=2;
    else if(tetae>=pi/3.0 && tetae<pi/2.0)
     tetan=3;
    else if(tetae>=pi/2.0 && tetae<2.0*pi/3.0)
     tetan=4;
    else if(tetae>=2.0*pi/3.0 && tetae<5.0*pi/6.0)
     tetan=5;
    else if(tetae>=5.0*pi/6.0 && tetae<pi)
     tetan=6;
    else if(tetae>=pi && tetae<7.0*pi/6.0)
     tetan=7;
    else if(tetae>=7.0*pi/6.0 && tetae<4.0*pi/3.0)
     tetan=8;
    else if(tetae>=4.0*pi/3.0 && tetae<3.0*pi/2.0)
     tetan=9;
    else if(tetae>=3.0*pi/2.0 && tetae<10.0*pi/6.0)
     tetan=10;
    else if(tetae>=10.0*pi/6.0 && tetae<11.0*pi/6.0)
     tetan=11;
```

```
else tetan=12;


// Syncronous link converter

err1=vdc_ref-vdc;
v_err=v_err+kpr*(err1-err0)+kir*h*err1;
err0=err1;
if(v_err>5.0)
 Im=5.0;
 else if(v_err<-5.0)
        Im=-5.0;
 else Im=v_err;
Ias_ref=Im*sin(wrs*t);
Ibs_ref=Im*sin(wrs*t-2.0*pi/3.0);
Ics_ref=Im*sin(wrs*t-4.0*pi/3.0);

if(Ias_ref-Ias<-hi) {sa1=1.0;sa2=0.0;}
else if(Ias_ref-Ias>hi) {sa1=0.0;sa2=1.0;}
else {sa1=0.0;sa2=0.0;}

if(Ibs_ref-Ibs<-hi) {sb1=1.0;sb2=0.0;}
else if(Ibs_ref-Ibs>hi) {sb1=0.0;sb2=1.0;}
else {sb1=0.0;sb2=0.0;}

if(Ics_ref-Ics<-hi) {sc1=1.0;sc2=0.0;}
else if(Ics_ref-Ics>hi) {sc1=0.0;sc2=1.0;}
else {sc1=0.0;sc2=0.0;}

vas=vm*sin(wrs*t);
vbs=vm*sin(wrs*t-2.0*pi/3.0);
vcs=vm*sin(wrs*t-4.0*pi/3.0);

vao=sa1*vdc1-sa2*vdc2;
vbo=sb1*vdc1-sb2*vdc2;
vco=sc1*vdc1-sc2*vdc2;

van=(1.0/3.0)*(2.0*vao-vbo-vco);
vbn=(1.0/3.0)*(2.0*vbo-vao-vco);
vcn=(1.0/3.0)*(2.0*vco-vao-vbo);

for(i=0;i<4;++i)
 {
 kc1[i]=h*(vas-van-Rr*Ia1)/lsr;
 kc2[i]=h*(vbs-vbn-Rr*Ib1)/lsr;
```

```
kc3[i]=h*(vcs-vcn-Rr*Ic1)/lsr;
kc4[i]=h*(sa1*Ia1+sb1*Ib1+sc1*Ic1-il)/c;
kc5[i]=-h*(sa2*Ia1+sb2*Ib1+sc2*Ic1+il)/c;

if(i==0||i==1)
{
Ia1+=kc1[i]/2.0;
Ib1+=kc2[i]/2.0;
Ic1+=kc3[i]/2.0;
vd1+=kc4[i]/2.0;
vd2+=kc5[i]/2.0;
}
if(i==2)
{
Ia1+=kc1[i];
Ib1+=kc2[i];
Ic1+=kc3[i];
vd1+=kc4[i];
vd2+=kc5[i];
}
}
Ias+=(kc1[0]+2.0*kc1[1]+2.0*kc1[2]+kc1[3])/6.0;
Ibs+=(kc2[0]+2.0*kc2[1]+2.0*kc2[2]+kc2[3])/6.0;
Ics+=(kc3[0]+2.0*kc3[1]+2.0*kc3[2]+kc3[3])/6.0;
vdc1+=(kc4[0]+2.0*kc4[1]+2.0*kc4[2]+kc4[3])/6.0;
vdc2+=(kc5[0]+2.0*kc5[1]+2.0*kc5[2]+kc5[3])/6.0;

Ia1=Ias;
Ib1=Ibs;
Ic1=Ics;
vd1=vdc1;
vd2=vdc2;

Idc1=sa1*Ias+sb1*Ibs+sc1*Ics;
Idc2=sa2*Ias+sb2*Ibs+sc2*Ics;
vdc=vdc1+vdc2;

//synchronous link converter end

// Selection of voltage vector from look up table

v=lookuptable[cf][ct+2][tetan-1];
switch(v)
{
case 11:
    vds=(1.0/3.0)*vdc;
```

```
            vqs=0.0;
            break;
    case 12:
            vds=(2.0/3.0)*vdc;
            vqs=0.0;
            break;
    case 21:
            vds=(1.0/6.0)*vdc;
            vqs=vdc/(2.0*1.732);
            break;
    case 22:
            vds=(1.0/3.0)*vdc;
            vqs=vdc/(1.732);
            break;
    case 31:
            vds=-(1.0/6.0)*vdc;
            vqs=vdc/(2.0*1.732);
            break;
    case 32:
            vds=-(1.0/3.0)*vdc;
            vqs=vdc/1.732;
            break;
    case 41:
            vds=-(1.0/3.0)*vdc;
            vqs=0.0;
            break;
    case 42:
            vds=-(2.0/3.0)*vdc;
            vqs=0.0;
            break;
    case 51:
            vds=-(1.0/6.0)*vdc;
            vqs=-vdc/(2.0*1.732);
            break;
    case 52:
            vds=-(1.0/3.0)*vdc;
            vqs=-vdc/(1.732);
            break;
    case 61:
            vds=(1.0/6.0)*vdc;
            vqs=-vdc/(2.0*1.732);
            break;
    case 62:
            vds=(1.0/3.0)*vdc;
            vqs=-vdc/1.732;
            break;
```

```
case 13:
        vds=(1.0/2.0)*vdc;
        vqs=vdc/(2.0*1.732);
        break;
case 23:
        vds=0.0;
        vqs=vdc/(1.732);
        break;
case 33:
        vds=-(1.0/2.0)*vdc;
        vqs=vdc/(2.0*1.732);
        break;
case 43:
        vds=-(1.0/2.0)*vdc;
        vqs=-vdc/(2.0*1.732);
        break;
case 53:
        vds=0.0;
        vqs=-vdc/(1.732);
        break;
case 63:
        vds=(1.0/2.0)*vdc;
        vqs=-vdc/(2.0*1.732);
        break;
case 7,8:
default:
        vds=0.0;
        vqs=0.0;
        break;
}
// printf("%f\t%f\n",vds,vqs);
// fprintf(fp9,"%0.4f\t%0.5f\t%d\t%d\t%d\t%d\t%0.1f\t%0.1f\n",t,tetae,cf,ct,tetan,v,vds,vqs);
 for(i=0;i<4;++i)
 {
 k1[i]=h*(vqs-(rs/lls)*(fqs1-((lm1/lls)*fqs1 + (lm1/llr)*fqr1)));
 k2[i]=h*(vds-(rs/lls)*(fds1-((lm1/lls)*fds1 + (lm1/llr)*fdr1)));
 k3[i]=h*(wr1*fdr1-(rr/llr)*(fqr1-((lm1/lls)*fqs1 + (lm1/llr)*fqr1))) ;
 k4[i]=h*(-wr1*fqr1-(rr/llr)*(fdr1-((lm1/lls)*fds1 + (lm1/llr)*fdr1))) ;
 k5[i]=h*(p/(2.0*j))*(te-tl-b*(2.0/p)*wr1);

 if(i==0||i==1)
 {
 fqs1+=k1[i]/2.0;
 fds1+=k2[i]/2.0;
 fqr1+=k3[i]/2.0;
 fdr1+=k4[i]/2.0;
```

```c
  wr1+=k5[i]/2.0;
}
if(i==2)
{
 fqs1+=k1[i];
 fds1+=k2[i];
 fqr1+=k3[i];
 fdr1+=k4[i];
 wr1+=k5[i];
}
}
fqs+=(k1[0]+2.0*k1[1]+2.0*k1[2]+k1[3])/6.0;
fds+=(k2[0]+2.0*k2[1]+2.0*k2[2]+k2[3])/6.0;
fqr+=(k3[0]+2.0*k3[1]+2.0*k3[2]+k3[3])/6.0;
fdr+=(k4[0]+2.0*k4[1]+2.0*k4[2]+k4[3])/6.0;
wr+=(k5[0]+2.0*k5[1]+2.0*k5[2]+k5[3])/6.0;

fs=sqrt(fds*fds+fqs*fqs);
fqs1=fqs;
fds1=fds;
fqr1=fqr;
fdr1=fdr;
wr1=wr;

fqm=((lm1/lls)*fqs + (lm1/llr)*fqr);
fdm=((lm1/lls)*fds + (lm1/llr)*fdr);

iqs=(fqs-fqm)/lls;
ids=(fds-fdm)/lls;
iqr=(fqr-fqm)/llr;
idr=(fdr-fdm)/llr;

te=(3.0/2.0)*(p/2.0)*(fds*iqs-fqs*ids);
is=sqrt(ids*ids+iqs*iqs);
wrm=wr*2.0/p;
wrm_ref=(wr_ref*2.0/p);

pm=te*wrm+3.0*is*is/2.0*rs;
il=pm/vdc;
if(fqs==0.0&&fds==0.0)
      tetae=0.0;
 else
      tetae=atan2(fqs,fds);
      if(tetae<0.0)
         tetae= tetae+2.0*pi;
```

```c
if(x>=100)
{
fprintf(fp1,"%f\t%f\t%f\n",t,te,tl);
fprintf(fp2,"%f\t%f\t%0.4f\n",t,wr*60.0/(2.*pi),wr_ref*60.0/(2.*pi));
fprintf(fp3,"%f\t%f\n",t,iqs);
fprintf(fp4,"%f\t%f\n",t,fqs);
fprintf(fp5,"%f\t%f\t%f\n",t,fs,fref);
fprintf(fp6,"%f\t%f\n",t,fds);
fprintf(fp7,"%f\t%f\n",fqs,fds);
fprintf(fp8,"%f\t%f\n",t,ids);
fprintf(fp10,"%f\t%f\t%f\t%f\t%f\t%f\t%f\n",t,il,pm,Im,v_err,Ias,Ias_ref);
fprintf(fp11,"%f\t%f\t%f\n",t,vas/10.0,Ias);
fprintf(fp12,"%f\t%f\t%f\n",t,vbs/10.0,Ibs);
fprintf(fp13,"%f\t%f\t%f\n",t,vcs/10.0,Ics);
fprintf(fp14,"%f\t%f\t%f\n",t,vdc_ref,vdc);
fprintf(fp15,"%f\t%f\t%f\t%f\n",t,Ias,Ibs,Ics);
fprintf(fp16,"%f\t%f\t%f\n",t,vdc1,vdc2);

x=0;
}
x++;
}

fclose(fp1);
fclose(fp2);
fclose(fp3);
fclose(fp4);
fclose(fp5);
fclose(fp6);
fclose(fp7);
fclose(fp8);
// fclose(fp9);
fclose(fp11);
fclose(fp12);
fclose(fp13);
fclose(fp14);
fclose(fp15);
fclose(fp16);

}
```

2. Listing of Real Time PC-Based Program

```c
#include<stdio.h>
#include<conio.h>
#include<stdlib.h>
#include<math.h>
#include <dos.h>
#include<time.h>
#define pi 3.14159
#define BASE 0x300
#define TRUE 1
void main()
{
int   p=4,f=50;
float vdc,vrated=415.0,vqs=0.0,vds=0.0;
float wrs,wrm;
float h=0.0002;
float lm=0.377,lr=0.403,ls=0.403,rs=1.0,rr=4.3;
float lls,llr,lm1;
float j=0.012,b=0.0;
float ids=0.0,iqs=0.0,idr=0.0,iqr=0.0,is=0.0,wr=0.0,wr1=0.0;
float fds=0.0,fqs=0.0,fdr=0.0,fqr=0.0,fs=0.0;
float fds1=0.0,fqs1=0.0,fdr1=0.0,fqr1=0.0;
float wre=0.0,wre0=0.0;
float wr_ref,wrm_ref=0.0,wr_rated,nr=1440.0,wc;

float fqm=0.0,fdm=0.0;
float te=0.0,tmx,tmn,ted,te_ref=0.0,tl=0.0,tl_rated=24.536;
float fref,fh,fl;
float tetae=0.0,ki=1.08,kp=2.5,ht1,ht2,hf;

float t,k;
int   i,ct=0,cf=0,tetan=0,v;

float k1[4],k2[4],k3[4],k4[4],k5[4];

int muxscan=0x30,swlogic;
int trigger=0x00;
int check,u;
int mb,lb,hb,msb[4],lsb[4];
float wra,va=0.0,vad=0.0,Ia,Ib,Ic;
float val[4];

clock_t strt=0,end=0;

int sa1=1,sa2=1,sb1=1,sb2=1,sc1=1,sc2=1;
```

```c
/* Lookup Table */
const int lookuptable[2][5][12]={
{
        {52,53,62,63,12,13,22,23,32,33,42,43},
        {51,53,61,63,11,13,21,23,31,33,41,43},
        {8,7,8,7,8,7,8,7,8,7,8,7},
        {31,33,41,43,51,53,61,63,11,13,21,23},
        {32,33,42,43,52,53,62,63,12,13,22,23},
},
{
        {62,63,12,13,22,23,32,33,42,43,52,53},
        {61,63,11,13,21,23,31,33,41,43,51,53},
        {7,8,7,8,7,8,7,8,7,8,7,8},
        {21,23,31,33,41,43,51,53,61,63,11,13},
        {22,23,32,33,42,43,52,53,62,63,12,13}
}
};

wrs=2.0*pi*f;
lls=ls-lm;
llr=lr-lm;
lm1=1/((1/lm)+(1/lls)+(1/llr));

fref=sqrt(2.0/3.0)*(vrated/wrs);
ht1=0.001*tl_rated;
ht2=0.002*tl_rated;
hf=0.01*fref;
wr_rated=nr*2.0*pi/60.0;
wr_ref=0.2*wr_rated;

tmx=2.0*tl_rated;
tmn=-2.0*tl_rated;

clrscr();

for(t=0.0;t<=50.0;t+=h)
{

if(t>=25.0)
wr_ref=-0.2*wr_rated;
if(t>=35.0)
wr_ref=0.2*wr_rated;
```

```c
/* SENSING OF ANALOG SIGNAL */

  outportb(BASE+2,muxscan);

 for(i=0;i<=3;i++)
  {
  outportb(BASE+0,trigger);

      while(1)
       {
       u=inportb(BASE+8);
       check=u;
       check&= 0x80;
       if(!check)
       break;
       }

   lsb[i]=inportb(BASE+0);
   msb[i]=inportb(BASE+1);
   }
 lsb[0]=lsb[0]>>4;
 msb[0]=msb[0]<<4;
 val[0]=lsb[0]+msb[0];
 val[0]=(val[0]-2047)*5/2047;
 Ia=val[0]*1.618;

// printf("Ia=%2.1f\t", Ia);

 lsb[1]=lsb[1]>>4;
 msb[1]=msb[1]<<4;
 val[1]=lsb[1]+msb[1];
 val[1]=(val[1]-2047)*5/2047;
 Ib=val[1]*1.678;

// printf("Ib=%2.1f\n", Ib);

 lsb[2]=lsb[2]>>4;
 msb[2]=msb[2]<<4;
 val[2]=lsb[2]+msb[2];
 val[2]=(val[2]-2047)*5/2047;
 vdc=val[2]*148.22;

// printf("vdc=%2.1f\n", vdc);

 lsb[3]=lsb[3]>>4;
```

115

```c
msb[3]=msb[3]<<4;
val[3]=lsb[3]+msb[3];
val[3]=(val[3]-2047)*5/2047;
wr=val[3]*377.47*(2*pi/30.0)*0.441;

// printf("wr=%2.1f\n", wr);

/* END OF SENSING SIGNALS */

Ic=-Ia-Ib;
ids=Ia;
iqs=(Ib-Ic)/sqrt(3.0);

wre=wr_ref-wr;
te_ref=te_ref+kp*(wre-wre0)+ki*h*wre;
if(te_ref>=tmx)
te_ref=tmx;
if(te_ref<=tmn)
  te_ref=tmn;
wre0=wre;
ted=te_ref-te;

if(ted>=0.0 && ted<ht1 && ct==0)
  ct=0;
else if(ted>=ht1 && ted <ht2 && ct==0)
  ct=1;
else if(ted>=ht2)
  ct=2;
else if(ted>=ht1 && ted<ht2 && ct==2)
  ct=2;
else if(ted<ht1 && ted>=0.0 &&ct==2)
  ct=1;
else if(ted<=0.0 && ct==1)
  ct=0;
else if(ted<=0.0 && ted>-ht1 && ct==0)
  ct=0;
else if(ted <= -ht1 && ted>-ht2 && ct==0)
  ct=-1;
else if(ted<=-ht2)
  ct=-2;
else if(ted<= -ht1 && ted>-ht2 && ct==-2)
  ct=-2;
else if(ted>-ht1 && ted<=0.0 &&ct==-2)
  ct=-1;
else if(ted<0.0 && ted>=-ht1 && ct==-1)
  ct=-1;
```

```
else if(ted>=0.0 && ct==-1)
  ct=0;


fh=fref+hf;
fl=fref-hf;
if(fs<=fl)
  cf=1;
if(fs>=fh)
  cf=0;

// Calculation of flux vector

if(tetae>=0.0 && tetae<pi/6.0)
   tetan=1;
  else if(tetae>=pi/6.0 && tetae<pi/3.0)
   tetan=2;
  else if(tetae>=pi/3.0 && tetae<pi/2.0)
   tetan=3;
  else if(tetae>=pi/2.0 && tetae<2.0*pi/3.0)
   tetan=4;
  else if(tetae>=2.0*pi/3.0 && tetae<5.0*pi/6.0)
   tetan=5;
  else if(tetae>=5.0*pi/6.0 && tetae<pi)
   tetan=6;
  else if(tetae>=pi && tetae<7.0*pi/6.0)
   tetan=7;
  else if(tetae>=7.0*pi/6.0 && tetae<4.0*pi/3.0)
   tetan=8;
  else if(tetae>=4.0*pi/3.0 && tetae<3.0*pi/2.0)
   tetan=9;
  else if(tetae>=3.0*pi/2.0 && tetae<10.0*pi/6.0)
   tetan=10;
  else if(tetae>=10.0*pi/6.0 && tetae<11.0*pi/6.0)
   tetan=11;
  else tetan=12;

// Selection of voltage vector from look up table

v=lookuptable[cf][ct+2][tetan-1];
switch(v)
{
case 11:
     vds=(1.0/3.0)*vdc;
     vqs=0.0;
     sa1=0;sa2=0;sb1=0;sb2=1;sc1=0;sc2=1;
```

```
        break;
case 12:
        vds=(2.0/3.0)*vdc;
        vqs=0.0;
        sa1=0;sa2=0;sb1=1;sb2=0;sc1=1;sc2=0;
        break;
case 21:
        vds=(1.0/6.0)*vdc;
        vqs=vdc/(2.0*1.732);
        sa1=0;sa2=0;sb1=0;sb2=0;sc1=0;sc2=1;
        break;
case 22:
        vds=(1.0/3.0)*vdc;
        vqs=vdc/(1.732);
        sa1=0;sa2=0;sb1=0;sb2=0;sc1=1;sc2=0;
        break;
case 31:
        vds=-(1.0/6.0)*vdc;
        vqs=vdc/(2.0*1.732);
        sa1=0;sa2=1;sb1=0;sb2=0;sc1=0;sc2=1;
        break;
case 32:
        vds=-(1.0/3.0)*vdc;
        vqs=vdc/1.732;
        sa1=1;sa2=0;sb1=0;sb2=0;sc1=1;sc2=0;
        break;
case 41:
        vds=-(1.0/3.0)*vdc;
        vqs=0.0;
        sa1=0;sa2=1;sb1=0;sb2=0;sc1=0;sc2=0;
        break;
case 42:
        vds=-(2.0/3.0)*vdc;
        vqs=0.0;
        sa1=1;sa2=0;sb1=0;sb2=0;sc1=0;sc2=0;
        break;
case 51:
        vds=-(1.0/6.0)*vdc;
        vqs=-vdc/(2.0*1.732);
        sa1=0;sa2=1;sb1=0;sb2=1;sc1=0;sc2=0;
        break;
case 52:
        vds=-(1.0/3.0)*vdc;
        vqs=-vdc/(1.732);
        sa1=1;sa2=0;sb1=1;sb2=0;sc1=0;sc2=0;
        break;
```

```
case 61:
    vds=(1.0/6.0)*vdc;
    vqs=-vdc/(2.0*1.732);
    sa1=0;sa2=0;sb1=0;sb2=1;sc1=0;sc2=0;
    break;
case 62:
    vds=(1.0/3.0)*vdc;
    vqs=-vdc/1.732;
    sa1=0;sa2=0;sb1=1;sb2=0;sc1=0;sc2=0;
    break;
case 13:
    vds=(1.0/2.0)*vdc;
    vqs=vdc/(2.0*1.732);
    sa1=0;sa2=0;sb1=0;sb2=1;sc1=1;sc2=0;
    break;
case 23:
    vds=0.0;
    vqs=vdc/(1.732);
    sa1=0;sa2=1;sb1=0;sb2=0;sc1=1;sc2=0;
    break;
case 33:
    vds=-(1.0/2.0)*vdc;
    vqs=vdc/(2.0*1.732);
    sa1=1;sa2=0;sb1=0;sb2=0;sc1=0;sc2=1;
    break;
case 43:
    vds=-(1.0/2.0)*vdc;
    vqs=-vdc/(2.0*1.732);
    sa1=1;sa2=0;sb1=0;sb2=1;sc1=0;sc2=0;
    break;
case 53:
    vds=0.0;
    vqs=-vdc/(1.732);
    sa1=0;sa2=1;sb1=1;sb2=0;sc1=0;sc2=0;
    break;
case 63:
    vds=(1.0/2.0)*vdc;
    vqs=-vdc/(2.0*1.732);
    sa1=0;sa2=0;sb1=1;sb2=0;sc1=0;sc2=1;
    break;
case 7:
    vds=0.0;
    vqs=0.0;
    sa1=1;sa2=1;sb1=1;sb2=1;sc1=1;sc2=1;
    break;
```

```
case 8:
   vds=0.0;
     vqs=0.0;
     sal=1;sa2=1;sb1=1;sb2=1;sc1=1;sc2=1;
     break;
default:
     vds=0.0;
     vqs=0.0;
     sal=1;sa2=1;sb1=1;sb2=1;sc1=1;sc2=1;
     break;
}
fqs1=ls*iqs+lm*iqr;
fds1=ls*ids+lm*idr;
fqr1=lr*iqr+lm*iqs;
fdr1=lr*idr+lm*ids;
wr1=wr;

for(i=0;i<4;++i)
{
 k1[i]=h*(vqs-(rs/lls)*(fqs1-((lm1/lls)*fqs1 + (lm1/llr)*fqr1)));
 k2[i]=h*(vds-(rs/lls)*(fds1-((lm1/lls)*fds1 + (lm1/llr)*fdr1)));
 k3[i]=h*(wr1*fdr1-(rr/llr)*(fqr1-((lm1/lls)*fqs1 + (lm1/llr)*fqr1))) ;
 k4[i]=h*(-wr1*fqr1-(rr/llr)*(fdr1-((lm1/lls)*fds1 + (lm1/llr)*fdr1))) ;


 if(i==0||i==1)
 {
  fqs1+=k1[i]/2.0;
  fds1+=k2[i]/2.0;
  fqr1+=k3[i]/2.0;
  fdr1+=k4[i]/2.0;

 }
 if(i==2)
 {
  fqs1+=k1[i];
  fds1+=k2[i];
  fqr1+=k3[i];
  fdr1+=k4[i];

 }
}
fqs+=(k1[0]+2.0*k1[1]+2.0*k1[2]+k1[3])/6.0;
fds+=(k2[0]+2.0*k2[1]+2.0*k2[2]+k2[3])/6.0;
fqr+=(k3[0]+2.0*k3[1]+2.0*k3[2]+k3[3])/6.0;
fdr+=(k4[0]+2.0*k4[1]+2.0*k4[2]+k4[3])/6.0;
```

```c
fs=sqrt(fds*fds+fqs*fqs);

fqm=((lm1/lls)*fqs + (lm1/llr)*fqr);
fdm=((lm1/lls)*fds + (lm1/llr)*fdr);

iqr=(fqr-fqm)/llr;
idr=(fdr-fdm)/llr;

te=(3.0/2.0)*(p/2.0)*(fds*iqs-fqs*ids);
is=sqrt(ids*ids+iqs*iqs);

if(fqs==0.0&&fds==0.0)
      tetae=0.0;
 else
      tetae=atan2(fqs,fds);
      if(tetae<0.0)
         tetae= tetae+2.0*pi;

/*********** SWITCHING OUT CONTROL PULSES************/

swlogic = 32 * sc1 + 16 * sc2 + 8 * sb1 + 4 * sb2 + 2 * sa1 + sa2;
outportb(BASE+3,swlogic);

/** SENDING ANALOG SIGNALS OUT************/
vad=2047.0+2047.0 *fqs/25.;
vad=floor(vad);
mb=vad/16;
lb=vad-mb*16;
lb=lb<<4;
outportb(BASE+6,lb);
outportb(BASE+7,mb);

vad=2047.0+2047. * te/15.0;
vad=floor(vad);
mb=vad/16;
lb=vad-mb*16;
lb=lb<<4;
outportb(BASE+4,lb);
outportb(BASE+5,mb);
 }
 end=clock();
 printf("%f\n",((end-strt)/CLK_TCK)*h);
// fclose(fp1);

}
```